

https://dspace.org/

Characterization of mouse cytomegalovirus MHC-1 homologs

Mans, Janet

2009-03-20T09:25:22Z
http://hdl.handle.net/10539/6768

Downloaded from a DSpace repository. https://dspace.org/

CHARACTERIZATION OF MOUSE CYTOMEGALOVIRUS MHC-I HOMOLOGS

Janet Mans

A thesis submitted to the Faculty of Health Sciences, University of the Witwatersrand, Johannesburg, for the Degree Doctor of Philosophy

Johannesburg, 2008

ABSTRACT

Mouse cytomegalovirus (MCMV), a β-herpesvirus, encodes the m145 family of glycoproteins. Several members of this family are predicted to adopt the MHC-I fold although their amino acid sequences exhibit less than 30% identity to classical MHC-I (MHC-Ia) proteins. Our aim was to determine how related the viral proteins are to MHC-Ia and characterize them in terms of cellular expression, structure and function. We studied the cellular localization of FLAG-tagged m17, M37, m145, m151, m152, m153 and m155 in transfected mouse fibroblasts. Flow cytometry analysis of transfected cells showed that M37, m145, m151 and m153 localize predominantly to the cell surface, whereas the majority of m17, m152 and m155 remain inside the cell. MHC-Ia proteins require assembly with β2-microglobulin (β2m) and peptide for stable cell surface expression. Transient transfection studies with β2m- or transporter associated with antigen (TAP)-deficient cell lines revealed that M37, m145, m151 and m153 could be expressed stably at the cell surface in the absence of β2m or TAP expression.

To generate protein material for crystallization screening we evaluated both bacterial and insect cell expression systems. Although most m145 family members could be expressed in bacteria in insoluble inclusion bodies, none of the proteins could be accurately refolded. Since M37, m151 and m153 are cell surface molecules with the potential to bind receptors on host cells, we focused our structure determination efforts on them and evaluated their expression in *Drosophila* S2 insect cells. The extracellular domains of all three proteins expressed at significant levels, however, m151 tended to aggregate and

precipitate over time. M37 and m153 were stable and could easily be purified to homogeneity. Size exclusion chromatography and SDS-PAGE analysis of m153 suggested that it forms a non-covalent homodimer. Analytical ultracentrifugation experiments confirmed this observation and provided an estimated molecular mass of 78.8 kDa. Enzymatic and mass spectrometry analyses showed that insect-expressed m153 is highly glycosylated. We tested a wide range of crystallization conditions for m153. It formed very fragile crystals and after optimization we obtained several that diffracted to 2.3 Å. To determine the structure of m153, we prepared a seleno-methionine derivative in insect cells, collected data on a single crystal and solved the phases by the single anomalous dispersion method. The m153 model was refined at 2.4 Å resolution to final R_{cryst} and R_{free} of 23% and 27.9%, respectively.

The m153 homodimer is formed by two MHC-I-like heavy chains, each consisting of two α-helices arranged on a platform of seven β-strands and an Ig-like α3 domain. The monomers are arranged "head-to-tail", with the α1α2 platform domain of one chain interacting with the Ig-like α3 domain of the other. The α1 and α2 helices are closely juxtaposed and do not form a peptide binding groove. Three N-linked carbohydrate residues were visualized in the crystal structure. Major deviations from the MHC-I fold include an extended N-terminus, which originates next to the α3 domain, and an elongated α2 helix (designated H2b) that reaches down towards the α3 domain. In addition, m153 has two unique disulfide bonds, one between strands of the platform domain and another that links the extended N-terminus to the H2b helix. Both unique disulfide bonds were verified by mass spectrometry. The canonical Ig-fold disulfide bond

is present in the α3 domain. Alanine mutation of four amino acids involved in interface hydrogen bonds abolished m153 dimer formation, validating the dimer interface visualized in the structure. The crystal structure of m153, together with the recently reported m157 structure, confirms the MHC-I fold for the MCMV m145 family and highlights shared structural features in the m145 family. We have demonstrated dimerization of full-length m153 in mammalian cells by bimolecular fluorescence complementation and co-immunoprecipitation studies. Further, we have shown that m153 is expressed at the surface of MCMV-infected cells at early times after infection.

To initiate a search for host ligands of m153, we generated a reporter cell line by introducing an m153-human zeta chain fusion protein into 43.1 cells that contain an NFAT-driven GFP construct. While a variety of mouse cell lines were unable to stimulate the m153-reporter cells, coculture with mouse splenocytes specifically induced GFP production in m153-reporters but not in the parental or control reporter cell lines. We identified conventional $CD11c^+$ and plasmacytoid dendritic cells (DCs) as the most potent m153-reporter cell stimulating populations in the spleen. The stimulation was shown to be m153-specific, dose- and cell contact-dependent. DCs derived from bone-marrow cultures also potently stimulated the m153-reporter cells. Macrophages and NK cells exhibited weaker stimulation of the reporter cells, indicating lower levels of ligand or that only small subsets of the cells express a ligand. DCs from several mouse strains, but not from the rat, stimulated m153-reporter cells. We evaluated DC surface phenotype and migratory capacity after coculture with m153-reporter cells or on m153-coated plates, but could not detect any changes induced specifically by the presence of m153.

The functional consequences of an interaction between MCMV m153 and mouse DCs remains to be explored. A viable approach to identify the m153 ligand/s is the generation and screening of DC-specific cDNA libraries with the m153-reporter cell line. Identification of a ligand will facilitate studies to establish m153's function during virus infection and provide greater insight into the immune manipulation strategies of herpesviruses.

DECLARATION

I declare that this thesis is my own, unaided work. It is being submitted for the degree of Doctor of Philosophy at the University of the Witwatersrand, Johannesburg. It has not been submitted before for any degree or examination at any other University.

_____

Janet Mans

_____ day of _____, 20___

ACKNOWLEDGEMENTS

I would like to sincerely thank:

David Margulies, for giving me the opportunity to work in his laboratory, for being a great mentor and giving me lots of support and encouragement,

Caroline Tiemessen, for her confidence in me, for providing invaluable support and encouragement and being an excellent long-distance mentor,

Kannan Natarajan, for his expert advice and help in the laboratory and critical discussion of experiments and results,

Ditza Levin for advice on flow cytometry and helpful discussions,

Howard Robinson at the Brookhaven National Synchrotron Light Source, Upton, New York, for collecting and processing X-ray diffraction data,

Stipan Jonjic at the Department of Histology and Embryology, University of Rijeka, Croatia, for providing the MCMV-GFP, production of monoclonal antibodies and advice and support,

Hvroje Simic at the Department of Histology and Embryology, University of Rijeka, Croatia, for production of the monoclonal antibodies,

Barbara Newman and Rose Mage at the Laboratory of Immunology, National Institute of Allergy and Infectious Diseases (NIAID), NIH, for the production of rabbit antibodies,

Peter Schuck and Andrea Balbo at the Protein Biophysics Resource, National Institute of Biomedical Imaging and Bioengineering, NIH, for performing the analytical ultracentrifugation experiments and data analysis,

Daniel Eikel and Sonja Hess at the Mass Spectrometry Facility, National Institute for Diabetes and Digestive and Kidney Diseases, NIH, for performing the m153 mass spectrometry experiments and data analysis,

Owen Schwartz, Meggan Czapiga and Juraj Kabat for their advice and help at the NIAID Biological Imaging Facility,

Sarah Tanksley at the NIAID Flow Cytometry Facility for cell sorting,

Mark Garfield at the NIAID Research Technology Branch for N-terminal sequencing,

Jack Bennink at the Laboratory of Viral Diseases, NIAID, NIH for advice and encouragement,

All the members of the Margulies laboratory for their friendship and support,

The NIAID for a pre-doctoral visiting fellowship,

The Poliomyelitis Research Foundation of South Africa for their financial support,

My family and friends in South Africa and the USA, whose support, constant encouragement and visits kept me motivated,

My husband Ben, for embarking on this adventure with me, for all his support, advice and insightful discussions.

PUBLICATIONS AND PRESENTATIONS

Publication arising from PhD

Mans J., Natarajan K., Schuck P., Balbo A., Eikel D., Hess S., Simic H., Jonjic S., Robinson H., Tiemessen C.T., Margulies D.H. Cellular expression and crystal structure of the murine cytomegalovirus MHC-I-like glycoprotein, m153. *Journal of Biological Chemistry*. 2007 Nov 30, 282 (48):35247-58

Publication arising from other work performed during PhD

Natarajan K., Hicks A., Mans J., Robinson H., Guan R., Mariuzza R.A., Margulies D.H. Crystal structure of the murine cytomegalovirus MHC-I homolog m144. *Journal of Molecular Biology*. 2006 358 (1):157-71

Presentations

Mans J., Natarajan K., Schuck P., Balbo A., Eikel D., Hess S., Simic H., Jonjic S., Robinson H., Tiemessen C.T., Margulies D.H. Cellular expression and crystal structure of the murine cytomegalovirus MHC-Iv glycoprotein, m153. NIH Immunology Retreat, October 1-3. 2007, Airlie Center, Warrenton, VA, USA. (Poster presentation)

Mans J., Natarajan K., Schuck P., Balbo A., Eikel D., Hess S., Simic H., Jonjic S., Robinson H., Tiemessen C.T., Margulies D.H. The crystal structure of mouse cytomegalovirus m153 reveals a novel dimerization mode for the MHC-I fold. 32nd Annual International Herpesvirus Workshop, July 2007, Asheville, NC, USA. (Poster presentation)

Eikel D., Mans J., Margulies D.H. and Hess S. Glycoprotein characterization using infusion chip technology combined with FT-ICR mass spectrometry and ECD/IRMPD fragmentation. 55th Conference of the American Society for Mass Spectrometry (ASMS), June 2007, Indianapolis, IN, USA. (Poster presentation)

Mans J., Natarajan K., Schuck P., Balbo A., Eikel D., Hess S., Simic H., Jonjic S., Robinson H., Tiemessen C.T., Margulies D.H. X-ray Crystallographic structures of murine cytomegalovirus MHC-I-like molecules reveal distinct modes of exploitation of the MHC-I fold. 94th Annual Meeting of The American Association of Immunologists, May 2007, Miami Beach, FL, USA. (Oral presentation)

Mans J., Natarajan K., Tiemessen C.T. and Margulies D.H. Insect cell expression and characterization of a mouse cytomegalovirus MHC class I homolog. NIH Graduate Student Research Symposium, May 5, 2006, Bethesda, MD, USA. (Poster presentation)

Mans J., Natarajan K., Tiemessen C.T. and Margulies D.H. MCMV encoded MHC-I like proteins that do not require β2m or peptide for cell surface expression. NK Hawaii - 9th Meeting of The Society for Natural Immunity, November 4-8, 2005, Poipu Beach, Kauai. (Poster presentation)

CONTENTS

ABSTRACT ii

DECLARATION vi

ACKNOWLEDGEMENTS vii

PUBLICATIONS AND PRESENTATIONS ix

CONTENTS xi

LIST OF TABLES xvi

LIST OF FIGURES xvii

LIST OF ABBREVIATIONS xx

CHAPTER 1

Literature Review

1.1 Introduction 1

1.2 The Herpesviridae 2

1.2.1 β-herpesvirinae 3

1.2.1.1 Human cytomegalovirus (HCMV) 3

1.2.1.2 Mouse cytomegalovirus (MCMV) 4

1.3 MCMV pathogenesis 6

1.3.1 Acute infection 6

1.3.2 Latency 7

1.4 The immune response to MCMV infection 8

1.4.1 Innate response....8
1.4.1.1 Dendritic cells....9
1.4.1.2 NK cells....11
1.4.2 Adaptive response....13
1.5 The *m145* gene family of MCMV....15
1.6 Interplay between MCMV and the host immune response....18
1.6.1 MCMV interference with NK cell activation....18
1.6.2 Manipulation of the MHC-I antigen presentation pathway by MCMV....19
1.6.3 Additional immune evasion mechanisms....23
1.7 Major Histocompatability Class I (MHC-I) molecules....23
1.8 MHC-I homologs encoded by human and murine CMVs....26
1.8.1 Homologs with significant amino acid sequence similarity....26
1.8.2 Distant viral homologs of MHC-I – Homology based on structural predictions....28
1.9 Aims of the study....29

CHAPTER 2

Materials and Methods

2.1 Cell lines....31
2.2 Mice....32
2.3 Antibodies....32
2.4 Vector constructs....32
2.4.1 Bacterial expression....33
2.4.2 Insect cell expression....33
2.4.3 Mammalian cell expression....34
2.4.3.1 FLAG-tagged constructs....34
2.4.3.2 m153-EYFP fusion construct....35
2.4.3.3 Bimolecular fluorescence complementation constructs....35
2.4.3.4 m144-human zeta and m153-human zeta fusion constructs....36
2.5 Transfection and FACS analysis of FLAG-tagged MCMV proteins....36

2.6 β2m and TAP-dependence....38
2.7 MCMV infection, cell surface staining and FACS....38
2.8 Bimolecular fluorescence complementation....39
2.9 Localization studies of m153....39
2.10 Immunoprecipitation and western blots....41
2.11 Bacterial expression in *E.coli* and refolding of proteins from inclusion bodies....42
2.12 *Drosophila* insect cell expression and purification of m153....44
2.13 Transient expression of wild type and mutant m153 in SF9 cells....45
2.14 Crystallization, structure determination and refinement....45
2.15 Analytical ultracentrifugation....47
2.16 Mass spectrometry....47
2.17 Retrovirus production and generation of reporter cell lines....48
2.18 Control antibody stimulation of reporter cell lines....49
2.19 Reporter cell coculture assays....50
2.20 Isolation of mouse or rat splenocytes....50
2.21 Isolation of different cell subsets from mouse or rat splenocytes....51
2.21.1 Dendritic cells (mouse - $CD11c^+$, rat – $OX62^+$)....51
2.21.2 Plasmacytoid dendritic cells....52
2.21.3 B cells, $CD11b^+$ cells, NK cells, $CD4^+$ and $CD8^+$ T cells....52
2.22 Generation of dendritic cells from mouse bone marrow cells....53
2.23 Cell-cell contact assay....53
2.24 Dendritic cell migration assay....54
2.25 DC surface phenotype analysis by FACS....55
2.26 Primer sequences....55

CHAPTER 3

Characterization and recombinant expression of predicted MHC-I-like proteins encoded by MCMV

3.1 Introduction....58
3.2 Results....60

3.2.1 Localization of MCMV MHC-I-like proteins in transfected cells.....60
3.2.2 Cell surface expression of M37, m145, m151 and m153 is independent of β2m and TAP expression.....62
3.2.3 Cell surface MHC-I levels are downregulated by m152 and to a lesser extent, by m153.....65
3.2.4 Optimization of recombinant expression of MCMV MHC-I homologs for structural characterization.....67
3.2.4.1 Expression in bacterial inclusion bodies.....67
3.2.4.2 Insect cell expression.....71
3.3 Discussion.....75

CHAPTER 4

Biochemical and cell biological characterization of MCMV m153

4.1 Introduction.....78
4.2 Results.....79
4.2.1 Localization of m153 in transfected NIH3T3 cells.....79
4.2.2 m153 is expressed on the surface of MCMV-infected fibroblasts.....83
4.2.3 Glycosylation of m153 in *Drosophila* S2 cells.....85
4.2.4 Recombinant m153 forms a stable, non-covalent dimer.....87
4.2.5 Full-length m153 is dimeric in mammalian cells.....90
4.3 Discussion.....92

CHAPTER 5

Crystal structure of the mouse cytomegalovirus glycoprotein, m153

5.1 Introduction.....94
5.2 Results.....96
5.2.1 The MHC-I fold of m153.....96

5.2.2 The m153 dimer 107
5.2.3 Comparison of m153 to the m145 family 113
5.3 Discussion 116

CHAPTER 6

Identification of spleen cell subpopulations that encode a putative ligand for MCMV m153

6.1 Introduction 120
6.2 Results 122
6.2.1 Generation of m153z_43.1 and m144z_43.1 reporter cell lines 122
6.2.2 Freshly isolated mouse splenocytes stimulate GFP production in 153z_43.1 cells 125
6.2.3 Generation of reporter cell lines 153z_43.1_H and 144z_43.1_H 129
6.2.4 Dendritic cells are the major population in mouse spleen that stimulates 153z_43.1_H reporter cells 131
6.2.5 Dendritic cells from a variety of mouse strains stimulate 153z_43.1_H reporter cells 138
6.2.6 Analysis of the surface phenotype and migration of $CD11c^+$ DCs after exposure to 153z_43.1_H reporter cells or plate-bound m153 140
6.3 Discussion 143

CHAPTER 7

Concluding Discussion 145

REFERENCES 151
LIST OF WEBSITES 166
APPENDIX A
Animal Ethics Clearance Certificate 167

LIST OF TABLES

Table number and title **Page**

2.1 Primer sequences 55-57

3.1 Predicted extracellular domains of the MCMV MHC-I homologs 68

3.2 Summary of expression of MCMV MHC-I homologs in bacterial inclusion bodies 69

3.3 Behavior of the MCMV proteins during the different steps of refolding 70

3.4 N-terminal sequence of M37, m151 and m153 that were expressed in insect cells 72

4.1 Analysis of glycosylation positions and content of recombinant m153 86

5.1 Data collection, refinement and validation statistics 97

5.2 Hinge angle between the $\alpha1\alpha2$ and $\alpha3$ domains of viral, MHC-Ia and MHC-Ib molecules.....106

LIST OF FIGURES

Figure number and title **Page**

1.1 Cartoon representation of the MCMV virion....4
1.2 Schematic representation of the MCMV genome....5
1.3 Multiple amino acid sequence alignment of the predicted MHC-I-like m145 family members and their homologs from the r145 family in RCMV 16-17
1.4 MCMV encoded glycoproteins downregulate ligands of the activating NK cell receptor NKG2D 19
1.5 Schematic representation of the interference with MHC-I trafficking in MCMV infected cells 21
1.6 Crystal structures of classical and non-classical MHC-I molecules....25
1.7 Structures of viral MHC-I homologs (MHC-Iv)....27

3.1 Cellular localization of MCMV MHC-I-like glycoproteins in transfected COS-7 cells 61
3.2 Surface expression of MCMV MHC-I-like proteins is independent of β2m 63
3.3 TAP-independent cell surface expression of M37, m145, m151 and m153....64
3.4 Effects of different m145 family members on MHC-I surface expression 65
3.5 Comparison of the MHC-I expression levels on the GFP-bright populations in m152-, m153- or vector control-transfected NIH3T3 cells 66
3.6 SDS-PAGE analysis of MCMV MHC-I-like proteins expressed in Rosetta DE3 *E.coli* 69
3.7 Size-exclusion chromatography of m151 after refolding from bacterial inclusion bodies 71
3.8 SDS-PAGE analysis of insect cell-expressed M37, m151 and m153 72
3.9 Size-exclusion chromatography of M37, m151 and m153 73
3.10 Anion-exchange chromatography of M37 and m153 74

4.1 Localization of m153 in transfected NIH3T3 cells....80
4.2 Punctate distribution of m153-EYFP fusion protein in transfected NIH3T3 cells...81
4.3 m153 expression in MCMV-infected cells....84
4.4 Recombinant m153, expressed in S2 insect cells, is glycosylated....85
4.5 m153 is a non-covalent dimer when expressed in S2 insect cells....87
4.6 SEDFIT analysis of m153 sedimentation velocity data....89
4.7 Sedimentation coefficient distribution *c(s)* derived from sedimentation velocity experiments at four different concentrations of m153....90
4.8 m153 forms a homodimer in mammalian cells....91

5.1 Ramachandran analysis of the m153 model with the Molprobity server....98
5.2 Conserved and unique features of the m153 monomer....100
5.3 Mass spectrum of a disulfide-linked tryptic peptide confirms the C16-C171 disulfide bond....102
5.4 Mass spectra of C*PVPQFNC*TITHR peptide before and after reduction with TCEP confirmed the C101-C108 disulfide bond....102
5.5 Comparison of m153 with m157, H-2K^b, Rae-1β and rat neonatal FcR....105
5.6 Overall structure of the m153 dimer....108
5.7 Dimer interface of m153....111
5.8 Mutations at the interface destabilize the m153 dimer....112
5.9 Amino acid sequence alignment of the m145 family....114
5.10 Conserved interaction between E70, R166 and W167 connects α1 and H2b helices....115

6.1 Infection of 43.1 reporter cells with GFP-, 153z- and 144z-retroviruses....123
6.2 Titration of mAb153.16 in a plate-bound 153z_43.1 stimulation assay....124
6.3 Antibody-specific triggering of GFP production in 43.1, 144z_43.1 and 153z_43.1 reporter cells....125
6.4 Mouse spleen cells stimulate GFP production in 153z_43.1 reporter cells....126

6.5 Dose response curve of spleen cell stimulation of 153z_43.1 reporter cells 127
6.6 Soluble m153 partially blocks stimulation of 153z_43.1 reporter cells by mouse splenocytes 127
6.7 $CD11c^+$ enriched spleen cells increases 153z_43.1 reporter cell stimulation 128
6.8 144z_43.1_H and 153z_43.1_H reporter cells 130
6.9 $CD11c^+$ cells are the most potent stimulators of 153z_43.1_H reporter cells 132
6.10 Comparison of 153z_43.1_H reporter cell stimulation by $CD11c^+$ DCs and $DX5^+$ NK cells 134
6.11 Plasmacytoid DC and bone marrow-derived $CD11c^+$ DC stimulate 153z_43.1_H reporter cells 135
6.12 The stimulation of 153z_43.1_H reporter cells by $CD11c^+$ cells is m153-specific and dose- and cell contact-dependent 137
6.13 Splenocytes and $CD11c^+$ cells from eight mouse strains stimulate 153z_43.1_H reporter cells 139
6.14 Rat $OX62^+$ dendritic cells do not stimulate the 153z_43.1_H reporter cells 140
6.15 $CD11c^+$ surface phenotype is not specifically affected by coculture with 153z_43.1_H cells 141
6.16 Migration of dendritic cells in response to MIP-3β (CCL19) is not affected by MCMV m153 142

LIST OF ABBREVIATIONS

3D-PSSM	Three-dimensional position-specific scoring matrix
AAALAC	Association for Assessment and Accreditation of Laboratory Animal Care
APC	Allophycocyanin
AUC	Analytical ultracentrifugation
B6	C57BL6
BiFC	Bimolecular fluorescence complementation
BM	Bone marrow
BSA	Bovine serum albumin
cDC	Conventional dendritic cell
cDNA	Complementary DNA
CID	Collision-induced dissociation
C-terminal	Carboxy-terminal
CTL	Cytotoxic T lymphocyte
DAPI	4',6-diamidino-2-phenylindole
DCs	Dendritic cells
DIC	Differential interference contrast
DMEM	Dulbecco's modified Eagle's medium
dsDNA	Double stranded deoxyribonucleic acid
DTT	Dithiothreitol
ECD	Electron capture dissociation
ECD	Extracellular domain
EDTA	Ethylenediaminetetraacetic acid
ER	Endoplasmic reticulum
ERGIC	ER-Golgi intermediate compartment
EYFP	Enhanced yellow fluorescent protein
FACS	Fluorescence activated cell sorting
FcRn	Neonatal Fc receptor
FCS	Fetal calf serum
FcγR	Fc gamma receptor

FT-MS/MS	Fourier transform – tandem mass spectrometry
FT-ICR	Fourier transform – ion cyclotron resonance
Fuc	Fucose
GFP	Green fluorescent protein
GM-CSF	Granulocyte macrophage colony-stimulating factor
GPI	Glycosyl-phosphatidylinositol
HA	Hemagglutinin
HCMV	Human cytomegalovirus
Hex	Hexose
HFE	Hemochromatosis gene product
HHV	Human herpes virus
HMA	Heteroduplex mobility assay
HPLC	High performance liquid chromatography
IE	Immediate early
Ig-like	Immunoglobulin-like
IPTG	Isopropyl-β,D-1-thiogalactopyranoside
IRES	Internal ribosome entry site
IRMPD	Infrared multi photon dissociation
kb	Kilobases
kDa	Kilodalton
LIR-1	Leukocyte immunoglobulin-like receptor 1
LPS	Lipopolysaccharide
m.o.i.	Multiplicity of infection
mAb	Monoclonal antibody
MCMV	Mouse cytomegalovirus
MHC-I	Major histocompatibility class I
MHC-Ia	Classical MHC-I
MHC-Ib	Non-classical MHC-I
MHC-II	Major histocompatibility class II
MHC-Iv	Viral major histocompatibility class I homolog
MICA	MHC-I related chain A

MM	Molecular mass markers
MME	Monomethyl ether
MULT-1	Murine UL16-binding protein-like transcript 1
Nac	N-acetyl
NCS	Non-crystallographic symmetry
NFAT	Nuclear factor of activated T cells
Ni-NTA	Nickel-nitrilotriacetic acid
NK	Natural killer
NKC	NK cell gene complex
NKG2D	NK group 2 member D
NKRP1	Natural killer receptor protein 1
N-linked	Asparagine-linked
NSLS	National Synchrotron Light Source
N-terminal	Amino-terminal
p.i.	Post infection
PBS	Phosphate buffered saline
PCR	Polymerase chain reaction
pDC	Plasmacytoid dendritic cell
PE	Phycoerythrin
PEG	Polyethylene glycol
PNGaseF	Peptide N-glycosidase F
Rae-1	Retinoic acid early inducible-1
RCMV	Rat cytomegalovirus
r.m.s.d.	Root mean square deviation
RNA	Ribonucleic acid
S2	Schneider 2
SAD	Single anomalous dispersion
SDS-PAGE	Sodium dodecyl sulfate polyacrylamide gel electrophoresis
SEC	Size exclusion chromatography
SeMet	Selenomethionine
SGV	Salivary gland-derived virus

SOE-PCR	Splicing by overlap extension PCR
TAP	Transporter associated with antigen processing
TBS	Tris buffered saline
TCEP	Tris-(2-carboxyethyl)-phosphine hydrochloride
TCR	T cell receptor
TCV	Tissue culture-derived virus
TLS	Translation, libration, screw
VIPRs	**V**iral proteins that **I**nterfere with antigen **Pr**esentation
VSV	Vesicular stomatitis virus
wt	Wild type
YFP	Yellow fluorescent protein
ZAG	Zn-alpha2-glycoprotein
β2m	Beta-2 microglobulin

CHAPTER 1

LITERATURE REVIEW

1.1 Introduction

Viruses follow one of two strategies to propagate themselves successfully and survive within the host population. In the first strategy, the infection is of short duration, the host cells are often killed as a consequence of the infection and the virus is easily transmitted to a series of successive hosts. In the second strategy, the virus establishes a long-term persistent infection in one host from which virus may spread at frequent or infrequent intervals to other hosts. Viruses with a small coding capacity, such as the RNA-viruses influenza or rhinovirus, adopt the first strategy and rely on high antigenic variation to escape the host immune response. Viruses that have larger DNA genomes, like the pox- or herpesviruses, follow the long-term strategy and often co-exist with their hosts for life. Larger genomes enable DNA viruses to encode numerous proteins that can interact with the host immune response and tip the balance in favor of the virus and result in the establishment of persistent infections. The main aim of persistent viruses is to avoid detection by the immune system. Viruses use many different mechanisms to achieve this goal. Some viruses, such as herpes simplex, hide from the immune system by infecting non-permissive cell types that act as reservoirs for their genetic material. Little or no transcription takes place until certain events reactivate the virus and allow for its replication and spread (Steiner et al., 1990). Other pathways of viral interference include blockade of antigen presentation, evasion of natural killer (NK) cell responses, disruption of normal cytokine signaling networks, inhibition of apoptosis in virus-

infected cells and evasion of antibody and complement responses (Finlay and McFadden, 2006; Tortorella et al., 2000). The herpesvirus family provides examples of virus-encoded proteins that target each of these different pathways.

1.2 The Herpesviridae

The herpesvirus family is divided into the alpha-, beta- and gamma-herpesvirinae. Historically the division was based on biological characteristics but more recent sequence-based phylogenetic analyses confirmed the major lineages (McGeoch et al., 1995). The DNA genomes range from 125-230 kb and encode 70-200 genes. All three subfamilies share a set of around 40 genes that have similar genomic positions and nucleotide sequences. The viruses share a common evolutionary origin and molecular phylogeny of the family suggests that the virus sublineages had developed by co-speciation with their hosts (McGeoch et al., 2006). Human pathogens are found in all three herpesvirus subfamilies. The α-herpesvirus HSV-1 causes cold sores, HSV-2 is the main cause of genital herpes, β-herpesviruses include the cytomegaloviruses and Epstein Barr virus and Kaposi's sarcoma-associated herpesvirus are γ-herpesviruses that are associated with the onset of several malignancies.

1.2.1 β-herpesvirinae

1.2.1.1 Human cytomegalovirus (HCMV)

The β-herpesvirus subfamily consists of human herpes virus (HHV)-6, HHV-7 and the cytomegaloviruses. These three groups have a similar genome organization and content. The cytomegaloviruses exhibit strict host-specificity and are characterized by a slow replication cycle and tropism to secretory glands and hematopoietic cells (Krmpotic et al., 2003). Cytomegaloviruses of many different species have been isolated. HCMV is the prototypic cytomegalovirus and derives its name from the characteristic enlargement of CMV-infected cells. Antibodies to HCMV can be detected in 50% to 90% of individuals and prevalence of the infection is linked to the socio-economic status of the population (Sissons et al., 2002). In healthy individuals the virus causes no clinical disease but infection of the immunocompromised host (transplant recipients, AIDS patients, neonates) can lead to serious and even fatal disease. Annually between 1% and 3% of infants in the United States are affected by congenital CMV infection that causes mortality and permanent disabilities (Pereira et al., 2006). Development of a vaccine to prevent congenital CMV infection is therefore a high priority. Immunocompromised individuals that suffer from HCMV disease benefit from anti-viral treatment with several nucleoside analogs that target the viral polymerase. The available drugs however, have poor oral bioavailability and toxic side effects, and development of improved drugs and identification of novel drug targets is needed.

The strict host specificity of HCMV has complicated the study of its pathogenesis. Several rodent models have been utilized (mouse (Simon et al., 2006), rat (Kaptein et al., 2006) and guinea pig (Schleiss and Lacayo, 2006)) and more recently non-human primates (chimpanzee and rhesus macaque (Britt, 2006)), the results of the latter would presumably be easier to translate to the human disease than findings from the rodent models. However, the rodent models will probably still be widely used because the primate models have disadvantages such as high cost and ethical considerations.

1.2.1.2 Mouse cytomegalovirus (MCMV)

MCMV causes acute, persistent and latent infection in mice (Sweet, 1999). The dsDNA genome of MCMV is 230 kb and encodes at least 170 genes. The MCMV virion consists of three major layers (Figure 1.1). The genome is surrounded by an icosahedral capsid. The tegument, a proteinaceous layer, covers the capsid and a host-derived lipid bilayer forms the envelope. Viral glycoproteins are found in the envelope and they act as receptors that facilitate virus entry into cells.

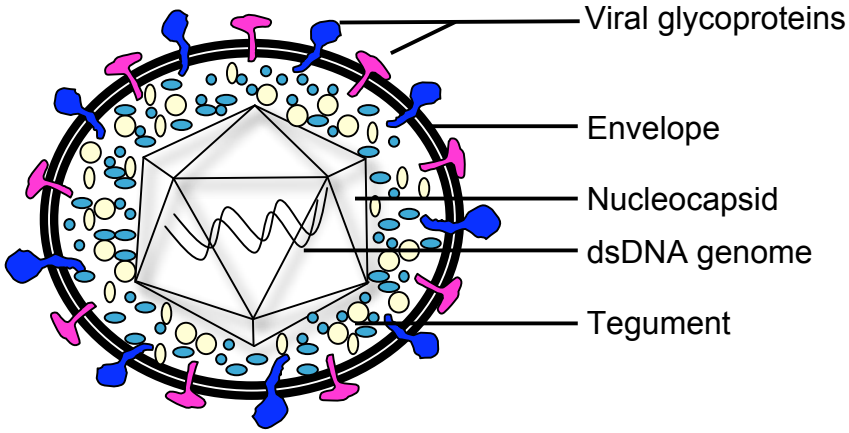

Figure 1.1. Cartoon representation of the MCMV virion.

The organization of the MCMV genome is such that the central genomic region encodes the genes essential for virus replication, which tend to be conserved among the CMVs of different species. The terminal genomic regions are more divergent and encode genes whose products are involved in immune evasion and are generally dispensable for virus growth *in vitro* (Figure 1.2).

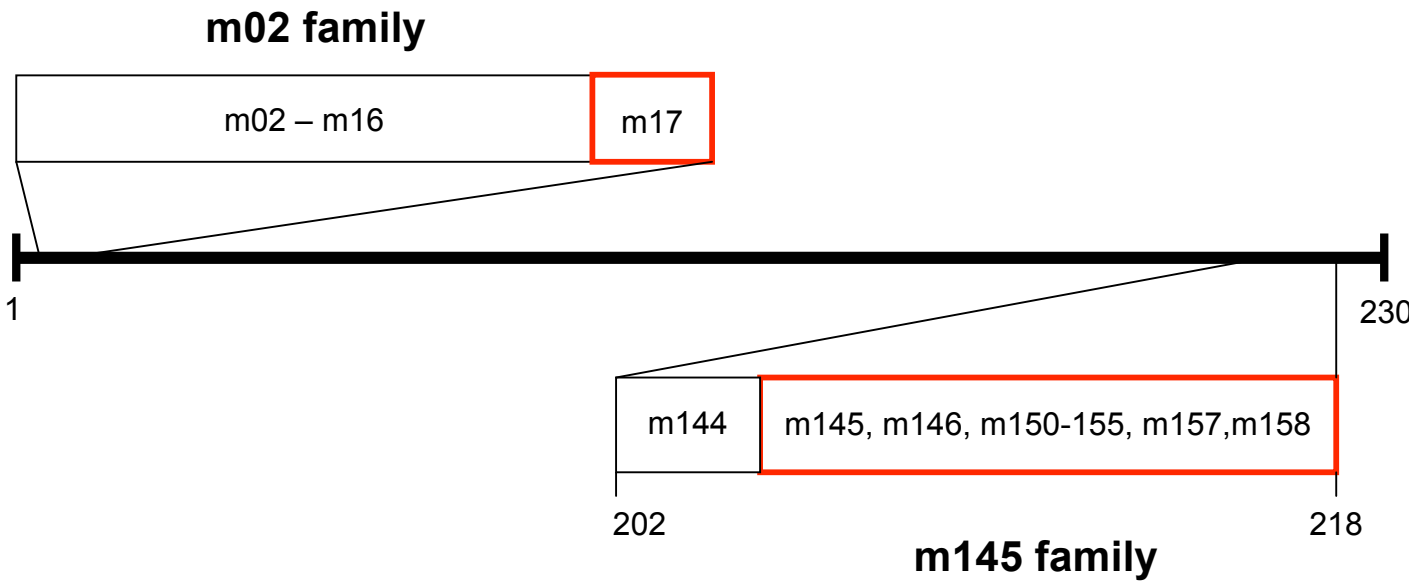

Figure 1.2. Schematic representation of the MCMV genome. Genes encoded in the central region of the genome are conserved between different herpesviruses and are often essential for virus replication. Genes found at the terminal regions of the genome are less conserved and contribute to immune evasion. Two of the best-studied immunoevasin families of MCMV are highlighted. The majority of the predicted MCMV MHC-I homologs are found within the m145 glycoprotein family. Positions in the genome are indicated in kb.

MCMV genes can be divided into three classes, α, β, and γ, based on the timing of their expression. The genes are expressed at immediate early (IE), delayed early (E) and late (L) stages of the replication cycle in infected cells. After virus entry into the host cells, IE transcription occurs independent of *de novo* viral protein synthesis. A second E phase then follows but the expression of these genes is dependent on the prior expression of one or more IE genes which transactivate E promoters. The L phase of expression begins

with the onset of virion DNA replication and viral structural proteins are then synthesized (Sweet, 1999).

1.3 MCMV pathogenesis

1.3.1 Acute infection

Natural transmission of MCMV is most likely through contact with saliva from infected animals. The routes by which the virus enters the host have not been clearly established. It has been shown that newborn mice can be infected via the oral route and that the virus spread is similar to that observed after intraperitoneal inoculation (Krmpotic et al., 2003), therefore it is likely that the virus enters the host via the upper respiratory and gastrointestinal tracts. Sexual transmission of MCMV could also be an important type of horizontal transmission (Krmpotic et al., 2003). Virus dissemination after intraperitoneal inoculation has been characterized well. Initially the virus replicates in macrophages and mesothelial cells that line the peritoneal cavity. From these sites the virus is spread by large mononuclear phagocytes to the spleen, liver and various other organs (Stoddart et al., 1994). MCMV can infect various cell types including different types of epithelial cells (glandular epithelial cells of the salivary gland, hepatocytes), endothelial cells, dendritic cells and tissue macrophages. In the spleen MCMV preferentially targets endothelial cells of the splenic stroma and induces changes in the microarchitecture of the spleen (Benedict et al., 2006).

In immunocompetent mice acute MCMV infection is usually controlled, whereafter a life-long persistent infection is established that is characterized by periods of latency and reactivation. The type of disease caused by MCMV infection in laboratory mouse models is highly dependent on the source of infectious virus (tissue culture-derived (TCV) or salivary gland extract-derived (SGV)), route and dose of inoculation, age and strain of mouse as well as the immune status of the animal. Infection of day-old BALB/c mice leads to ~ 40% mortality in the third week post infection with virus replication detectable in several organs. Survivors display growth retardation until they are 4-6 weeks of age. At this time virus replication is restricted to the salivary glands, where the virus persists for 4-6 months. After 6 months the infection becomes latent. In contrast, MCMV infection in adult immunocompetent mice does not cause mortality, significant organ damage is not observed and virus replication seems to be confined mostly to the salivary glands. After about two months the infection in the salivary glands is cleared and a latent infection is established (Reddehase et al., 1994). Disease manifestations in immunodeficient mice include interstitial pneumonia (Reddehase et al., 1985), adrenal necrosis (Reynolds et al., 1993; Shanley and Pesanti, 1986), bone-marrow aplasia (Mutter et al., 1988) and retinitis (Zhang and Atherton, 2002). These all correlate with clinical manifestations of HCMV infection in immunocompromised humans (Vancikova and Dvorak, 2001).

1.3.2 Latency

The mechanisms by which the MCMV genome enters into and is maintained in the latent state are not well understood. Latency is defined as a persistent infection in which the viral genome is present but gene expression is limited and infectious virus is not

produced (Roizman and Sears, 1987). In mice, several organs (liver, kidney, heart, lungs, spleen, adrenal and salivary glands) as well as whole blood have been shown to be sites of latent MCMV infection (Reddehase et al., 2002). The lungs are a major site of latency in the mouse and have an up to 10-fold higher burden of viral DNA than other tissues (Balthesen et al., 1993). Stromal and / or parenchymal cells are sites of MCMV latency in most organs. In addition endothelial cells, lung alveolar macrophages and bone marrow cells have been shown to contain MCMV DNA during latency (Koffron et al., 1998). Reactivation of MCMV from latency occurs *in vitro* in tissue explants (Jordan and Mar, 1982) and *in vivo* when latently infected mice are immunosuppressed (Balthesen et al., 1993). The reactivated virus replicates in salivary gland epithelial cells and recurring and persistent shedding from the salivary gland can be detected.

1.4 The immune response to MCMV infection

1.4.1 Innate response

The innate immune response coordinates the initial attack on invading pathogens, containing viral infections until the adaptive response is generated and able to clear the infection. Cells such as dendritic cells, macrophages and NK cells combine forces to limit CMV infection. IFN-α/β cytokines are produced early after MCMV infection. They are crucial in establishing an antiviral state and are required for the survival of the host (Dalod et al., 2002). A specialized subset of dendritic cells, the plasmacytoid DCs, are the main producers of IFN-α/β (Dalod et al., 2003) in response to MCMV infection. It seems that IFN-α/β cytokines play a central role in regulating both innate and adaptive immune responses to MCMV challenge. Apart from the induction of an antiviral state,

IFN-α/β induce NK cell cytotoxicity and they control the maturation and cytokine production of the various dendritic cell subsets, thereby indirectly contributing to CD8 T cell activation (Dalod et al., 2003).

1.4.1.1 Dendritic cells

Dendritic cells (DCs) are a heterogeneous group of cells of hematopoietic origin. They occur at a low frequency and are found throughout the peripheral tissues, primary and secondary lymphoid organs, and are specialized to capture, process and present antigens to naïve T cells. In the classical description of DCs, peripheral DCs are in an immature state, which is characterized by low surface levels of MHC class II and co-stimulatory molecules, and the cells are highly efficient in antigen uptake and processing. Upon encounter with foreign antigen or upon entering a milieu rich in pro-inflammatory cytokines, these cells undergo phenotypic changes and migrate to the lymph nodes where they interact with naïve or resting T cells and initiate an immune response (Banchereau et al., 2000). More recently, studies in mice have revealed that most of the DCs in the spleen and thymus and about half of the lymph-node DCs develop from bone-marrow precursor cells within the lymphoid organs and do not traffic throughout the peripheral tissues (Villadangos and Heath, 2005). Therefore not all DCs follow the classical pathway.

The nomenclature of mouse DC subtypes in the literature varies. In a recent review it was suggested that DCs should be divided into conventional DCs (cDCs), which already have a dendritic form and function, and precursors of DCs (pre-DCs), cells that require further development to acquire full DC function and the typical dendritic form

(Shortman and Naik, 2007). The conventional DCs are subdivided into migratory and resident cells. The migratory cDCs include interstitial DCs and Langerhans cells that migrate from the dermis and epidermis, respectively, to subcutaneous lymph nodes. Three different types of resident cDCs can be distinguished based on their expression of CD4 and CD8: $CD4^+$, $CD8^+$ and double negative (i.e. $CD4^-CD8^-$) DCs. Plasmacytoid dendritic cells (pDC), also known as natural interferon-producing cells, are a type of pre-DC. The pDCs circulate as spherical cells, have a relatively long life span and produce large amounts of type I interferons in response to viral and bacterial stimulation. They acquire a dendritic shape and an enhanced ability to take up and present antigen after activation.

Both cDC and pDC play pivotal roles in orchestrating the immune response to virus infection. Several groups have shown that DCs can be infected by HCMV and MCMV (Andrews et al., 2001; Jahn et al., 1999; Mathys et al., 2003; Moutaftsi et al., 2002; Raftery et al., 2001), but the reports differed on the effects of CMV infection on the surface phenotype and T cell priming activity of infected DC. The most recent study by Mathys and colleagues (Mathys et al., 2003) revealed that although both immature and mature DC are permissive to MCMV infection, only immature DC support virus replication. They further showed that the expression of MHC class I, class II, CD40, CD80 and CD86 increased during early times after MCMV infection of immature and mature DC, but at 48 h after infection these surface molecules were significantly downregulated from the cell surface. The viral Fc receptor, m138, was subsequently identified as the molecule responsible for the downregulation of CD80 from the surface of infected DC (Mintern et al., 2006).

Infected DC were able to prime autologous naïve T cells against MCMV at early times after infection. By 48 h after infection however, the DC were unable to prime T cells, consistent with the marked downregulation of MHC and costimulatory molecules from the cell surface (Mathys et al., 2003). Thus MCMV infection induces the activation of DC and first initiates and then restricts T cell activation. It has been proposed that productive infection of immature DC, which will migrate upon activation, could aid the dissemination of the virus (Mathys et al., 2003).

1.4.1.2 NK cells

Patients that lack NK cells suffer from severe HCMV infections (Biron et al., 1989) and mice that have been depleted of NK cells or genetically lack NK cells are also highly susceptible to MCMV infection. Furthermore, adoptive transfer of NK cells can prevent MCMV disease in both adult and newborn mice (Bukowski et al., 1985; Bukowski et al., 1988). Therefore NK cells must play an important role in the innate immune response to MCMV. As mentioned earlier, the genetic makeup of a mouse strain has a profound effect on susceptibility to MCMV infection. Mice can be divided into susceptible (e.g. BALB/c) or resistant strains (e.g. C57BL/6 (B6)) based on their ability to control MCMV replication at early times after infection. Studies in the early eighties indicated that there are both MHC- (H2) as well as non-H2 loci that confer resistance to MCMV infection (Grundy and Melief, 1982; Grundy et al., 1982). The non-H2 loci were identified in the B6, C3H and CBA mouse strains. The *Cmv1* resistance locus was identified by analysis of the genetic basis of the differences in MCMV susceptibility of BALB/c and B6 mice. The locus was subsequently mapped to the NK cell gene complex (NKC) on mouse chromosome 6. The NKC region encodes both activating and

inhibitory NK cell receptors. By further genetic and physical mapping studies *Cmv1* was identified as *Ly49h* (*Klra8*) (Forbes et al., 1997; Lee et al., 2003).

Ly49h encodes a lectin-like activating NK cell receptor, which is expressed on approximately 50% of B6 NK cells (Smith et al., 2000). The viral ligand that binds Ly49H and activates B6 NK cells was identified as m157, which is a member of the m145 glycoprotein family encoded by MCMV (Arase et al., 2002; Smith et al., 2002). B6 mice are thus resistant to MCMV infection because m157 engages the activating receptor Ly49H and this interaction leads to the activation and expansion of $Ly49H^+$ NK cells and clearance of virus-infected cells. It does not make sense for the virus to encode a ligand for activating NK cell receptors. However, m157 was also shown to bind Ly49I, which is an inhibitory NK cell receptor expressed in the 129/J strain (Arase et al., 2002; Smith et al., 2002). Therefore the more logical function of m157 would be to engage inhibitory receptors. Notably, in an experiment where MCMV was serially passaged through resistant B6 ($Ly49H^+$) mice, several virus clones could be isolated that contained mutations in the *m157* gene. The mutations all prevented the expression of m157 or its binding to Ly49H (Voigt et al., 2003). These results indicate that the virus quickly adapts under selective pressure from the host innate immune system.

Recently it was shown that early control of MCMV replication by NK cells attenuates the IFNα/β response by pDCs. Thus, rapid control of MCMV prevents IFNα/β-related immunosuppressive effects and enables earlier development of an effective $CD8^+$ T cell response (Robbins et al., 2007). Mice that are deficient only in the adaptive immune response but have normal NK cells can limit early MCMV replication, but they cannot sustain virus control and eventually succumb to disseminated viral infection. Thus NK

cells play an important role during the initial stages of infection but the adaptive response is essential for resolution of the infection.

1.4.2 Adaptive response

The first studies implicating T cell subsets in the protective response to MCMV infection utilized adoptive transfer of T cells. T lymphocytes, obtained from the draining lymph nodes of MCMV-infected immunocompetent mice, were transferred into syngeneic sublethally irradiated mice either 2 h prior to infection or 6 days after infection of the recipients. Both prophylactic and therapeutic T cell transfers were able to prevent mortality (Reddehase et al., 1985). Furthermore it was shown that the $CD8^+$ T cell subset is protective and that $CD4^+$ T cells are not required to prevent mortality. This kind of preemptive $CD8^+$ T cell immunotherapy has been applied successfully to immunosuppressed patients after bone marrow transplantation (Riddell et al., 1992).
Although $CD4^+$ T cells are not essential to prevent death, mice depleted of $CD4^+$ T cells were unable to eliminate virus production in the salivary glands even though large numbers of $CD8^+$ T cells had infiltrated the salivary glands (Jonjic et al., 1989). Antibodies are not crucial to the resolution of MCMV infection, since B-cell deficient mice clear primary infection and establish latency with the same kinetics as wild type mice (Jonjic et al., 1994). It can be concluded that $CD8^+$ T cells represent the major protective part of the adaptive immune response to MCMV but that $CD4^+$ T cells are necessary for the elimination of virus from the salivary glands. The salivary gland is the site of persistent infection and virus shedding, therefore $CD4^+$ T cells are important in preventing horizontal transmission of MCMV.

In the B cell-deficient mouse model of MCMV latency, it has been shown that stringent immune surveillance, rather than cell intrinsic factors, maintains the CMV genome in the latent state. In latently infected mice, stepwise or combined depletion of NK cells or different T cell subsets, is followed by productive virus replication, indicating that the virus frequently initiates productive replication cycles that are kept in check by the immune response. Antibodies to MCMV seem to play a protective role when reactivation from latency occurs, since mice devoid of B cells and antibodies develop higher MCMV titers when NK and T cells are depleted and reactivation takes place (Polic et al., 1998).

In conclusion, the immune response to MCMV infection is a complex process involving many different innate and adaptive cytokines and cell types and may vary in different organs and during the different stages of virus infection.

1.5 The *m145* gene family of MCMV

The genome sequence of the Smith strain of MCMV was determined by Rawlinson and colleagues (Rawlinson et al., 1996). The authors grouped eleven putative transmembrane glycoproteins together in the m145 family (m17, m145, m146, m150-155, m157, m158). Ten genes are found towards the right end of the genome arranged in tandem on the complementary strand. One family member, m17 lies at the opposite end of the genome adjacent to the m02 glycoprotein family (see Figure 1.2). All genes contain putative signal peptides, transmembrane regions and potential N-linked glycosylation sites, except for m157, which is predicted to be glycophosphatidylinositol (GPI)-linked. A homologous but expanded family is encoded by the rat CMV (RCMV), however all members of the mouse m145 family are not conserved. Rat homologs with both sequence and positional homology are *r145, r150, r151, r152, r155* and *r157* (Vink et al., 2000). An interesting feature of the mouse m145 family is that eight members are predicted to adopt an MHC-I-like fold despite no significant sequence similarity to MHC-I molecules (Smith et al., 2002). A multiple alignment of the predicted MHC-I-like m145 proteins and their rat homologs (including signal peptide, transmembrane and intracellular domains) is shown in Figure 1.3. The viral proteins share low levels of amino acid similarity (7-28%) and there are very few amino acid residues conserved in all family members. The predicted extracellular regions of the proteins are most similar, whereas the N-terminal and C-terminal (predicted intracellular domain) regions show very little conservation. A number of cysteine residues, which are presumably involved in disulfide bonds, are conserved. Several important immune evasion functions of MCMV are attributed to members of the m145 family. These will be discussed in the following section.

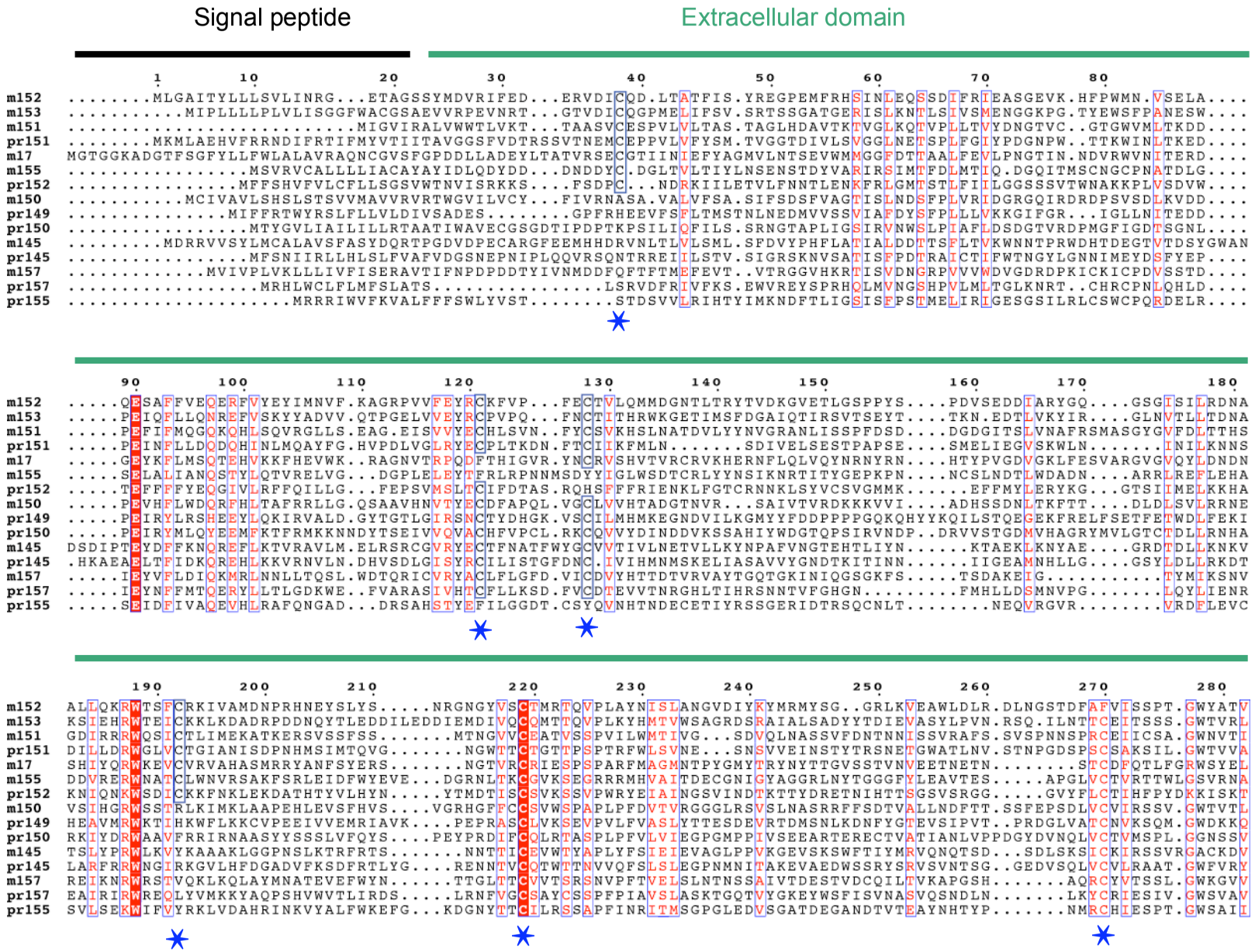
Signal peptide
Extracellular domain
m152
m153
m151
pr151
m17
m155
pr152
m150
pr149
pr150
m145
pr145
m157
pr157
pr155

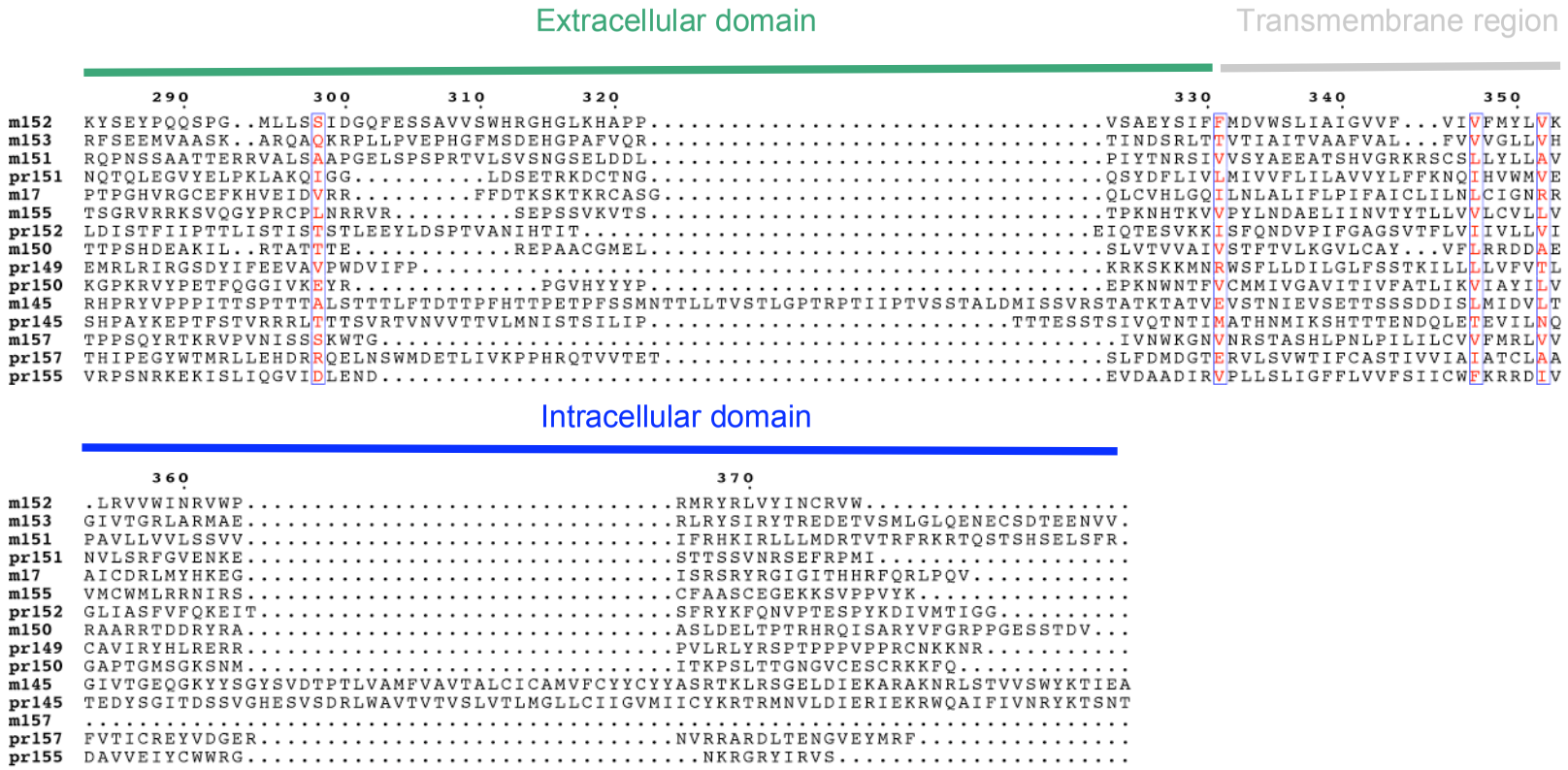

Figure 1.3. Multiple amino acid sequence alignment of the predicted MHC-I-like m145 family members and their homologs from the r145 family in RCMV. The full-length proteins were aligned. The approximate signal peptide region, extracellular domain, transmembrane region and intracellular domains are indicated. Risler amino acid similarity scoring was used (Risler et al., 1988). Similar residues are colored red, and identical residues white on a red background. The positions of conserved cysteines are indicated by blue stars.

1.6 Interplay between MCMV and the host immune response

A wide variety of immune evasion strategies have been described for MCMV. Notably, the virus has evolved multiple proteins that interfere with the activation of NK cells and subvert antigen presentation (Lodoen and Lanier, 2005; Pinto and Hill, 2005).

1.6.1 MCMV interference with NK cell activation

Four members of the m145 family of MCMV interfere with the NK cell response. m145, m152 and m155 have all been shown to downregulate distinct ligands of the activating NK cell receptor NKG2D. m145 targets MULT-1 (murine UL-16 binding protein-like transcript 1), m152 affects the Rae-1 family of ligands and m155 is specific for H60 (Figure 1.4, (Hasan et al., 2005; Krmpotic et al., 2005; Lodoen et al., 2003; Lodoen et al., 2004)). Rae-1 (α, β, γ, δ, ε isoforms), H60 and MULT-1 are NKG2D ligands that are induced in cells subjected to stress, cancerous transformation or virus infection (Cerwenka and Lanier, 2003). Whether the viral proteins directly interact with the NKG2D ligands or effect their retention/degradation in an indirect way is not yet known. Rae-1, H60 and MULT-1 are related to MHC-I in structure, but consist of only the α1 and α2 domains of classical MHC-I and lack the Ig-like α3 domain (see section 1.8). MCMV m157 was the first viral ligand to be identified for an activating NK cell receptor (Arase et al., 2002; Smith et al., 2002). The interaction of m157 with activating and inhibitory receptors of the Ly49 lectin-like NK cell receptors was discussed in detail in the preceding section on the innate immune response to MCMV. Another MCMV encoded protein interferes with NKG2D ligand expression. The viral Fc receptor (fcr-1) encoded by the *m138* gene was recently shown to reduce the surface expression levels of

H60 and MULT-1 in MCMV-infected cells (Lenac et al., 2006). The study revealed that fcr-1 uses distinct domains and possibly different mechanisms to downregulate H60 and MULT-1.

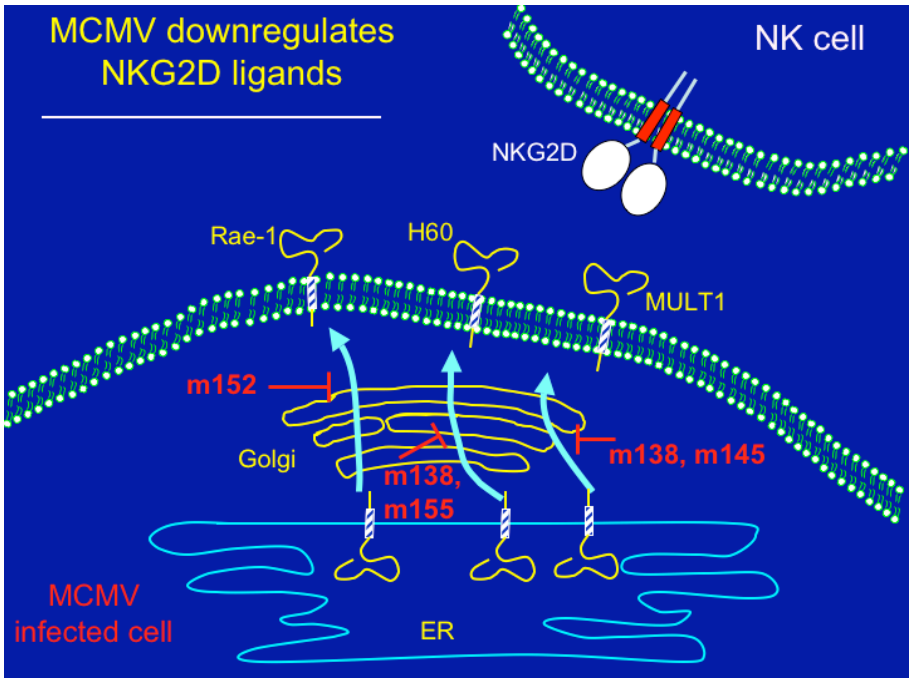

Figure 1.4. MCMV encoded glycoproteins downregulate ligands of the activating NK cell receptor NKG2D. m138 interferes with surface expression of H60 and MULT-1, m145 targets MULT-1, m152 retains members of the Rae-1 ligand family and m155 affects H60 cell surface expression.

1.6.2 Manipulation of the MHC-I antigen presentation pathway by MCMV

MCMV encodes three different proteins that target antigen presentation by MHC class I molecules (Figure 1.5). They were named VIPRs -**V**iral proteins that **I**nterfere with antigen **Pr**esentation- to distinguish them from other immunoevasins. The *m04* and *m06* genes encode gp34 and gp48 respectively and they affect MHC-I trafficking in different ways. The *m152* gene encodes the gp40 glycoprotein and has a dual function. In addition to the downregulation of Rae-1, which was described in the preceding section, m152

reduces MHC-I surface expression. The VIPRs all use different mechanisms to regulate MHC-I. m04/gp34 associates with MHC-I in the ER and these complexes are transported to the cell surface where the proteins remain associated (Kleijnen et al., 1997). m06/gp48 redirects MHC-I molecules to lysosomes, where they are subsequently degraded. m06/gp48 has a di-leucine motif in its cytoplasmic tail that facilitates binding to adaptor proteins AP-1A and AP-3A and sorting into the lysosomal pathway. Both *m04* and *m06* belong to the *m02* gene family of MCMV. Other *m02* family members have not been characterized functionally. m152, which is part of the m145 family, was the first MCMV VIPR to be described (Krmpotic et al., 1999). Initial observations showed that an MHC-I presented epitope derived from the IE protein pp89 was presented during immediate early MCMV gene expression but not when early genes were expressed (Del Val et al., 1989; Reddehase et al., 1989). Further studies revealed that the virus blocks antigen presentation by retaining the tri-molecular MHC-I complex (heavy chain, β2-microglobulin and peptide) in the ER/cis-Golgi compartment (del Val et al., 1992). The region affecting MHC-I transport was mapped to the *Hin*dIII E fragment of the viral genome (Thale et al., 1995), and *m152* was identified as the gene responsible for MHC-I downregulation (Ziegler et al., 1997). The luminal domain of m152 was implicated in catalyzing the retention of MHC-I molecules (Ziegler et al., 2000). There is no evidence of a stable m152/MHC-I interaction and the exact mechanism of retention remains a mystery.

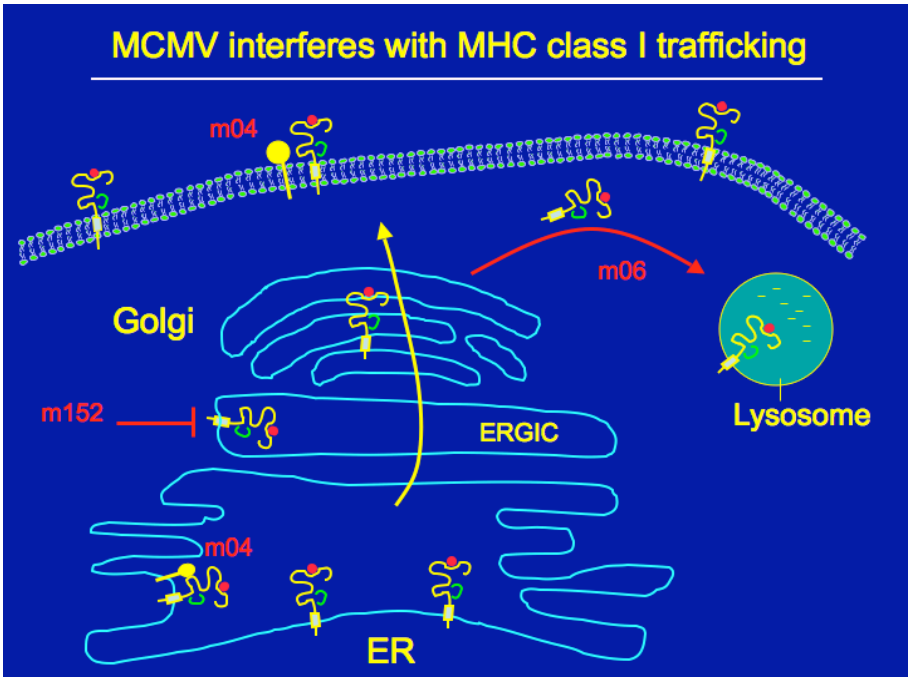

Figure 1.5. **Schematic representation of the interference with MHC-I trafficking in MCMV infected cells.** m04 associates with MHC-I and the complex is transported to the cell surface. m06 reroutes MHC-I molecules from the secretory pathway into lysosomes for their degradation. m152 catalyzes the retention of MHC-I in the ER Golgi Intermediate Compartment (ERGIC).

The biological consequences of the concerted action of m04, m06 and m152 are not well understood. A complex picture has emerged from studies utilizing viruses that have had individual or combinations of immunoevasins deleted. All three viral genes exhibit different efficiencies in targeting different MHC-I alleles (Pinto et al., 2006). Early studies indicated that m04 could inhibit CTL lysis of MCMV infected cells (Kavanagh et al., 2001). It was proposed that m04 prevents the T cell receptor (TCR) from recognizing MHC-I, thereby reducing CTL activity. m04 was thus considered a negative regulator of antigen presentation (Lilley and Ploegh, 2005). More recently, a comprehensive analysis of the effect of m04 on antigen presentation both *in vitro* and *in vivo* was undertaken (Holtappels et al., 2006). These experiments provided important new insight, namely that m04 instead acts as a positive regulator of antigen presentation. Cells that were infected

with a mutant MCMV, in which m04 and m06 were deleted, successfully evaded CTL stimulation and lysis. Thus, m152 expression is sufficient to block antigen presentation and evade CTL attack. However, when m04 was expressed in combination with m152, the infected cells became susceptible to CTL lysis, suggesting that m04 restores antigen presentation by escorting MHC-I to the cell surface. Wild type MCMV-infected cells, where m04, m06 and m152 are expressed in combination, were able to evade CTL responses. Therefore, m06 counters the positive effect of m04 and allows escape from immune recognition (Holtappels et al., 2006).

It was assumed that VIPR function was essential for MCMV to establish persistent infection in mice. However, a deletion mutant for m04, m06 and m152 did not differ in its ability to establish acute, persistent and latent infection in adult B6 mice. Furthermore, the size and effector memory phenotype of the $CD8^+$ T cell response elicited after infection with the triple mutant virus was comparable to the response against wild type virus (Gold et al., 2004). As mentioned before, MCMV infection in salivary gland acinar epithelial cells cannot be controlled by $CD8^+$ T cells and is only cleared by $CD4^+$ T cells. The effect of deleting all three VIPRs on virus replication in the salivary gland was recently tested. Mice infected with the m04+m06+m152 knockout virus had 10-fold lower salivary gland titers than mice infected with wt MCMV. The virus titers could be restored to the levels reached in a wt MCMV infection by depleting $CD8^+$ T cells (Lu et al., 2006). Taken together, it seems that the MCMV VIPRs affect antigen presentation to $CD8^+$ T cells in the salivary gland epithelial cells and may be important to sustain virus production in the salivary glands and promote transmission to new hosts.

1.6.3 Additional immune evasion mechanisms

Early after infection with MCMV, IL-10 is prematurely and transiently activated. This causes substantial downregulation of MHC class II molecules from the cell surface from infected macrophages and prevents antigen presentation to $CD4^+$ T cells (Redpath et al., 1999). MCMV further encodes two molecules that influence chemokine function during infection. MCK-2, a CC chemokine homolog, promotes dissemination of the virus to the salivary glands (Fleming et al., 1999) and M33, a viral chemokine receptor, has been shown to be very important for successful virus replication in the salivary glands (Davis-Poynter et al., 1997). MCMV can infect dendritic cells and encodes the modB7-2 protein that selectively downregulates CD86 in antigen presenting cells (Loewendorf et al., 2004). Other viral products that modulate the complement pathway (Nomura et al., 2002) and prevent apoptosis in infected cells have also been described (Menard et al., 2003).

1.7 Major Histocompatability Class I (MHC-I) molecules

MHC-I molecules are type I transmembrane cell surface receptors that are expressed on most cell types and consist of a heavy chain, a β2-microglobulin (β2m) light chain, and peptides of 8-10 residues (Figure 1.6). They are poised for recognition by clonotypic αβ receptors on $CD8^+$ T cells or by inhibitory or activating receptors on NK cells. MHC-I are classified as classical (Ia) or non-classical (Ib) molecules based on their amino acid sequence polymorphism, function, and tissue-specific expression. The heavy chain consists of an α1α2 domain unit containing two α-helices set atop an eight-stranded β-sheet platform and an Ig-like α3 domain (Figure 1.6A) (Bjorkman and Parham, 1990).

The peptide-binding groove is formed by the α1 and α2 helices (Figure 1.6B). β2m associates with the heavy chain below the platform domain adjacent to the α3 domain. Two conserved disulfide bonds stabilize the heavy chain, one bond is found in the α1α2 domain (strand β5 - α2 helix) and the second bond links the B and G strands of the Ig-like α3 domain. MHC-Ib molecules exhibit less polymorphism than the classical molecules, most do not bind peptide, and they vary in their association with β2m (Natarajan et al., 1999). MHC-Ib proteins function both in immune recognition and in other physiological settings (Margulies et al., 2007). The Rae-1 family of stress-induced molecules are examples of MHC-Ib proteins that are expressed in mouse cells. In humans, MICA and MICB molecules are induced by stress signals and they are also non-classical MHC-I proteins. These molecules act as ligands for the activating NK cell receptor NKG2D. The structures of Rae-1β and MICA have been determined (Li et al., 2002; Li et al., 2001). These molecules do not bind peptide, Rae-1β is truncated with no α3 domain (Figure 1.6C) and MICA consists of a full-length heavy chain but does not associate with β2m (Figure 1.6D).

Figure 1.6. Crystal structures of classical and non-classical MHC-I molecules. A) Structure of the classical MHC-I molecule H-2K^b in complex with a peptide derived from the VSV nucleoprotein (Fremont et al., 1992). Ribbon diagram of MHC heavy chain (*cyan*) α1, α2 and α3 domains, β2m (*magenta)* and peptide (*red*). B) Top view of the peptide binding groove. Disulfide bonds are shown in *yellow*. C) Rae-1β, an example of an MHC-I-like protein that consists only of the α1α2 domain (Li et al., 2002). D) MICA, a non-classical MHC-I protein that has the α1α2 and α3 domains, but does not associate with peptide or β2m and displays an unusually large angle between the α1α2 and α3 domains (Li et al., 2001).

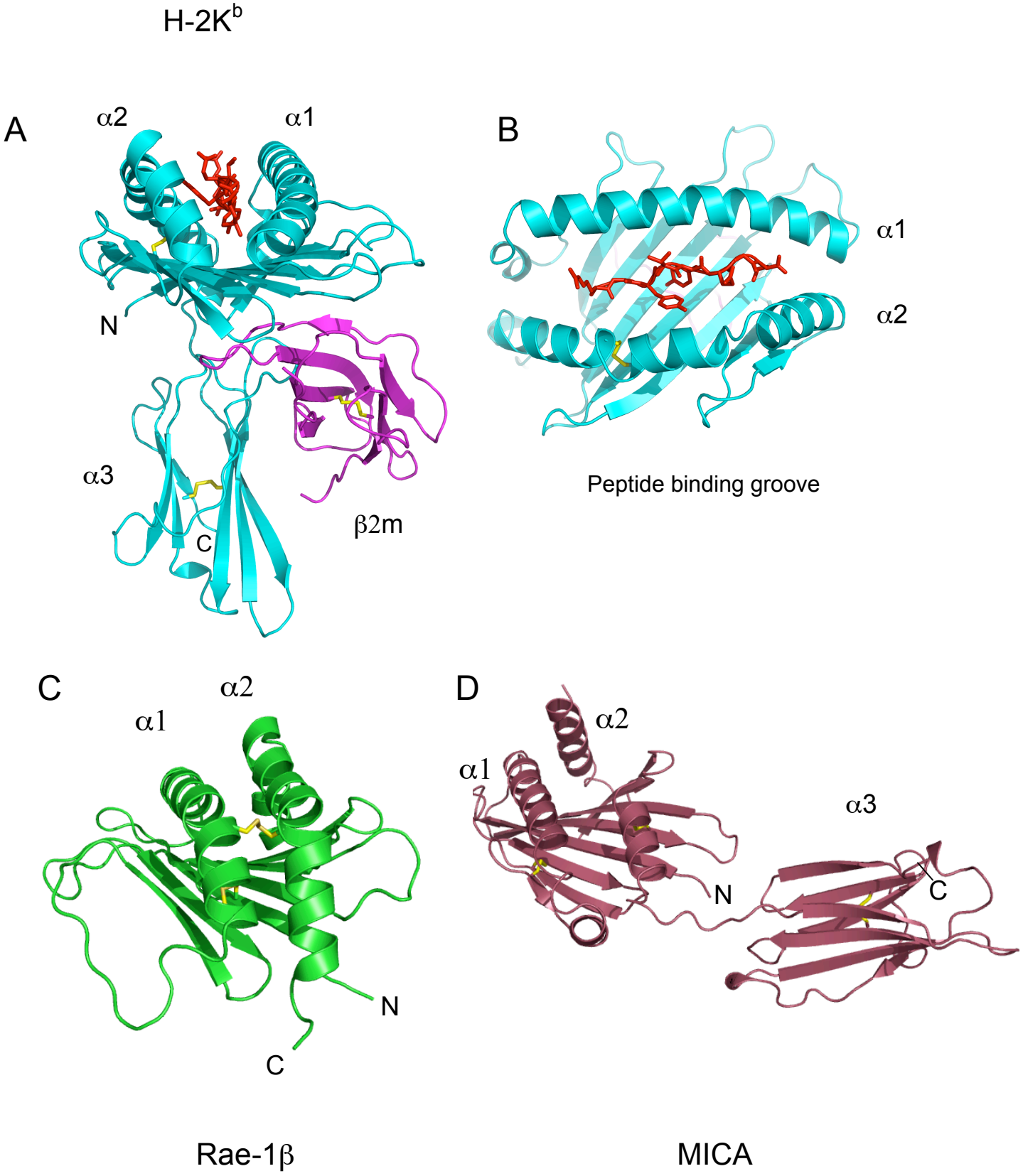
H-2K^b
A
α2
α1
N
α3
C
β2m
B
α1
α2
Peptide binding groove
C
α2
α1
N
C
Rae-1β
D
α2
α1
α3
N
C
MICA

Figure 1.6.

1.8 MHC-I homologs encoded by human and murine CMVs

1.8.1 Homologs with significant amino acid sequence similarity

HCMV encodes two different MHC-I homologs. UL18 shares 25% identity and 40% similarity with classical MHC-I molecules and it associates with β2m and peptide (Figure 1.7A). UL18 is a ligand for the leukocyte Ig-like receptor 1 (LIR-1) (Cosman et al., 1997), an inhibitory receptor that is expressed on some NK cells, T cells, dendritic cells, monocytes and B cells. LIR-1 binds to UL18 with a 1000-fold higher affinity than to other MHC-I molecules. A recent report indicated that UL18 inhibits LIR-1^+ NK cells but has an activating effect on LIR-1^- NK cells (Prod'homme et al., 2007). Another study revealed that soluble UL18 protein can affect the phenotype of monocyte-derived dendritic cells and impairs their capacity to migrate and stimulate T cells (Wagner et al., 2008). However, the function of UL18 during HCMV infection is not yet well understood. UL142 is the other identified MHC-I homolog expressed by HCMV. This protein is shorter than the classical MHC-I heavy chain and is predicted to consist of only an α1 and α2 domain (Wills et al., 2005). UL142 downregulates some alleles of the human stress-induced ligand MICA and thereby protects the infected cell from NK cell cytotoxicity (Chalupny et al., 2006). m144 is the counterpart of UL18 expressed by MCMV. m144 differs from UL18 in several respects, it does not bind peptide and can be stably expressed in the absence of β2m (Natarajan et al., 2006). MCMV lacking m144 is attenuated *in vivo* and the attenuation can be reversed by depletion of NK cells (Cretney et al., 1999; Farrell et al., 1997). The mechanism by which m144 affects NK cell function is not known, since no ligand has been identified. The crystal structure of m144 has been determined (Natarajan et al., 2006). It revealed a peptide-free, class I-like heavy

chain, associated with β2m (Figure 1.7B). Crystal structures of UL18 and UL142 have not yet been determined.

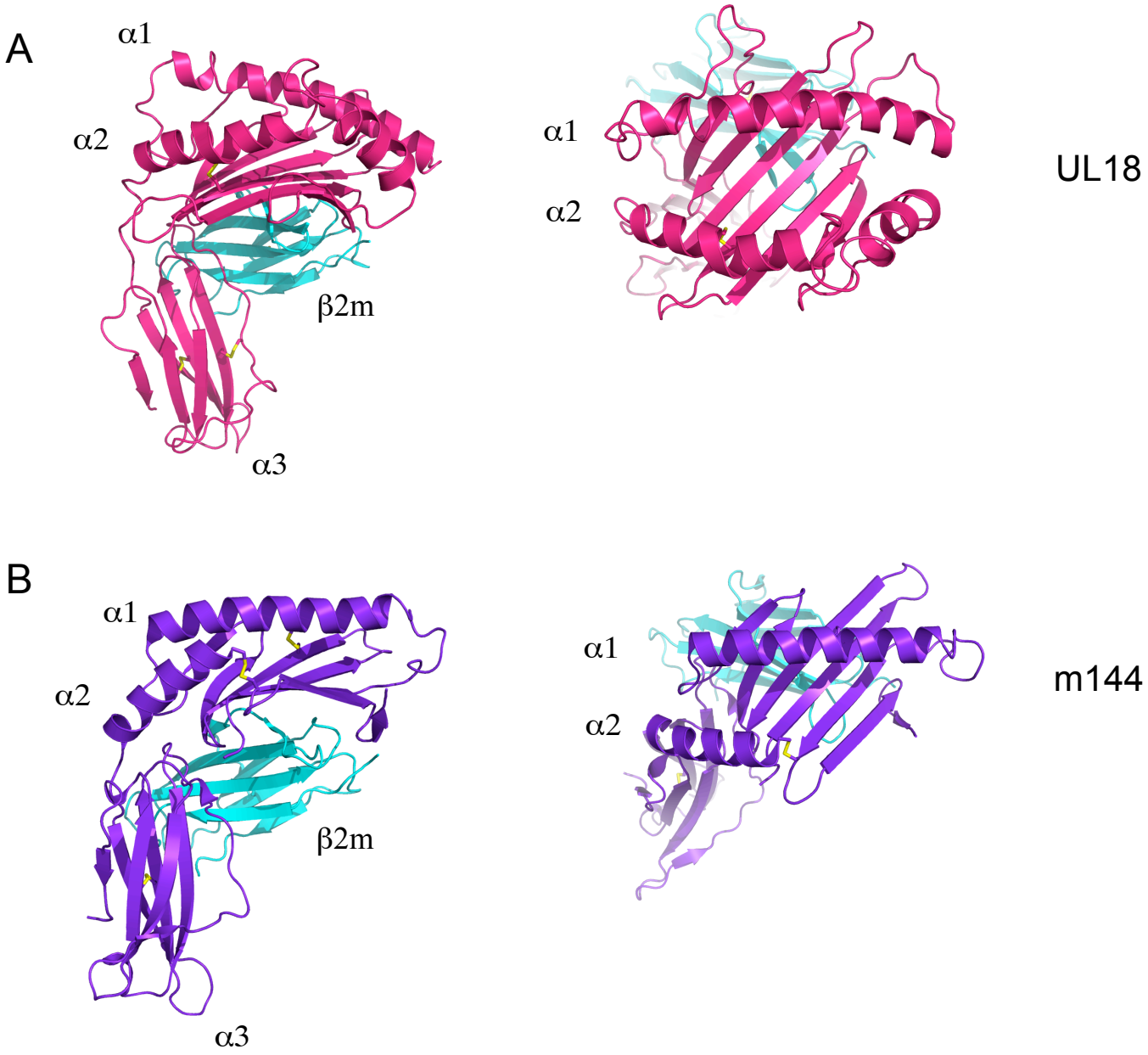

Figure 1.7. Structures of viral MHC-I homologs (MHC-Iv). A) Side and top views of a molecular model of HCMV UL18 based on the crystal structure of the HLA-A2/LIR-1 complex (Wagner et al., 2007) (PMDB access code PM0074971). Heavy chain (*pink*), β2m (*cyan*). No peptide was included in the model. B) Crystal structure of MCMV m144 (PDB ID = 1U58). Heavy chain (*purple*), β2m (*cyan*). Disulfide bonds are shown in *yellow*.

1.8.2 Distant viral homologs of MHC-I - Homology based on structural predictions

Protein structure prediction from amino acid sequence is complicated by a low level of sequence identity between the target protein and proteins of known structure. The majority of programs for secondary structure prediction use multiple sequence alignments to predict regions of alpha helix, beta sheet and coil. When working with sequences within the "twilight zone" (<30% homology), multiple alignments often do not provide reliable predictions. The 3D-PSSM method incorporates structural alignments of homologous proteins with standard multiple sequence alignments and is therefore able to detect distant relationships between proteins (Kelley et al., 2000). Smith and colleagues subjected the MCMV genome to structural prediction analysis using 3D-PSSM (Smith et al., 2002). The program uses one- and three-dimensional sequence alignments in combination with secondary structure and solvation potential information to assign a protein fold. Twelve MCMV open reading frames in total were predicted to encode proteins with MHC-I-like folds (Smith et al., 2002). Eight of these proteins form part of the m145 family of MCMV. The other proteins were m144, the known MHC-I homolog, and M37, m90 and m159, all proteins of unknown function. The confidence of the fold prediction ranged from 70-95% and a variety of MHC-I molecules made out the top hits.

Of the predicted MHC-I-like proteins, only m144, m145, m152, m155 and m157 have established functions. The exact mechanism of action has only been determined for m157. It is intriguing that MCMV should encode MHC-I-like molecules that interact with either host MHC-I molecules (m152), endogenous MHC-I-like proteins (m145, m152 and m155) or receptors that usually recognize MHC-I proteins (m157). The unique

functions of m145, m152, m155, and m157 suggest that each member of the m145 family is important in modulating the response of the host to MCMV infection. The low degree of sequence similarity within the m145 family implies that the members of the m145 family may have evolved significant structural deviations from typical MHC-I to solve novel difficulties in their encounter with the immune system.

1.9 Aims of the study

An understanding of the evolution and function of the MHC-I-like molecules of MCMV demands examination of the cellular expression, immunological function, and molecular structure of each of these molecules. The aims of this study were to characterize the MCMV MHC-I-like proteins in recombinant and mammalian cell expression systems, select a suitable candidate and determine its crystal structure. Structural information on the m145 family could confirm the validity of the MHC-I fold prediction, help to evaluate how closely related these proteins are to host MHC-I and to each other, and possibly yield insight into other members of the family. Since the functions of several family members are still unknown, structural characterization may be complementary to functional characterization of this important MCMV protein family.

Specific objectives:

1. To characterize the predicted MHC-I-like proteins encoded by MCMV in terms of cellular localization and cell surface expression requirements for β2m and peptide

2. To evaluate recombinant expression systems for yield and quality of the viral proteins for structural studies

3. To screen the proteins for crystallization and determine the crystal structure of a successful candidate

4. To construct a reporter cell line for the specific MCMV MHC-I-like protein

5. To screen primary cells and cell lines for possible ligands

The characterization of several MCMV MHC-I-like proteins in terms of cellular localization and association with β2m and peptide as well as their recombinant expression is presented in Chapter 3. m145 family member m153 presented a suitable candidate for structure determination, since it could be expressed at high levels in recombinant form, is of a very stable nature and could be crystallized. We have studied m153 in both transfected and MCMV-infected cells in detail and this is presented in Chapter 4. We demonstrate that *m153* is a functional gene that directs the expression of its encoded protein to the surface of MCMV-infected cells. Surface expression of m153 is independent of the transporter associated with antigen processing (TAP) or β2m. In surprising contrast to MHC-I molecules, recombinant soluble m153 is homodimeric. The crystal structure of m153 described in Chapter 5 confirms that m153 adopts an MHC-I-like fold and reveals the mode of dimerization in addition to other distinguishing features. In Chapter 6 we report the m153-reporter cell construction and the identification of dendritic cells as a cell type that can stimulate m153-specific reporter cells.

CHAPTER 2

MATERIALS AND METHODS

2.1 Cell lines

COS-7 (ATCC CRL-1651), NIH3T3 (ATCC-1658), RMA, RMA-S and Phoenix E cells were grown in DMEM containing 10% fetal bovine serum, 5 x 10^{-5} M 2-mercaptoethanol, 1x non-essential amino acids (Biowhittaker, Lonza, Allendale, NJ, USA) and 50 μg/ml gentamicin at 37 °C in 5% CO_2. R1.1, R1E and 43.1 and its derivatives 153z_43.1, 153z_43.1_H, 144z_43.1 and 144z_43.1_H, mouse bone marrow and spleen cells were cultured in RPMI containing the same supplements as above. RMA-S cells have a defect in the *Ham-2* gene and do not express a functional transporter associated with antigen processing (Attaya et al., 1992). R1E cells do not express β2m (Allen et al., 1986). 43.1 cells contain an NFAT-driven GFP construct and express GFP upon cross-linking of the T cell receptor (Ohtsuka et al., 2004). *Drosophila* S2 cells were maintained in Insect Express medium (BioWhittaker) supplemented with 50 μg/ml gentamicin except where mentioned otherwise. SF9 cells were cultured in BacVector Insect Cell Medium (Novagen, Madison, WI, USA) supplemented with 50 μg/ml gentamicin.

2.2 Mice

BALB/cJ, BALB/cByJ, CBA/J, C3H/HeJ, C57BL/6, DBA2/J, FVB/NJ and NOD/ShiLtJ mice were obtained from NIH-NCI-DCT (Frederick, MD, USA). Male and female mice, ranging from 6 weeks to 3 months of age were used in the experiments. Dr. Anderson Nunes (LVMR, NIAID) kindly provided female Wistar rat spleens. All animal based studies were performed under an approved protocol of the NIH Animal Care and Use Committee under AAALAC guidelines.

2.3 Antibodies

Rabbit antiserum was produced against m153 expressed as inclusion bodies in *E. coli*. Reduced, denatured SDS-gel purified m153 was emulsified in complete Freund adjuvant prior to immunization. The mouse monoclonal antibody mAb153.16 was generated with the extracellular domain of mature m153 (amino acids 1-314) expressed in S2 cells, and stains m153 transfected cells and immunoprecipitates m153 from transfected or virus-infected cells. The mouse monoclonal antibody to MCMV m144, 15C6, was obtained from the American Type Culture Collection (Cat. No. CRL-2431, ATCC - Manassas, VA, USA).

2.4 Vector constructs

The PCR primer sequences are listed at the end of this Chapter under section 2.26.

2.4.1 Bacterial expression

The extracellular regions of the MCMV proteins (m17, M37, m90, m145, m150, m151, m152, m153, and m155) were predicted using the Signal P 3.0 server (Bendtsen et al., 2004; Nielsen et al., 1997) and hydrophilicity plots from the Macvector program (Olson, 1994). Restriction enzyme sites for BamHI and NdeI were incorporated in the DNA primers designed to amplify the extracellular domains from MCMV genomic DNA (Smith strain, catalog no. VR-1399, American Type Culture Collection, Manassas, VA, USA). These sites were used to insert the PCR products in the bacterial expression vector pET21b (Novagen, Madison, WI, USA). A termination codon was inserted in all the 3'-oligos to prevent addition of the vector encoded His-tag to the proteins. The primers used to amplify the MCMV proteins are listed under Section 2.26 on page 51. All constructs were sequence verified.

2.4.2 Insect cell expression

cDNAs encoding the predicted mature extracellular domain of M37 (residues 1-246), m151 (residues 1-317) and m153 (residues 1-315) were PCR-amplified from MCMV-infected cell culture supernatants (Smith strain, ATCC, catalog no. VR-1399). BamHI (m151, m153) or BglII (M37) restriction sites were incorporated in the forward primers and a thrombin cleavage site (LVPRG, m151 and m153) or an enterokinase site (DDDDK, M37), a 6xHis tag, a termination codon, and a KpnI restriction site were incorporated in the reverse primers. The PCR products were directly cloned into the pCR4-Topo-TA vector (Invitrogen, Carlsbad, CA, USA), the sequences verified, and

then the M37, m151 and m153 fragments were inserted in the BglII and KpnI sites of pMT-Bip-V5-His (Invitrogen).

To generate the interface mutant, alanine mutations were introduced at four residues (T128, S131, R225 and S241) in the m153-N-YFP construct using the QuickChange Multi mutagenesis kit (Stratagene, La Jolla, CA, USA). An alanine mutation was introduced at a site distant from the interface at Asp 194 in the control mutant. The wild type and mutated forms of m153 (residues 1-315) were PCR-amplified from the wt m153-N-YFP or the mutated plasmids and cloned in the pIEx-4 SF9 expression vector (Novagen, Madison, WI, USA).

2.4.3 Mammalian cell expression

2.4.3.1 FLAG- and HA-tagged constructs

The FLAG-tag DYKDDDDK was inserted two amino acids after the predicted signal peptide cleavage site of each MCMV protein. Overlapping primers were designed to encode the FLAG sequence and the N-terminal sequence of the proteins. Three to five sequential PCRs were performed using MCMV Smith strain (ATCC VR-1399) DNA as template to amplify the full-length gene and insert the FLAG-tag in ORFs, m17, M37, m90, m144, m145, m150, m151, m152, m153, m155 and m159. The PCR products were inserted in the TOPO-TA vector (Invitrogen, Carlsbad, CA, USA) and sequence verified. EcoRI or MfeI and BamHI or BglII restriction enzyme sites were incorporated in the 5' and 3' oligonucleotides, respectively, to facilitate cloning of the tagged genes in the EcoRI and BamHI sites of the pIRES-hr-GFP-II vector (Stratagene, La Jolla, CA, USA).

This vector will be referred to as pIRES-GFP. The HA-tag YPYDVPDYA was inserted at the N-terminus of m153 by sequential PCR with m153-pcDNA as template. The HA-tagged m153 was then inserted in the EcoRI and BamHI sites of pIRES-GFP.

2.4.3.2 m153-EYFP fusion construct

EYFP was fused to the C-terminus of full-length m153. Residues minus 22-383 of m153 were amplified from an existing construct using forward and reverse primers with BamH1 and EcoRI restriction sites respectively. The PCR product was then inserted into the corresponding sites of pEYFP-N1 (Clontech, Mountain View, CA, USA). Expression of the fusion protein is driven by the CMV IE promoter.

2.4.3.3 Bimolecular fluorescence complementation constructs

Mammalian expression vectors encoding the N-terminal 1-154 residues (N-YFP) or the C-terminal 155-238 residues (C-YFP) of YFP were a kind gift from Dr. Keiko Ozato, NICHD, NIH. m153 and m144 were amplified from existing full-length constructs. The PCR products were digested and inserted in the BglII and EcoRI sites of N-YFP and C-YFP and the sequences verified. The resulting constructs encode fusion proteins of m153 and m144 linked at their C-termini to either the N- or C-terminal fragments of YFP. A 12-13 amino acid spacer separates the viral proteins from the YFP fragments.

2.4.3.4 m144-human zeta and m153-human zeta fusion constructs

The transmembrane and cytoplasmic domain of the human T cell receptor zeta chain was fused to the extracellular domain of m153 using splicing by overlap extension (SOE) PCR. The extracellular domain (residues minus 22-315) of m153 and the human zeta chain (residues 30-163) were amplified from existing constructs. The resulting PCR products were used as template for the SOE reaction using the outer primer pairs. The fused m153-human zeta PCR product was cloned in the TOPO-TA vector (Invitrogen, Carlsbad, CA, USA) and sequence verified. The construct was then excised from the TA vector with BamHI and EcoRI and inserted in these sites of the pMXs retrovirus vector (a kind gift of Dr. Toshio Kitamura, University of Tokyo, Tokyo, Japan) (Onishi et al., 1996). A construct consisting of the extracellular domain of m144 (residues minus 20-249) fused to the transmembrane and cytoplasmic domain of the human zeta chain was obtained from Dr. Kannan Natarajan, NIAID, NIH. This fusion construct was amplified and inserted in the BamHI and EcoRI sites of pMXs.

2.5 Transfection and FACS analysis of FLAG-tagged MCMV proteins

Fugene 6 (Roche Diagnostics, Indianapolis, IN, USA) was used according to the manufacturer's instructions to transfect COS-7 cells with the parental pIRES-hr-GFP-II vector (Stratagene, La Jolla, CA, USA) or pIRES-hr-GFP-II constructs encoding FLAG-tagged versions of m17, M37, m144, m145, m151, m152, m153 and m155. Forty-eight hours after transfection the surface expression of the viral proteins was assessed. One million cells were stained with 0.5 μg anti-FLAG M2 (Sigma-Aldrich, St. Louis, MO, USA) in PBS, 5% FCS, 0.1% NaN_3 for 30 min. on ice. After washing, the bound

antibodies were detected with sequential 30 min. incubations with anti-mouse IgG_1–Biotin and Streptavidin-PE (BD Pharmingen, San Jose, CA, USA).

For intracellular staining of m152- and m155-transfected samples the cells were fixed with 4% paraformaldehyde for 20 min. at room temperature, washed twice with PBS and permeabilized in PBS, 0.1% BSA, 0.5% Triton X-100. One million cells were stained with 1 μg M2 for 30 min. at room temperature, and after washing the bound antibodies were detected with anti-mouse IgG_1-PE (Southern Biotech, Birmingham, AL, USA). Cells transfected with the pIRES-hr-GFP-II vector served as a negative control for non-specific staining in all experiments. The stained cells were analyzed with a Becton Dickenson FACScan (BD Biosciences, San Jose, CA, USA).

To assess the effect of the MCMV proteins on MHC-I expression in mouse cells, NIH3T3 cells were transfected with FLAG-tagged versions of m17, M37, m144, m145, m151, m152, m153 and m155 in the pIRES-hr-GFP-II vector. The Amaxa nucleofector (Amaxa Biosystems, Cologne, Germany) was used to introduce 2 μg of DNA into 1 x 10^6 NIH3T3 cells (Solution R, program U30). Eighteen hours after transfection the cells were stained for MHC-I expression with the anti-H-$2D^{l/q}$ antibody followed by anti-mouse IgG-APC (BD Biosciences, San Jose, CA, USA) and analyzed with a FACSCalibur (BD Biosciences).

2.6 β2m and TAP-dependence

The Amaxa nucleofector (Amaxa Biosystems, Cologne, Germany) was used to introduce the pIRES-hr-GFP-II vector (Stratagene, La Jolla, CA, USA) encoding the different FLAG-tagged MCMV genes or H-2D^d into R1.1 and R1E cells (solution V, program A30) or into RMA and RMA-S cells (solution T, program A30) according to the manufacturer's instructions. In the RMA and RMA-S experiments serum-free medium was used after transfection, to avoid stabilization of MHC-I molecules by peptides derived from serum proteins in the medium. Eighteen to 24 h post transfection the cells were stained for surface expression of the FLAG-tagged viral proteins with the M2 monoclonal antibody (Sigma-Aldrich, St. Louis, MO) and a PE labeled anti-mouse IgG_1 antibody (Southern Biotech, Birmingham, AL, USA). H-2D^d was detected using the PE-labeled 34-5-8S antibody (BD Biosciences, San Jose, CA, USA). Propidium iodide staining was used to exclude dead cells from the analysis.

2.7 MCMV infection, cell surface staining and FACS

Seventy percent confluent NIH3T3 cells were infected with MCMV-GFP at a multiplicity of infection (m.o.i) of two. Twenty-four hours post infection (p.i.) the cells were detached with a non-enzymatic cell dissociation solution (Cellstripper, Cellgro, Herndon, VA, USA) and resuspended in PBS containing 5% FCS and 0.1% NaN_3. $F(ab')_2$ fragments were generated from monoclonal antibody mAb153.16 with the Immunopure IgG_1 $F(ab')_2$ kit (Pierce, Rockford, IL, USA). Infected and uninfected cells were incubated with the $F(ab')_2$ followed by anti-mouse IgG-APC. Dead cells were excluded by propidium iodide gating. Cells were analyzed with a FACSCalibur (Becton-

Dickinson, Franklin Lakes, NJ, USA) and virus-infected cells were gated on GFP expression.

For time-course analysis of m153 expression in MCMV-infected cells, cells were infected as described above and harvested at 3, 6, 12, 24 and 48 h p.i. The cells were processed for immunoprecipitation and Western blot as described in Section 2.10.

2.8 Bimolecular fluorescence complementation

NIH3T3 cells were transfected with 153-N-YFP and 153-C-YFP or 144-N-YFP and 144-C-YFP using the Amaxa nucleofector (Amaxa Biosystems, Cologne, Germany, solution R, program U30). Cells were then seeded on chambered coverslides and incubated for 48 h at 37 °C. A Leica TCS AOBS SP2 confocal microscope (Leica Microsystems, Bannockburn, IL, USA) equipped with a 63x 1.4 NA PL APO objective was used to examine live cells at room temperature for YFP fluorescence complementation. Leica TCS v2.1547 software was used to capture the images. After analysis the cells were detached with trypsin and the YFP positive cells were quantified by flow cytometry.

2.9 Localization studies of m153

NIH3T3 cells (1×10^6) were transfected with 1 – 2 μg of m153-EYFP-pcDNA or 153-pcDNA using the Amaxa nucleofector (Solution R, Program U30) and seeded in Lab-Tek coverglass chambers (Nalge Nunc International). Eighteen hours post transfection the cells were fixed for 15 min. at room temperature with 4% paraformaldehyde and washed once with PBS. All subsequent steps were performed at room temperature. The

intracellular staining samples were permeabilized with 0.1% Triton X-100 for 15 min. and washed once with PBS. Both surface and intracellular staining samples were then treated with Image It Enhancer (Molecular Probes, Invitrogen Carlsbad, CA, USA) for 30 min., washed with PBS and blocked for 30 min. with 10 mg/ml goat serum. After rinsing in PBS the cells were incubated with mAb153.16 for 1 h, washed three times in PBS, and incubated with anti-mouse IgG-Alexa 594 for 30 min. The staining patterns were then studied by confocal microscopy as described in section 2.8.

m153-EYFP (2 μg) was transfected in 1 x 10^6 NIH3T3 cells (Amaxa nucleofector, solution R, program U30) and the cells were seeded on Lab-Tek chambered coverglass (Nalge Nunc International, Rochester, NY, USA). Eighteen to 24 h after transfection the cells were fixed with 4% paraformaldehyde (15 min. room temperature), stained for the Golgi apparatus (anti-human Golgin, Molecular Probes) or early endosomes (anti-EEA1, Abcam, Cambridge, MA, USA) and detected with anti-mouse or -rabbit Alexa 594 secondary antibodies (Molecular Probes). For visualization of mitochondria and lysosomes, live cells were treated with Mitotracker-Red and Lysotracker-Red (Molecular Probes) according to the manufacturer's instructions. Nuclei were stained with DAPI (Molecular Probes). The confocal microscope and image capturing software described in section 2.8 were used.

2.10 Immunoprecipitation and Western blots

NIH3T3 cells (2 x 10^6) were co-transfected with FLAG-m153-pcDNA (1 μg) and HA-m153-pcDNA (1 μg) (Amaxa Nucleofector, solution R, program U30) and seeded in 10 cm plates. For infection experiments 70-80% confluent NIH3T3 cells seeded in 10 cm plates were infected with MCMV-GFP at an m.o.i. of two. After overnight incubation for transfections and 24 h incubation for infections, the cells were washed twice in ice-cold PBS and lysed in the plates with 1 ml of 1% NP40, 50 mM Tris-HCl pH 8, 300 mM NaCl, 5 mM EDTA, 1x protease inhibitor cocktail (Pierce, Rockford, IL, USA), 10 mM iodoacetamide, 0.02% sodium azide. The cells were removed from the plate with a cell scraper and incubated for 15 min. on ice. All subsequent steps were performed on ice or at 4 °C. The lysate was centrifuged for 15 min. at 13,000 rpm, and supernatants were precleared by incubating with 50 μl of anti-mouse IgG beads (eBioscience, San Diego, CA, USA) for 30 min. For transfected cells the precleared cell lysates were divided into three aliquots, and either 5 μg of FLAG M2 antibody (Sigma-Aldrich, St. Louis, MO, USA), anti-HA (Sigma-Aldrich) or mAb153.16 were incubated with the lysates for 1 h. For infection experiments 5 μg of mAb153.16 were incubated with infected and uninfected cell lysates for 1 h. Then 50 μl of anti-mouse IgG beads were added to the lysates and incubated for 1 h with rotation. The beads were washed 5x with lysis buffer containing 0.1% NP40. Reducing SDS-PAGE sample buffer (Pierce) was added to the beads and the samples heated to 100 °C for ten minutes prior to electrophoresis on an 8-20% gradient Tris-Glycine SDS-PAGE gel (Invitrogen, Carlsbad, CA, USA). The proteins were transferred to polyvinylidene fluoride (PVDF) membranes using standard protocols. The membrane was blocked overnight with 5% non-fat dried milk in 0.1% Tween 20/PBS. The proteins were detected by incubation with either anti-FLAG M2,

anti-HA (Sigma-Aldrich) or anti-m153 rabbit serum for 1 h at room temperature. After washing in 0.1% Tween 20/PBS the membranes were incubated with secondary antibody for 1 h at room temperature (anti-mouse or anti-rabbit Trublot-eBioscience), and washed again. The blots were developed with the Supersignal West Dura Extended Duration substrate (Pierce) and exposed to Biomax XAR film (Kodak, Rochester, NY, USA).

To determine whether m153 is glycosylated, immunoprecipitated samples on beads were incubated with 1000 U PNGaseF (New England Biolabs, Ipswich, MA, USA) in PBS at 37 °C overnight before processing for SDS-PAGE and Western blot analysis as described above.

2.11 Bacterial expression in *E.coli* and refolding of proteins from inclusion bodies

The MCMV constructs were evaluated for expression in bacterial inclusion bodies in Rosetta DE3 cells (Novagen, Madison, WI, USA). One liter of LB medium with 250 μg/ml carbenicillin and 34 μg/ml chloramphenicol was inoculated with a 50 ml overnight culture of the MCMV/pET21 construct and grown at 37 ºC and 250 rpm until an OD_{600} of 0.8 was reached. The cultures were then induced with 0.5-1 mM IPTG. After two hours the cells were harvested by centrifugation at 5000 x g for 5 min. The cell pellet was resuspended in 100 mM Tris-HCl, 2 mM EDTA pH 8, 0.1% deoxycholate and 0.5 mg/ml lysozyme and the cells were lysed overnight at 4 ºC. The viscous mixture obtained after lysis was sonicated 4 x 20 sec with a Sonicator cell disruptor set at output = 7 and duty cycle = 50% (Misonix, Inc. Farmingdale, NY, USA). The inclusion bodies were pelleted at 20,000 x g for 20 min. and washed three times with TE/0.1% DOC and once with TE. The final pellet was dissolved in 6 ml TE to which 5.7 g guanidine-HCl or

4.8 g urea was added to produce a final concentration of 6 M GdHCl or 8 M urea respectively. The inclusion bodies were incubated for several hours at room temperature until the solution was clear.

The solubilized proteins were then diluted drop-wise with rapid stirring in one liter of a 0.4 M arginine-HCl, 100 mM Tris-HCl, 2 mM EDTA, 4 mM reduced glutathione, 0.4 mM oxidized glutathione pH 8 buffer, that was pre-chilled to 4 °C. The refolding mixture was incubated for 4 days at 4 ºC. Precipitates were removed by filtering through a 0.45 μm membrane and the solution was dialyzed against TBS pH 8. After dialysis, precipitated material was removed by filtration and the protein solution concentrated using a 10 000 MW cutoff membrane (Millipore, Danvers, MA, USA) in a stir-cell concentrator (Amicon-Millipore). The concentrated proteins were analyzed on a size exclusion column (Shodex KW 802.5, Thomson Instrument Company, Clear Brook, VA, USA) to assess the efficiency of refolding.

The Research Technology Branch of the NIAID provided N-terminal sequencing services. Liquid or blotted protein samples were sequenced by automated Edman degradation.

2.12 *Drosophila* insect cell expression and purification of m153

The pMT-Bip-His constructs encoding M37, m151 or m153 were transfected, together with puromycin and blasticidin resistance-encoding plasmids (10:1:1 ratio by weight), into S2 cells using Fugene6 (Roche, Indianapolis, IN, USA) according to the manufacturer's protocol. Forty-eight hours after transfection the cells were transferred to selective medium containing 5 μg/ml puromycin (Sigma-Aldrich, St. Louis, MO, USA) and 5 μg/ml blasticidin (Calbiochem, San Diego, CA, USA). Resistant cells were maintained in selective medium in shaker cultures (28 °C, 100 rpm). Expression of M37, m151 or m153 was induced with 1 mM $CuSO_4$ at a cell density of 2 x 10^7 /ml. The proteins were purified on Ni-NTA columns (Qiagen, Valencia, CA) and then subjected to SEC (Shodex KW802.5 or Pharmacia Superdex 75). The His-tags were removed by thrombin or enterokinase (M37) cleavage at 37 °C for 2 h, and the proteins were purified by anion exchange chromatography (Mono Q, Pharmacia, Uppsala, Sweden). For preparation of a SeMet derivative of m153, the m153/S2 cells were grown in Orbigen insect cell medium to 2 x 10^7 cells/ml. The cells were then washed in methionine-free medium (Orbigen, San Diego, CA, USA) and starved in this medium for 6 h under normal growth conditions. Protein expression was induced by simultaneous addition of 1 mM $CuSO_4$ and 60 μg/ml SeMet (Sigma-Aldrich). The SeMet labeled protein was purified as described for the native protein.

2.13 Transient expression of wild type and mutant m153 in SF9 cells

Two hundred micrograms of m153-pIEx-4, interface mutant-m153-pIEx-4 or control mutant-m153-pIEx-4 were transfected into 1 x 10^8 exponentially growing SF9 cells in 100 ml with 1 ml of Insect GeneJuice transfection reagent (Novagen, Madison, WI, USA). Seventy-two hours after transfection the cell supernatants were collected. Wild type and mutant proteins were then purified on Ni-NTA and SEC columns as described for S2 insect cell expression.

2.14 Crystallization, structure determination and refinement

Crystal Screen, Crystal Screen 2 (Hampton Research, Aliso Viejo, CA, USA) and the PEGs Suite (Qiagen, Valencia, CA, US) were used to screen for m153 crystallization conditions. Both native m153 and the SeMet derivative of m153 crystallized in 25% PEG 2000 MME, 0.1 M Tris-HCl pH 8. The crystals were grown in 2 μl hanging drops at 18 ºC. The crystals were very fragile and did not diffract well. We used an additive screen (Hampton Research) and found that addition of 0.5% β-D-maltoside to the drops yielded crystals that diffracted to 2.3 Å. Diffraction data for SAD phasing were collected on a single SeMet derivative crystal on beamline X29A at the NSLS, Brookhaven, at a wavelength of 0.9791 Å and processed with HKL2000 (Otwinowski and Minor, 1997). The automated SOLVE/RESOLVE scripts as incorporated in the AutoSol module of the PHENIX suite (Adams et al., 2002) were used with data truncated at 2.8 Å to obtain SAD phases followed by automated model building and docking to the m153 sequence. Ambiguously placed residues were rebuilt manually into the SAD-phased map in COOT as alanines (Emsley and Cowtan, 2004). To extend the resolution to 2.4 Å a molecular

replacement search was carried out in Phaser (Read, 2001) with the partially built model yielding Z-scores of 11.0 and 23.7 for the rotation and translation functions, respectively, for one dimer in the asymmetric unit. Rigid body refinement specifying α1α2 and α3 as separate domains yielded a model with initial R and R_{free} of 36.9% and 38.6%, respectively. Refinement at 2.4 Å was continued in Refmac5 (Murshudov et al., 1997) with tight NCS restraints between chains A and B with further model building guided by 2Fo-Fc and Fo-Fc maps generated in COOT 0.1.3. Residues in the 231-237 loop which had little or no electron density were omitted from the NCS restraints. Optimal domains for TLS refinement were identified and input files for TLS refinement were generated using the TLSMD web server (Painter and Merritt, 2005). TLS refinement using 10 TLS groups per chain decreased R_{free} from 29.9% to 28%. Finally, waters were added with CNS 1.1 (Brunger et al., 1998) and a final round of refinement was performed without NCS restraints. The final model has R_{cryst}=23% and R_{free}=27.9%, includes residues 2-230 and 238-277 of chain A and residues 5-277 of chain B and has 57 waters. The atomic coordinates and structure factors have been deposited in the Protein Data Bank (Berman et al., 2000) under accession number 2O5N. Buried surface area calculations were performed in CNS. Hinge angles were calculated using HINGE, a program written by Peter Sun. HINGE calculates an ellipsoid (defined by axes a, b and c) for each indicated domain, and reports the angle between the long axes of the adjacent domains as the hinge angle. HINGE is available at: http://sis.niaid.nih.gov/programs/hinge.html.

The following residue ranges were used to define the α1α2 and α3 domains in the respective proteins: m153 (20-178, 179-277), m157 (20-175, 176-268), m144 (1-142, 143-242), H-2K^b (1-180, 181-274), CD1d (1-184, 185-279), T22 (1-180, 181-276), ZAG (1-182, 183-277), MICA (1-175, 176-274). Figures were generated using PyMOL

(DeLano, 2002). Sc values were calculated using the default settings of the Sc program (Lawrence and Colman, 1993) of the CCP4 Suite.

2.15 Analytical ultracentrifugation

Sedimentation velocity experiments were conducted with a ProteomeLab XLI ultracentrifuge (Beckman Coulter, Fullerton, CA, USA). 400 µl samples were loaded at concentrations of 0.3 mg/ml for m153 wild type and 0.5 and 0.1 mg/ml for the m153 mutant and centrifuged at 50,000 rpm at 20 °C. Sedimentation data were acquired with the Rayleigh interference optical system at 1 min. intervals, and data were analyzed using SEDFIT software (Schuck, 2000). Additional details on experimental and data analysis protocols can be found at http://www.analyticalultracentrifugation.com.

2.16 Mass spectrometry

For mass spectrometry infusion experiments, samples were diluted with ultrapure water (LC-MS-Chromasolv grade, Sigma-Aldrich, St. Louis, MO, USA), heated to 65 °C for 5 min. and desalted twice in ultrapure water using Centri•Sep™ desalting spin columns according to the manufacturer's procedures (Princeton Separations, Inc. Adelphia, NJ, USA). After further enzymatic or chemical treatment with 0.1 µg trypsin (Promega, Madison, WI, USA), 0.5 mU PNGaseF (QA-Bio, Palm Desert, CA, USA), 2 µg tris-(carboxyethyl)-phosphine hydrochloride (TCEP, Sigma-Aldrich) or 2 µg dithiothreitol (DTT, Sigma-Aldrich) and incubation at 37 °C for 1 – 48 h, the respective samples were diluted 1:1 in spraying buffer (40% Isopropanol, 40% Acetonitrile, 20% Ultrapure Water and 0.2% formic acid, all Sigma-Aldrich). Infusion nano-electrospray was performed

using the TriVersa™-NanoMate chip technology (Advion Biosystems, Ithaca, NY, USA) coupled to an LTQ-FT™ ICR mass spectrometer (Thermo Electron, Thermo Scientific, Waltham, MA, USA).

Five microliters solution pick-up (ca. 2-15 pmol/μL) was sufficient for ~ 45 min. analysis time (1.5 kV, 0.3 bar pressure assistance). MS and MS^n fragmentation data were recorded applying collision-induced dissociation (CID, 35% energy), electron capture dissociation (ECD, 5 x 10^5 energy, 10 ms delay, 70 ms duration) or infrared multi photon dissociation (IRMPD, 90% energy, 10 ms delay, 90 ms duration) of indicative precursor ions. MS spectra recorded were the average of three or more FT-MS scans (max. ion injection time 3000 ms, resolution 100,000 to 500,000, ion accumulation values according to the manufacturer's standard values). MS^n spectra were recorded as the average of three FT-MS scans (5 Da window for precursor ion selection).

2.17 Retrovirus production and generation of reporter cell lines

The m144-zeta-pMX and m153-zeta-pMX (2 μg) constructs were transfected in the Phoenix E packaging cell line (a kind gift of Dr. Toshio Kitamura, University of Tokyo, Tokyo, Japan) using Fugene 6 (Roche, Indianapolis, IN, USA) according to the manufacturer's protocol. Retrovirus containing supernatants were collected 48 h after transfection and stored at -80 °C. The 43.1 cell line (Ohtsuka et al., 2004) contains an NFAT-driven GFP construct and was used as the parental reporter cell line. One and a half million 43.1 cells were suspended in 3 ml of m144-zeta or m153-zeta retroviral supernatants in one well of a 6 well plate. Polybrene (hexadimethrine bromide, Sigma-Aldrich, St. Louis, MO, USA) was added to a final concentration of 4 μg/ml and the

cells were centrifuged at 1000 x g for two hours at room temperature to enhance the infection efficiency. Forty-eight hours after infection the cells were stained for surface expression of m144 and m153 using anti-m144 15C6 or mAb153.16 followed by anti-mouse IgG-PE and FACS analysis to determine the infection efficiency. Forty-three percent of m144-zeta infected cells expressed m144 and 70% of m153-zeta infected cells expressed m153. Limited dilution cloning was then performed to obtain cell lines in which all cells express the respective viral molecules at high levels. 153z_43.1 or 144z_43.1 cells were seeded at different concentrations in 96 well plates (50, 25, 10 and 1 cell per well) and cultured at 37 °C / 5% CO_2. The cells that grew out were expanded and stained for m153 or m144 expression and the populations with homogeneous viral protein expression were selected for further use.

2.18 Control antibody stimulation of reporter cell lines

Control stimulation of 43.1, m144z_43.1 and m153z_43.1 cell lines was performed in flat bottom 96 well plates coated overnight with the TCR specific antibody H57 (1 µg/ml), anti-m144 15C6 (1 µg/ml) or anti-m153 mAb153.16 (4 µg/ml) in PBS. Reporter cells (1 x 10^5/well) were incubated for 16-18 h at 37 °C / 5% CO_2 before the cells were harvested by centrifugation and analyzed for GFP expression by FACS.

2.19 Reporter cell coculture assays

Screening of cell lines and primary cells was performed in round-bottom 96 well plates. One hundred thousand reporter cells were cocultured with different numbers of stimulator cells ranging from 1 x 10^5 to 1 x 10^6 in a total volume of 250 µl for 18 h. Reporter cells were discriminated from stimulator cells based on forward- and side-scatter profiles or by staining with a PE-labeled antibody to the Vβ3 TCR chain (clone KJ25, BD Pharmingen, BD Biosciences, San Jose, CA, USA) and analyzed by FACS (FACSCalibur, BD Biosciences, San Jose, CA, USA). The number of Vβ3 positive cells that express GFP represents the percentage of cells stimulated by the "test" cell line or primary cells. Dead cells were excluded from the analysis by gating on propidium iodide negative cells.

2.20 Isolation of mouse or rat splenocytes

Each freshly isolated spleen was flushed three times with 3 ml of 6 mg/ml Liberase Blendzyme 2 (Roche, Indianapolis, IN, USA) and 0.5 mg/ml DNAse (Roche) in complete RPMI. The spleen was then cut into fine pieces and combined with the cell/enzyme suspension and incubated at 37 °C for 30 min. and vortexed every 5 min. The cells were passed through a 45 µm cell strainer (BD Falcon) and the remaining pieces of tissues dissociated with a plunger. The cells were then centrifuged for 10 min. at 300 x g at 4 °C. The red blood cells were lysed by addition of ACK lysing buffer (155 mM NH_4Cl, 0.1 mM EDTA, 10 mM $KHCO_3$, Quality Biological Inc., Gaithersburg, MD, USA) and were subsequently washed twice in RPMI medium containing 50 µg/ml

gentamicin and 10% fetal bovine serum. The yield of cells per spleen ranged from 1.2 to 1.6 x 10^8.

2.21 Isolation of different cell subsets from mouse or rat splenocytes

2.21.1 Dendritic cells (mouse – $CD11c^+$, rat – $OX62^+$)

$CD11c^+$ cells were isolated by positive selection with anti-CD11c microbeads from Miltenyi Biotec (Auburn, CA, USA). Cells were resuspended at 10^8 cells/400 μl in ice-cold PBS containing 0.5% BSA and 2 mM EDTA. To increase the purity of the final $CD11c^+$ population, the cells were incubated with anti-CD32/CD16 (clone 2.4G2, 4 μg/ml, BD Pharmingen, San Jose, CA, USA) for 10 min. on ice, to block Fc receptor on the spleen cells. Then 100 μl anti-$CD11c^+$ beads were added per 10^8 cells and the cells were incubated for 15 min. at 4-8 °C. The cells were subsequently washed with the PBS/BSA/EDTA buffer (1-2 ml/ 10^8 cells) and resuspended at 10^8/500 μl. The $CD11c^+$ cells were then isolated using an LS positive selection column and MACS separator (Miltenyi Biotec) according to the manufacturer's instructions. The purity of the population was determined by staining with an anti-CD11c-PE antibody (clone HL3, BD Pharmingen) and FACS analysis (FACSCalibur, BD Biosciences). Routinely, $CD11c^+$ populations with purity of $\geq$ 90% were obtained.

Rat (Wistar strain) dendritic cells were isolated by positive selection using rat anti-DC (OX62) Microbeads (Miltenyi Biotec), according to the manufacturer's instructions.

2.21.2 Plasmacytoid dendritic cells

For plasmacytoid DC (pDC) isolation spleen single cell suspensions were prepared by mechanical disaggregation. The pDC were isolated using the plasmacytoid dendritic cell isolation kit II from Miltenyi Biotec according to the manufacturer's instructions. This kit allows the isolation of untouched pDC from single cell suspensions of the spleen. The purity of the population, as assessed by staining with the anti-mPDCA-1-PE antibody (Miltenyi Biotec), was usually ~ 90%.

2.21.3 B cells, $CD11b^+$ cells, NK cells, $CD4^+$ and $CD8^+$ T cells

For B cell and monocyte/macrophage ($CD11b^+$) isolation the spleen cell suspensions were prepared by enzymatic disaggregation as described for $CD11c^+$ cells. The cells were isolated using positive selection with CD19 or CD11b microbeads from Miltenyi Biotec. NK, $CD4^+$ and $CD8^+$ cells were isolated from spleen cell suspensions prepared by mechanical disaggregation. NK cells were isolated by positive selection using anti-NK (DX5) microbeads (Miltenyi Biotec) or by a combination of first negative selection using the NK cell isolation kit from Miltenyi Biotec followed by positive selection. $CD4^+$ and $CD8^+$ T cells were isolated by negative selection using the CD4 and CD8-specific T cell isolation kits from Miltenyi Biotec. The purity of the final populations was 98% for B cells, 80% for $CD11b^+$ cells, 70% for NK cells by positive selection), 91% by combination, 94% for $CD4^+$ T cells and 89% for CD8 T cells as determined by staining for specific cell markers and FACS analysis.

2.22 Generation of dendritic cells from mouse bone marrow cells

Bone marrow cells were flushed from the femora of BALB/c mice and the cells were treated with ACK buffer to remove red blood cells. The cell suspension was then incubated with PE-labeled antibodies to B220, MHC class II (IE/IA), CD90.2 and CD11b (all from BD Pharmingen) for 10 min. at 4-8 °C. Anti-PE magnetic beads (Miltenyi Biotec) were added to the cell suspension and a further incubation of 15 min. at 4-8 °C was performed. The labeled cells were removed using an LS MACS separation column (Miltenyi Biotec). The unlabeled fraction was seeded at 3 x 10^6 cells per well in a 6 well plate in RPMI containing GM-CSF (5 ng/ml, Chemicon International, Millipore, Danvers, MA, USA). The medium was changed every 2 days and after 6 days of culture $CD11c^+$ cells were isolated from the bone-marrow cultures using the CD11c Microbeads as described above.

2.23 Cell-cell contact assay

$CD11c^+$ cells were isolated from BALB/c spleens as described in section 2.21.1. As a positive control for reporter cell stimulation, 1.2 x 10^6 $CD11c^+$ cells were cocultured in 24 well plates overnight with 5 x 10^5 153z_43.1_H reporter cells in 700 µl complete RPMI medium at 37 ºC / 5% CO_2. As a negative control, the parental 43.1 reporter cells were cocultured with $CD11c^+$ cells under the same conditions. To test whether cell-cell contact was required for reporter cell stimulation, the cocultures were performed in 24 well plates with 0.4 µm polycarbonate membrane 6.5 mm transwell inserts (Costar, Corning, NY, USA) that separated the reporter and stimulator cells. $CD11c^+$ cells (1.2 x 10^6) were incubated in 100 µl in the transwell (upper chamber) and 5 x 10^5 reporter cells

were added in 600 μl to the well of the 24 well plate (lower chamber) and vice versa. The assay was performed in duplicate wells. After overnight incubation at 37 ºC / 5% CO_2 the reporter cells were collected, stained for Vβ3 expression and analyzed by FACS to determine the number of GFP^+ cells. Dead cells were excluded by propidium iodide gating.

2.24 Dendritic cell migration assay

The migration assay was performed using polycarbonate transwell inserts with a 6.5 mm diameter and a pore size of 5 μm (Costar, Corning, NY, USA). $CD11c^+$ cells were isolated as described and cultured overnight in complete RPMI at a concentration of 1 x 10^6 cells/ml on 24 well plates coated in PBS, 10 μg/ml m152 in PBS or 10 μg/ml m153 in PBS. Half of the cells cultured on the PBS coated plates were stimulated with 1 μg/ml lipopolysaccharide (LPS, Sigma-Aldrich, St. Louis, MO, USA). Two hundred and fifty-thousand cells were then added to the transwell inserts in 100 μl. The bottom chambers were filled with 600 μl complete RPMI medium or medium supplemented with 200 ng/ml recombinant mouse CCL19 (also known as MIP-3β, R&D Systems, Minneapolis, MN, USA). The cells were incubated at 37 °C / 5% CO_2 for 6 h. Cells that had migrated to the bottom chamber were collected, stained for CD11c and counted by FACS. The migration is expressed as the ratio of cells migrating in CCL19 to cells migrating in medium alone. The assay was performed in triplicate.

2.25 DC surface phenotype analysis by FACS

One million $CD11c^+$ cells were cultured alone or with 1 x 10^6 43.1 or m153z_43.1H cells for 16-18 h. The surface phenotype of the $CD11c^+$ cells after the coculture was assessed by staining with anti-CD11c-PE and FITC-labeled antibodies to CD40 (3/23), CD80 (16-10A1), CD86 (GL1) or I-A^d (AMS-32.1) and appropriate isotype controls followed by FACS analysis (FACScan, BD Biosciences). All antibodies were from BD Pharmingen (BD Biosciences, San Jose, CA, USA).

2.26 Primer sequences

Table 2.1. Primer sequences

Bacterial expression	
MCMV ORF	Primer sequence
m17	A 5' GCTAGGGCTAGCCGTGCGCAGAACTGCGGCGTCAGTTTC B 5' GAGTCAGGATCCTTAGCTCGCGCAGCGTTTTGTTTTTGACTT
M37	A 5' GCTAGGGCTAGCCTCGGGGCCCGAATCGGGCGTCTTCGA B 5' GAGTCAAGATCTTTACTTGGGCAGGGGATCGCCGGCCACGTA
m90	A 5' GCTAGGGCTAGCGGCACGGCGGACTTATATACCTGGATA B 5' GAGTCAGGATCCTTAGGTGTAAGCCTCCTGGGGTTCTCTGCC
m145	A 5' GCTAGGGCTAGCAGCTACGATCAACGTACCCCCGGCGAC B 5' GAGTCAGGATCCTTACGTATCTACCGAATAGCCCGAGTAATA
m150	A 5' GCTAGGGCTAGCTCCCTGAACGATAGCTTTCCCCTCGTA B 5' GAGTCAGGATCCTTAGGCCGGCTCCCTCTCTGTCGTCGTTGC
m151	A 5' GCTAGGGCTAGCGCCGGGCTTCATGATGCGGTCACAAAG B 5' GAGTCAGGATCCTTAACAAGATCTTTTGCGACCGACATGCGA
m152	A 5' GCTAGGGCTAGCGGCGAGACGGCGGGCAGCAGCTATATG B 5' GAGTCAGGATCCTTACGCGGAGACGGGAGGAGCGTGCTTGAG
m153	A 5' GCTAGGGCTAGCGTCGTGCGGCCCGAAGTTAACAGGACG B 5' GAGTCAGGATCCTTAGGTCAGTCTCGAATCGTTGATCGTCCT
m155	A 5' GCTAGGGCTAGCATCGATTTACAAGACTATGATGATGAC B 5' GAGTCAGGATCCTTAGGCGTCGTTTAGGTACGGAACCACTTT
m159	A 5' GCTAGGGCTAGCTTCAGTCAGGAGTGTCTATACATGCCT B 5' GAGTCAGGATCCTTAGCTGCCCATGGGTAGCGGTCCGTAAGG
Insect cell expression	
pMT-Bip-V5-His / Drosophila S2 cells	
M37	A 5'*AGATCT*GGGCCCGAATCGGGCGTCTTCG B 5'*GGTACC*TCAATGGTGATGGTGATGATGCTTGTCATCGTCATCCTTGGGCAGGGGATCGCCGGCCAC
m151	A 5'*GGATCC*TCTGTGTGTGAGTCGCCGGTCCTCG B 5'*GGTACC*TCAATGGTGATGGTGATGATGGCTGCCGCGCGGCACCAGACAAGATCTTTTGCGACCGACATG
m153	A 5'*GGATCC*GAGGTCGTGCGGCCCGAAGTTAAC B 5'*GGTACC*TCAATGGTGATGGTGATGATGGCTGCCGCGCGGCACCAGGGTCAGTCTCGAATCGTTGATCGTC

pIEx-4 / SF9 cells	
m153	5'CGTCAC*CCATGG*CAATTCCCCTTCTCCTTCTGCCGTTGGTTCTC 5'ACTTCG*CTCGAG*GGTGAGTCTCGAATCGTTGATCGTCCTCTG
Interface Mutation primers	5'GACGGTGCTATACAGGCCATACGAGCCGTGACATCGGAATAC (T128A, S131A) 5'AGCGCCGGCCGGGACTCCGCTGCGATAGCCTTGTCCGCG (R225A) 5'ATCGAAGTGGCTGCCTATCTGCCGGTC (S241A)
Control mutation primers	5' GAAGATGACATTCTAGAAGCTGACATCGAGATGGATATCG (D194A, forward) 5' CGATATCCATCTCGATGTCAGCTTCTAGAATGTCATCTTC (D194A, reverse)
Mammalian expression	
Insertion of N-terminal FLAG tags	
ORF	Primer Sequence
m17	A 5'TCTAGTGGATCCATGGGGACGGGAGGAAAGGCGGACGGTACGTTCTCGGGTTTCTATCTG B 5'ACGTTCTCGGGTTTCTATCTGCTGTTCTGGCTCGCCCTCGCCGTGCGTGCGGACTACAAG C 5'GCCGTGCGTGCGGACTACAAGGATGACGATGACAAGCAGAACTGCGGCGTCAGTTTC D 5'TCGACTGAATTCTTAGACTTGGGGCAGACGCTGAAATCG
M37	A 5'CCTGCCAGATCTATGGTCCTGACACATAAGTCCGAATCTCGGGCGGATTCTCTCGTC B 5'TCTCGGGCGGATTCTCTCGTCAGGATGACAGCGGGGGGGCTCGGGATCGCGGCGGTG C 5'GGGCTCGGGATCGCGGCGGTGGCCACGCGTGCCACCACTCTCTGTTGTTGCCTCGCGATCGCC D 5'TGTTGTTGCCTCGCGATCGCCGCGCGGACGGCGGTCTCGGGGCCCGAATCGGACTAC E 5'TCGGGGCCCGAATCGGACTACAAGGATGACGATGACAAGGGCGTCTTCGAGTGCTCCTAC F 5'AGCGTCGAATTCTTACACGTTTTCCGCGGCGAAATC
m144	A 5'GCTACGGGATTCATGAGGGCTCTGGCGCTGATATGCGTGGTGTGGGTGTGTTGGCGAGAG B 5'GTGTGGGTGTGTTGGCGAGAGAGTTGCGCTCGCCACGGGGACTACAAGGATGACGAT C 5'CACGGGGACTACAAGGATGACGATGACAAGACAGAGGACTCGTCCGAGTCCGGACTG D 5'TACGCTGAATTCTTAAATGCTGGGATCCGGGACCGTGACGAT
m145	A 5'ACGGCTGGATCCATGGACCGTCGGGTGGTCTCATACCTAATGTGCGCCTTG B 5'TCATACCTAATGTGCGCCTTGGCGGTTTCGTTCGCTAGCTACGATTAC C 5'TCGTTCGCTAGCTACGATTACAAGGATGACGATGACAAGCAACGTACCCCCGGCGACGTA D 5'ACAGTTGAATTCTTACGCCTCTATCGTCTTATACCA
m152	A 5'GCTACGGGATTCATGATTGGCGTGATACGTGCGCTCGTGTGGTGGACTTTGGTG B 5'CTCGTGTGGTGGACTTTGGTGAAGACGACCGCAGCCTCTGTGGACTACAAG C 5'GCAGCCTCTGTGGACTACAAGGATGACGATGACAAGTGTGAGTCGCCGGTCCTCGTT D 5'TACGCTCAATTGTTATCGAAAGCTGAGCTCGCTGTGGGA
m152	A 5'GGATCCATGCTGGGCGCTATCACCTACTTGCTCCTCTCGGTTCTCATAAAC B 5'CTCCTCTCGGTTCTCATAAACCGAGGCGAGACGGCGGGCGACTACAAG C 5'GAGACGGCGGGCGACTACAAGGATGACGATGACAAGAGCAGCTATATGGACGTGCGC D 5'GAATTCTTACCACACGCGGCAGTTGATGTA
m153	A 5'GCTACGGGATCCATGATTCCCCTTCTCCTTCTGCCGTTGGTTCTCATCTCAGGAGGG B 5'TTGGTTCTCATCTCAGGAGGGTTCTGGGCGTGCGGCTCAGCGGAGGTCGACTACAAG C 5'TCAGCGGAGGTCGACTACAAGGATGACGATGACAAGGTGCGGCCCGAAGTTAACAGG D 5'TACGCTGAATTCTTACACCACATTCTCCTCCGTATCCGAGCA
m155	A 5'GGATCCATGTCTGTACGAGTATGTGCTCTCCTGCTCTTGATCGCT B 5'CTCCTGCTCTTGATCGCTTGTGCCTACGCCTACATCGATTACAAG C 5'TACGCCTACATCGATTACAAGGATGACGATGACAAGTTACAAGACTATGATGATGAC D 5'CAATTGTTATTTGTAGACGGGCGGGACGCT
Insertion of N-terminal HA-tag	
m153	A 5'GCTACGGGATCCATGATTCCCCTTCTCCTTCTGCCGTTGGTTCTCATCTCAGGAGGG B 5'TCAGCGGAGGTCTACCCATACGATGTTCCAGATTACGCTGTGCGGCCCGAAGTTAACAGG C 5'TTGGTTCTCATCTCAGGAGGGTTCTGGGCGTGCGGCTCAGCGGAGGTCTACCCATAC D 5'TACGCTGAATTCTTACACCACATTCTCCTCCGTATCCGAGCA

m153-EYFP fusion	
Forward Reverse	A 5'ACG*GGATCC*ATGATTCCCCTTCTCCTTCTGCCG B 5'ACG*GAATTC*GCACCACATTCTCCTCCGTATCCG
BiFC constructs	
m144_5YFP m144_3YFP	A 5'ACG*AGATCT*ATGAGGGCTCTGGCGCTG B 5'ACG*GAATTC*GCAATGCTGGGATCCGGGACCGTG
m153_5YFP m153_3YFP	A 5'ACG*GGATCC*ATGATTCCCCTTCTCCTTCTGCCG B 5'ACG*GAATTC*GCCACCACATTCTCCTCCGTATCCG
m144 and m153 – human zeta chain fusion constructs	
153_YFP 153-hzeta-reverse	5'ACG*GGATCC*ATGATTCCCCTTCTCCTTTCTGCCG 5'TCCATCCAGCAGGTAGCAGAGTTTGGTCAGTCTCGAATCGTTGATCGTCCTCTGG
153_hzeta_forward human_zeta_reverse	5'CCAGAGGACGATCAACGATTCGAGACTGACCAAACTCTGCTACCTGCTGGAT 5'*GAATTC*TTAGCGAGGGGGCAGGGCCTGCATGTGAAC
m144_5YFP human_zeta_reverse	5'ACG*AGATCT*ATGAGGGCTCTGGCGCTG 5'*GAATTC*TTAGCGAGGGGGCAGGGCCTGCATGTGAAG

CHAPTER 3

CHARACTERIZATION AND RECOMBINANT EXPRESSION OF PREDICTED MHC-I-LIKE PROTEINS ENCODED BY MCMV

3.1 Introduction

The predicted MHC-I-like proteins of MCMV comprise m144, eight members of the m145 family (m17, m145, m150, m151, m152, m153, m155 and m157) and three additional proteins of unknown function M37, m90 and m159. We did not include m157 in our characterization experiments, since several other groups were already studying it. m144, previously studied in the laboratory, was used as a control in some experiments.

The MCMV MHC-I-like proteins all have putative N-terminal signal sequences, transmembrane regions or in the case of m157, a GPI-anchor signal sequence, and N-linked glycosylation sites (Rawlinson et al., 1996). It is therefore likely that they are cell surface expressed molecules, similar to classical MHC-I proteins. However, the capacity of proteins like m145, m152 and m155 to cause downregulation of host proteins argues that the family members may localize either to the surface or remain inside the cell, in the secretory/surface pathway, depending on their function. To learn more about the cellular expression of the MCMV m145 family we used transient transfection studies in mammalian cells. As a first step to examine the relationship of these proteins to classical MHC-I molecules, we determined whether the proteins are expressed predominantly inside the cell or at the cell surface. MHC-Ia proteins are only stably expressed at the cell surface when they have peptide bound in the $\alpha1\alpha2$ domain groove and are associated with the $\beta2$m light chain. We therefore evaluated whether the viral proteins are

dependent on association with β2m or the availability of peptides in the ER for stable surface expression.

We applied bioinformatics to predict the soluble extracellular domain of the viral MHC-I-like molecules and tested different recombinant expression systems to identify the optimal expression system for this protein family, identify the best candidates for structure determination and obtain suitable material for crystallization trials.

3.2 Results

3.2.1 Localization of MCMV MHC-I-like proteins in transfected cells

The cellular localization of several members of the m145 family as well as M37 was studied in transfected cells. Constructs encoding N-terminally FLAG-tagged molecules were transfected into COS-7 cells and the surface expression of the proteins was assessed 48 h post transfection by staining with the FLAG-specific monoclonal antibody M2 and flow cytometry analysis. Due to technical difficulties m90, m150 and m159 could not be studied in the transfection experiments. Of the six m145 family members tested, m145, m151 and m153 were localized predominantly at the cell surface. M37 was also detected readily at the cell surface (Figure 3.1A). m144, which is expressed on the surface of MCMV-infected cells (Andrews et al., 2001), was used as a positive control for surface localization. The percentage of cells that expressed m17, m152 and m155 at detectable levels at the cell surface ranged from 10 to 36%. Subsequent intracellular staining for m152 and m155 confirmed that these proteins are more abundant inside the cell than on the surface (Figure 3.1B), consistent with the observation that they cause the retention of NKG2D ligands Rae-1 and H60 in MCMV infected cells (Hasan et al., 2005; Lodoen et al., 2003). Thus even though the m145 family members all have predicted signal peptides and transmembrane regions, their localization is not necessarily at the cell surface and is probably dictated by their individual functions.

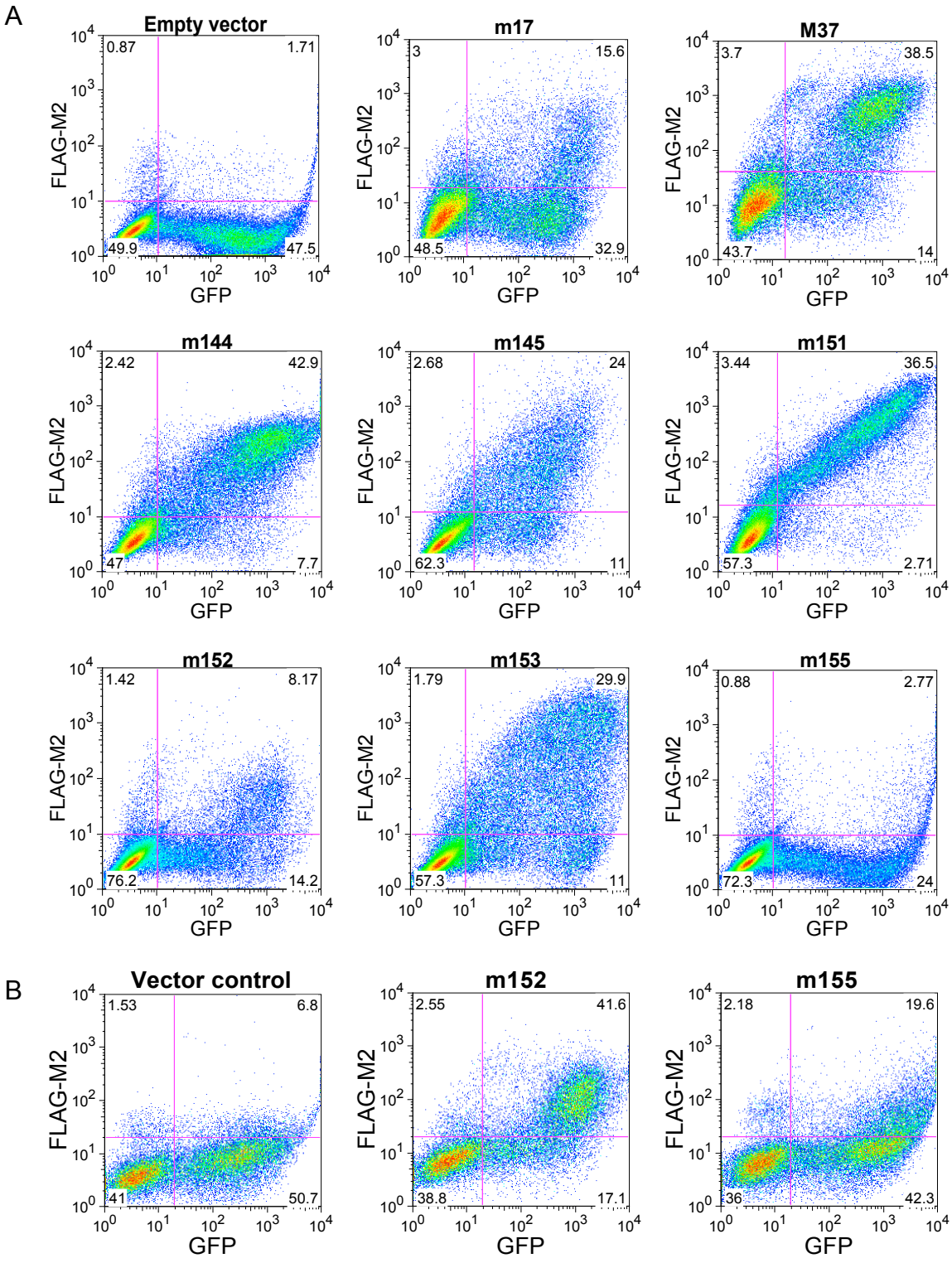

Figure 3.1. Cellular localization of MCMV MHC-I-like glycoproteins in transfected COS-7 cells. A) pIRES-GFP vectors encoding N-terminally FLAG-tagged constructs of the indicated proteins were transfected into COS-7 cells. Surface expression was evaluated 48 h after transfection by staining with the anti-FLAG M2 monoclonal antibody and anti-mouse IgG_1-PE followed by FACS analysis. B) Intracellular staining of COS-7 cells transfected with m152- or m155-pIRES-GFP using the same antibodies as in A. Experimental details are described in Chapter 2, section 2.5.

3.2.2 Cell surface expression of M37, m145, m151 and m153 is independent of β2m and TAP expression

Since the MHC-I fold was predicted for all members of the MCMV m145 family as well as M37 (Smith et al., 2002), we next determined whether the MCMV proteins that localize to the cell surface (m145, m151, m153 and M37), share the requirements of classical MHC-I molecules for β2m and peptide for stable expression. To investigate their requirement for β2m we transfected N-terminally FLAG-tagged constructs into a cell line deficient in β2m (R1E (Allen et al., 1986)) as well as its β2m sufficient counterpart (R1.1). The surface expression of all four proteins was equivalent in both cell types indicating that none of them require β2m for stable surface expression (Figure 3.2).

To evaluate the requirement for bound peptide we examined surface expression of M37, m145, m151 and m153 in RMA-S, a TAP deficient cell line that fails to transfer peptides from the cytosol to the ER (Townsend et al., 1989). MHC-Ia molecules expressed in such cells are unstable at the cell surface. We transfected RMA-S and RMA (TAP^+) cells with each of the four FLAG-tagged constructs and evaluated surface expression of the viral proteins in comparison to transfected H-$2D^d$, an MHC-Ia molecule (Figure 3.3). TAP deficiency had no effect on M37, m145, m151 or m153 surface expression, whereas expression of H-$2D^d$ was clearly reduced. We conclude that these MCMV proteins do not require β2m or bound peptide for stable surface expression. The structural implication of this finding is that these MCMV proteins fold properly and have a compact three-dimensional structure in the absence of peptide or β2m.

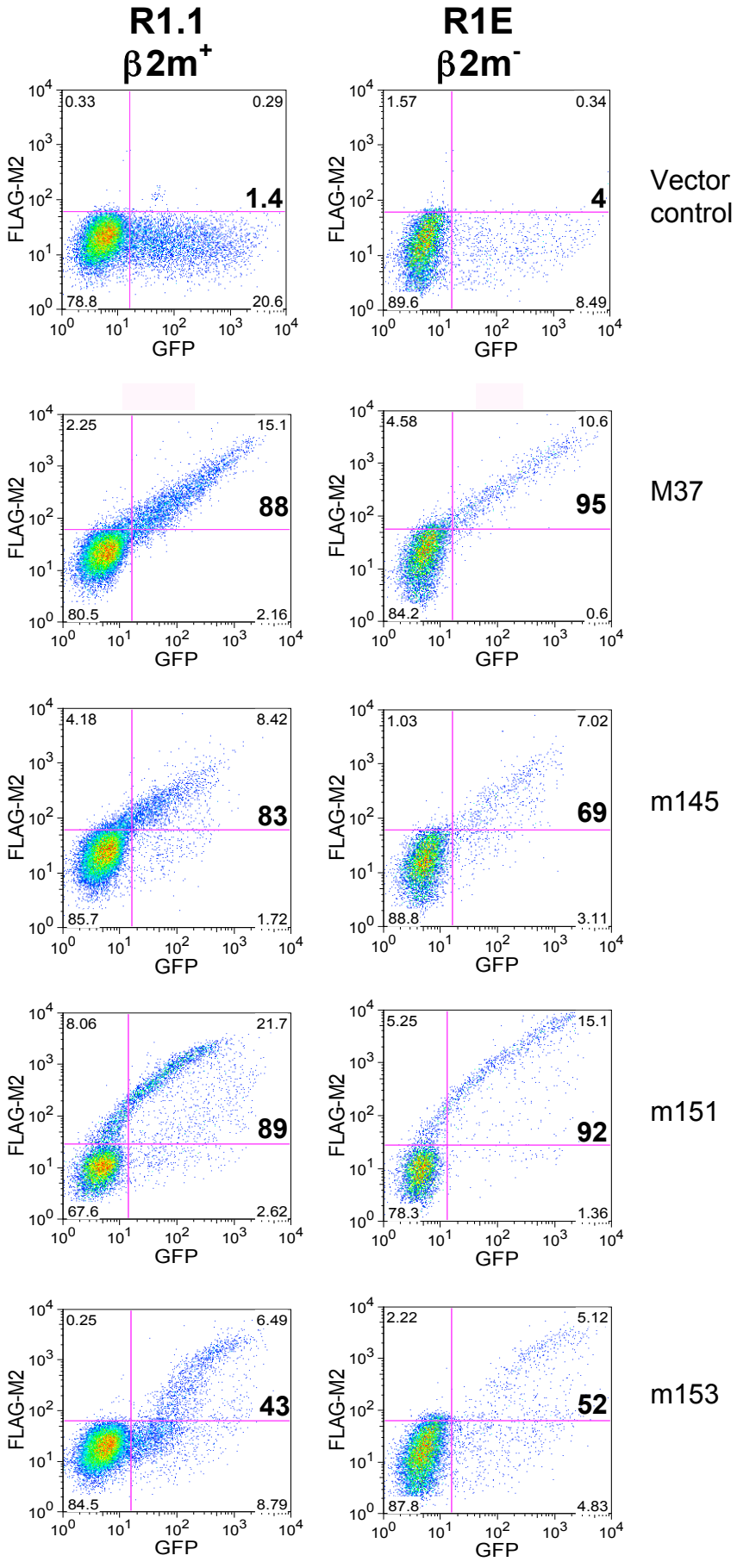

Figure 3.2. Surface expression of MCMV MHC-I-like proteins is independent of β2m.
R1.1 ($\beta2m^+$) and R1E ($\beta2m^-$) cells were transfected with the indicated FLAG-tagged viral genes in pIRES-GFP or H-$2D^d$-pIRES-GFP as a control. Eighteen hours post transfection surface levels of the viral proteins and H-$2D^d$ were determined as described in Chapter 2, section 2.6. The number of GFP positive cells indicates transfection efficiency. The percentage surface expression is indicated in bold in the upper right quadrant (percentage of GFP^+ cells that stain for either FLAG-M2 or H-$2D^d$). The results are representative of at least two independent experiments.

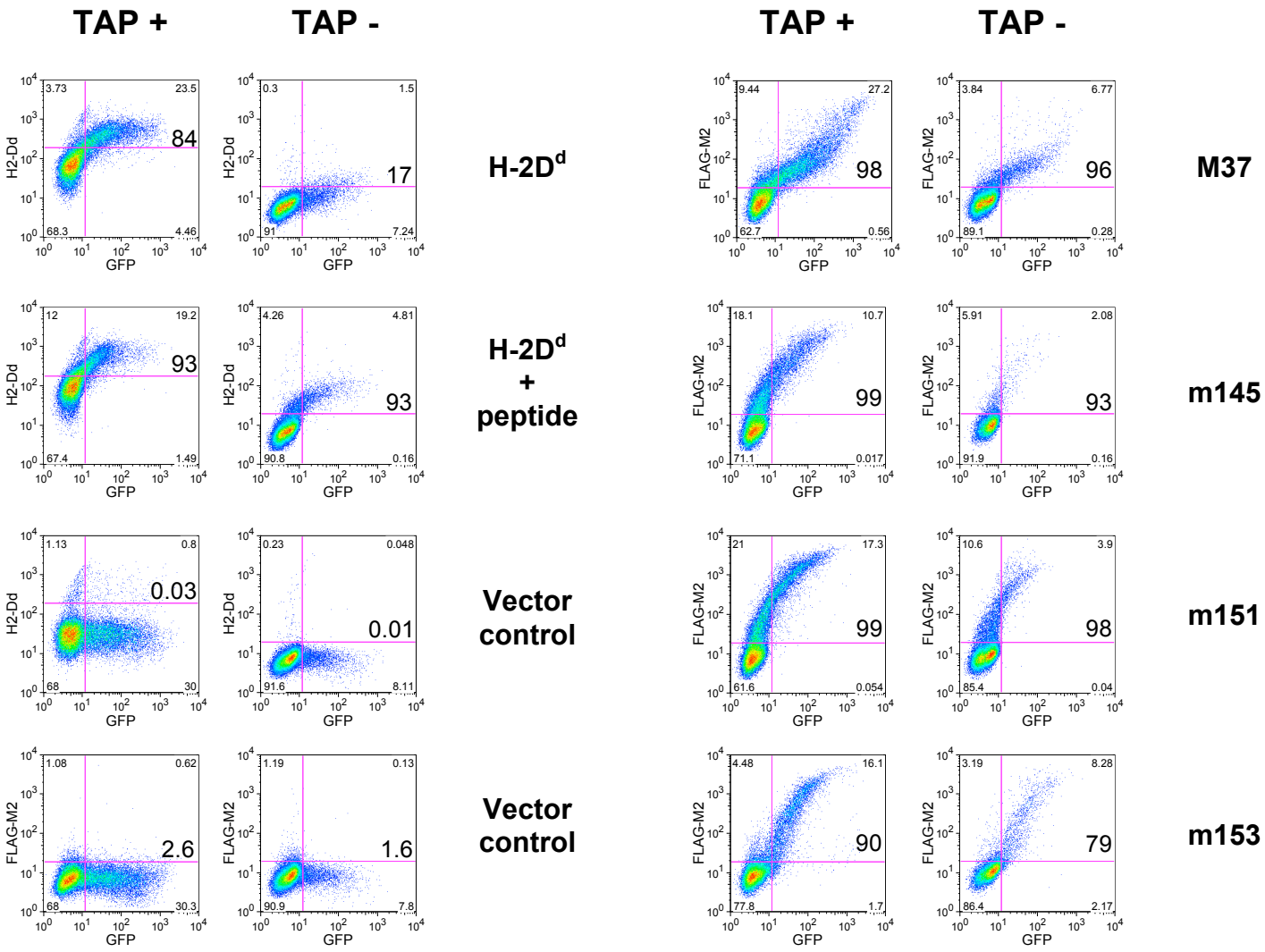

Figure 3.3. TAP-independent cell surface expression of M37, m145, m151 and m153. RMA (TAP^+) and RMA-S (TAP^-) cells were transfected with the indicated FLAG-tagged viral genes in pIRES-GFP or H-$2D^d$-pIRES-GFP as a control. Eighteen hours post transfection surface levels of the viral proteins and H-$2D^d$ were determined as described in Chapter 2, section 2.6. The number of GFP positive cells indicates transfection efficiency. The percentage surface expression is shown in the upper right quadrant in bold (percentage of GFP^+ cells that stain for either FLAG-M2 or H-$2D^d$). The results are representative of at least two independent experiments.

3.2.3 Cell surface MHC-I levels are downregulated by m152 and to a lesser extent, by m153

It has long been known that m152 downregulates surface MHC-I in MCMV-infected cells. To determine whether any of the other m145 family members have an effect on MHC-I expression, we transfected NIH3T3 fibroblasts with the FLAG-tagged constructs encoding the individual family members and 18 h after transfection stained the cells for H-2D^q expression (Figure 3.4). As expected, m152 reduced the surface levels of H-2D^q significantly in the majority of transfected cells. The only other family member that affected MHC-I expression was m153.

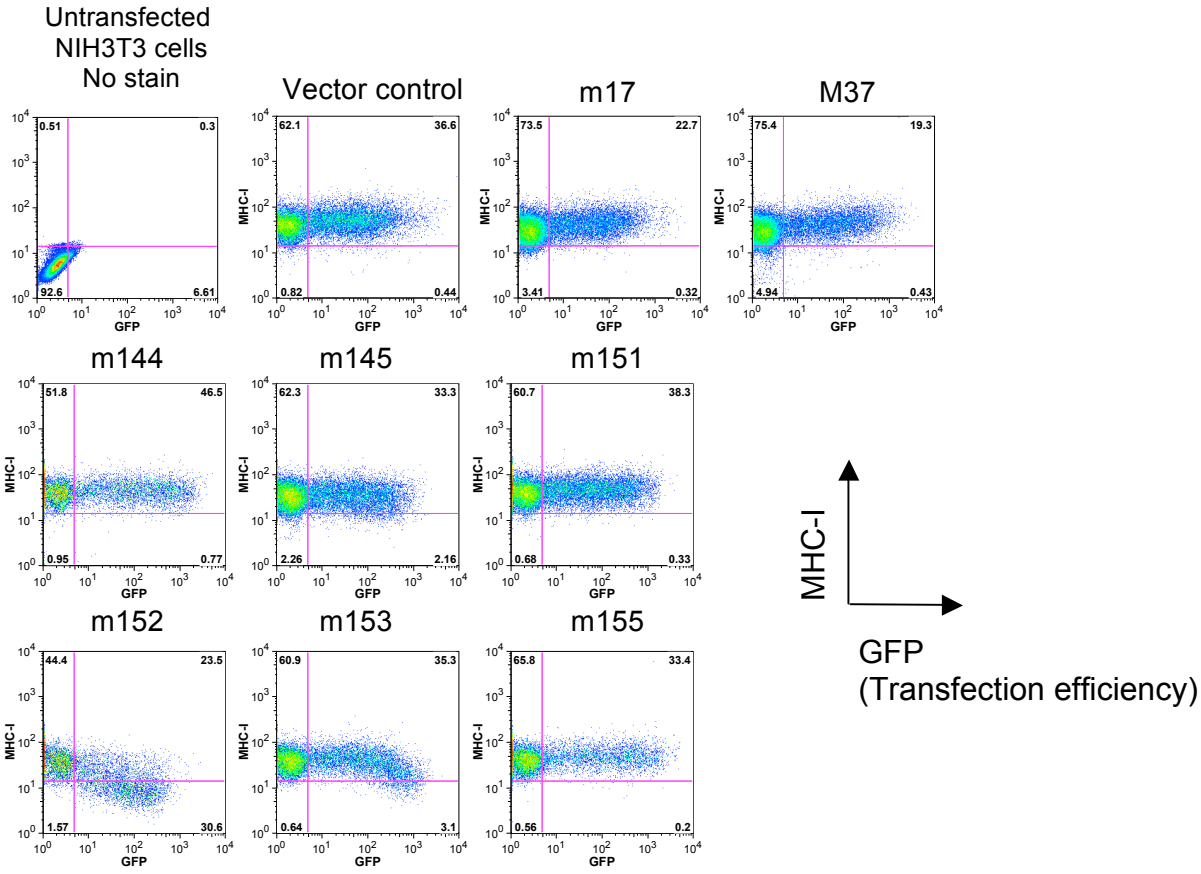

Figure 3.4. Effects of different m145 family members on MHC-I surface expression. FLAG-pIRES-GFP constructs of the indicated viral proteins were transfected in NIH3T3 cells. Eighteen hours after transfection the cells were surface stained for MHC-I (H-2D^q) expression (for details see Chapter 2, section 2.5) and analyzed by flow cytometry.

The effect of m153 on MHC-I surface expression levels was only observed in GFP-bright cells (Figure 3.4). Since GFP and m153 expression is linked in the pIRES-GFP vector, the GFP-bright population should represent cells that express high levels of m153. MHC-I expression is thus only affected when a very high concentration of m153 is present. This effect was not observed for any of the other family members, and is therefore unlikely to be an artefact of the transfection system. In conclusion, even though m153 causes significant reduction in the surface MHC-I levels, it does not downregulate MHC-I expression to the same extent as m152 (Figure 3.5).

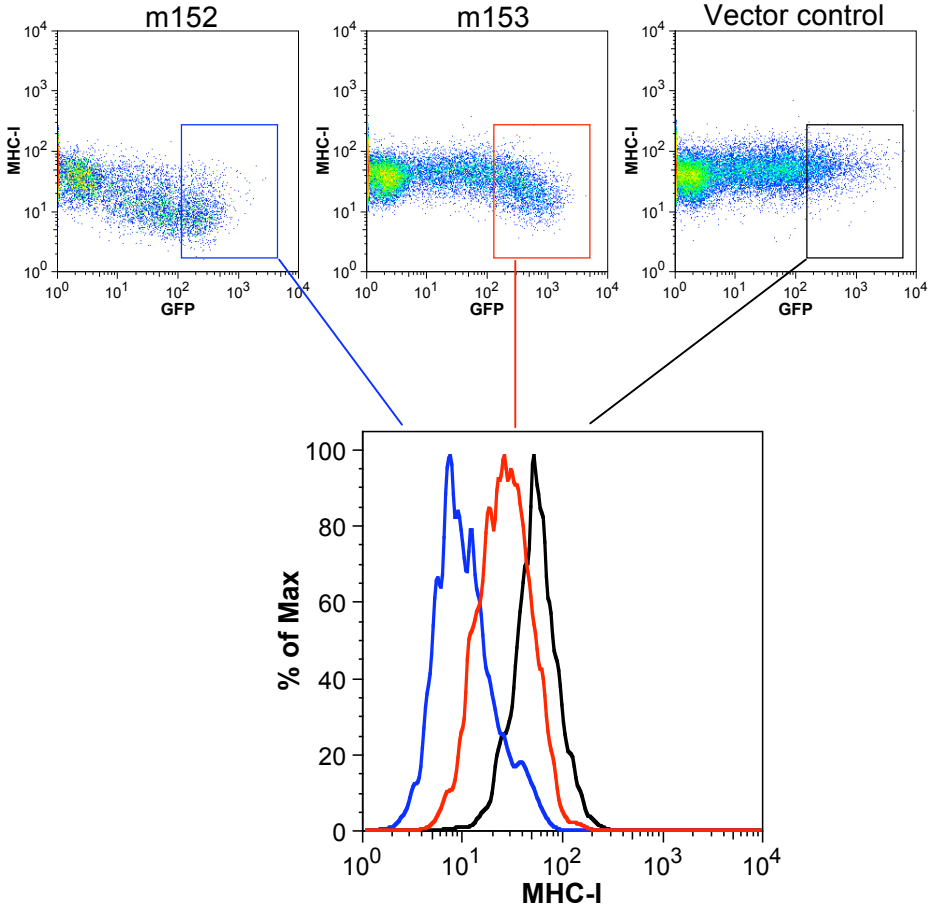

Figure 3.5. Comparison of the MHC-I expression levels on the GFP-bright populations in m152-, m153- or vector control-transfected NIH3T3 cells.

3.2.4 Optimization of recombinant expression of MCMV MHC-I homologs for structural characterization

Bacterial expression in insoluble inclusion bodies is a widely used approach to generate protein material for structural studies (Yokoyama, 2003) and the majority of the protein structures available in the Protein Data Bank (PDB) were determined from bacterially expressed recombinant proteins. Inclusion bodies, the insoluble product of the highly expressed recombinant protein, are frequently highly enriched with the recombinant protein accounting for as much as 75-90% of their content. If a protein can be refolded successfully from bacterial inclusion bodies, relatively high yields of protein can be prepared in a short time. Since bacterially expressed proteins lack glycosylation, the preparations are highly homogeneous and therefore more likely to crystallize than glycosylated insect- or mammalian-cell expressed proteins. Another advantage of bacterial expression is that it allows for the quick generation of various mutant proteins.

MHC-I molecules can be expressed in bacteria and refolded from inclusion bodies in combination with β2m and peptide (Garboczi et al., 1992). Thus, we first tested expression of the predicted MCMV MHC-I homologs in bacteria.

3.2.4.1 Expression in bacterial inclusion bodies

The extracellular domains (ECD) of the MCMV encoded MHC-I homologs were predicted with the SignalP 3.0 server, that recognizes signal peptides (Bendtsen et al., 2004), and the Kyte/Doolittle hydrophilicity plots of the MacVector program (Olson, 1994) that predicts the transmembrane regions (Table 3.1). The ECD of each of the proteins were cloned in the pET21b bacterial expression vector.

Table 3.1. Predicted extracellular domains of the MCMV MHC-I homologs.

MCMV ORF	Predicted extracellular domain		
	Size (kDa)	Signal peptide (SignalP 3.0 server)*	Transmembrane domain (Macvector)
m17	33.7	MGTGGKADGTFSGFYLLFWLALAVR	GQLCVHLGQILNLALIFLPIFAICLILNLCI
M37	27.3	MVLTHKSESRADSLVRMTAGGLGIAAVATRA TTLCCCLAIAARTAVS	KMVGMFFFVFGGLALLILFCFMT
m90	23.3	MDSARRNTSSRVSCSMPAFLSSPRITFMLLG VLLCFALASGGTA	TFLHVLIAFLFCIGTGLIVCLYAIL
m145	44.9	MDRRVVSYLMCALAVSFA	TPTLVAMFVAVTALCICAMVFCYYC
m150	27.4	MCIVAVLSHSLSTSVVMAVVRVRTWGVILVC YFIVRNASA	ACGMELSLVTVVAIVSTFTVLKGVLCAYVF
m151	33.3	MIGVIRALVWWTLVKTTAA	CSLLYLLAVPAVLLVVLSSVVIF
m152	33.9	MLGAITYLLLSVLINRGET	EYSIFFMDVWSLIAIGVVFVIVFMYLVKLRVVWIN
m153	37.4	MIPLLLLPLVLISGGFWACGSA	TTVTIAITVAAFVALFVVVGLLVHGIV
m155	34.1	MSVRVCALLLLIACAYAYIDL	AELIINVTYTLLVVLCVLLVVMCWM
m159	37.2	MWTTSYFLIGLGTLVLS	EVPVMLVAAIVAVLVVFLMIGCIGFCSFV

*The SignalP 3.0 server: http://www.cbs.dtu.dk/services/SignalP

The expression of the MHC I-like proteins listed in Table 3.1 was evaluated in BL21 DE3 *E. coli* cells. Only m90 could be expressed in the BL21 DE3 cells (data not shown). We next tested expression in the Rosetta DE3 strain of *E. coli*. The Rosetta strain contains the pRARE plasmid, which encodes tRNAs for six rare mammalian codons, and enables the expression of proteins that are limited by codon usage (Brinkmann et al., 1989; Kane, 1995). Seven of the viral proteins could be expressed at varying levels in the Rosetta DE3 strain of *E. coli* (Figure 3.6).

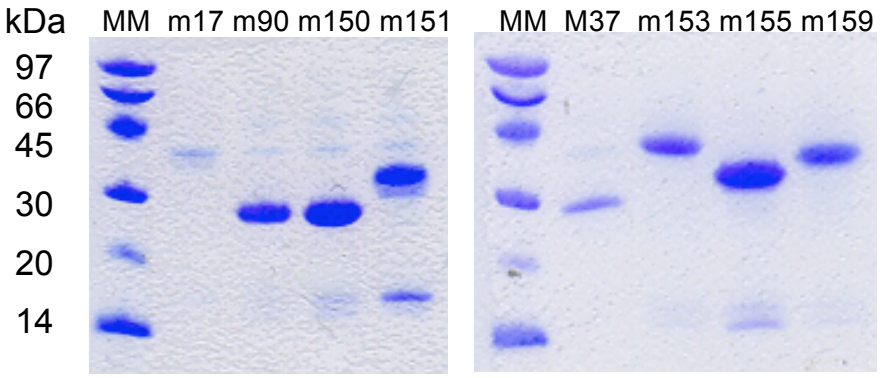

Figure 3.6. SDS-PAGE analysis of MCMV MHC-I-like proteins expressed in Rosetta DE3 *E. coli*. Inclusion bodies were solubilized in SDS-PAGE sample buffer and separated on a 20% acrylamide gel. The proteins were visualized by Coomassie brilliant blue staining. The sizes of the molecular weight markers (MM) are indicated in kDa. Experimental details in Chapter 2, section 2.11.

The identity of the dominant protein present in each inclusion body preparation was confirmed by N-terminal sequencing (Table 3.2)

Table 3.2. Summary of expression of MCMV MHC-I homologs in bacterial inclusion bodies.

MCMV ORF	BL21 DE3	Rosetta DE3	N-terminal sequence *
m17	-	-	-
M37	-	+	#
m90	+	+	XTADLYT(T)IQATP
m145	-	-	-
m150	-	+	XLNDSFPLVRIDG
m151	-	+	AGL(H)DAVTK
m152	-	-	-
m153	-	+	VV(I)PEVN(N)TGXVD
m155	-	+	IDLQDYXDDNNX(Y)
m159	-	+	FSQE(I)LYMPQINL

*The identity of each expressed protein was verified by N-terminal sequencing
X – no amino acid identified, ( ) – possible amino acid
Due to low yields the N-terminal sequence could not be determined

We attempted to refold the proteins from inclusion bodies by rapid dilution into a 0.4 M arginine refolding buffer generally used to refold MHC class I molecules (Garboczi et al., 1992). After 4 days of refolding at 4 °C the proteins were dialyzed against Tris-buffered saline, pH 8 and concentrated before analysis of the efficiency of refolding with

size exclusion chromatography (SEC). The proteins precipitated from the refolding solution at different stages as summarized in Table 3.3.

Table 3.3. Behavior of the MCMV proteins during the different steps of refolding.

MCMV Protein	Dilution in Arginine	Dialysis against TBS	Concentration of refolded protein
M37	Small precipitates	Lots of fine precipitation	Large precipitate
m90	Clear	Small precipitates	Large precipitate
m150	Clear	Small precipitates	Large precipitate
m151	Clear	Small precipitates	Small precipitate
m153	Clear	Clear	Small precipitate
m155	Clear	Large precipitate	-
m159	Large precipitate	-	-

Experimental details are described in Chapter 2, section 2.11.

Analysis of the recovered, refolded proteins by SEC revealed that the majority of every protein had aggregated and eluted at a retention time corresponding to a very large size (150 – 650 kDa). The SEC profile obtained for m151 is representative of the other proteins and is presented in Figure 3.7. No significant elution of protein at the retention time corresponding to 30 - 40 kDa was observed for any of the expressed proteins. To optimize the refolding conditions we used the FoldIt Screen from Hampton Research. We screened a number of refolding conditions for m153 and at a small scale a few conditions showed promise, but upon large-scale refolding the proteins again formed aggregates (data not shown). Therefore bacterial expression could not be used to generate large quantities of the MCMV MHC-I-like proteins for structural characterization.

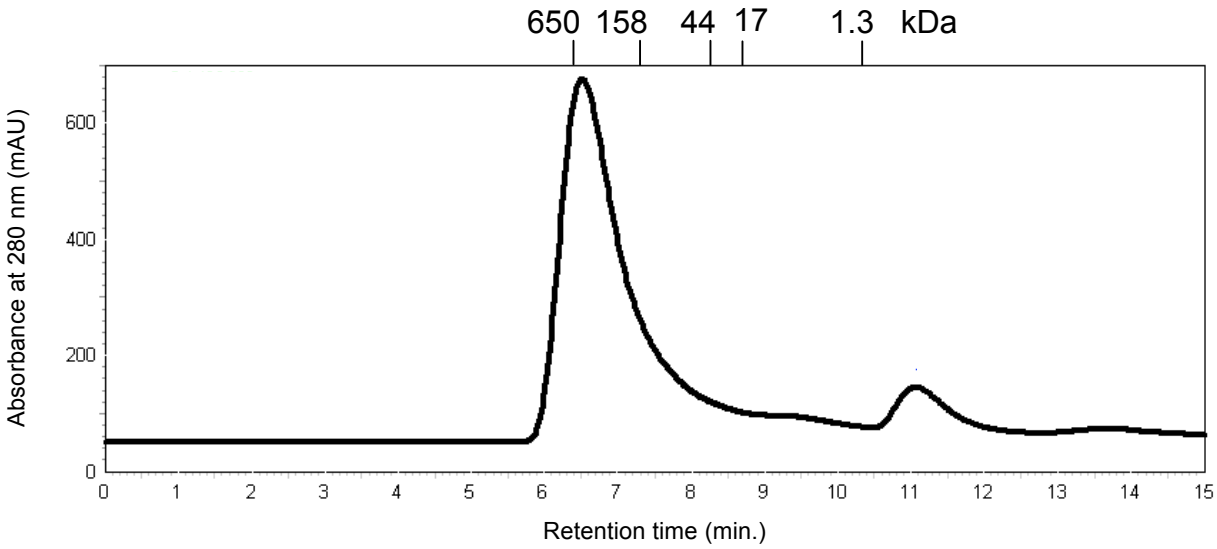

Figure 3.7. Size-exclusion chromatography of m151 after refolding from bacterial inclusion bodies. The major protein peak elutes at a retention time of 6.6 min. and represents aggregated material. The distribution of several size markers (kDa) is indicated above the graph.

3.2.4.2 Insect cell expression

Since M37, m151 and m153 were shown to localize to the cell surface (Figure 3.1) and are therefore likely to engage cell surface receptors on other cells, we focused on these three proteins for further recombinant expression studies. The extracellular domains of M37, m151 and m153 were expressed as secreted proteins in stably transfected Schneider S2 Drosophila cells. A C-terminal 6x histidine tag facilitated purification of the expressed proteins from culture supernatants on nickel-NTA columns. Subsequent purification steps consisted of size exclusion chromatography, protease cleavage to remove the histidine tag and anion-exchange chromatography. The identity of each protein was confirmed by N-terminal amino acid sequencing (Table 3.4).

Table 3.4. N-terminal sequence of M37, m151 and m153 that were expressed in insect cells

M37	RSGPESGVFEESYDV
m151	RSSVXESPVLVLTAS
m153	EVVRPEVNRTGRVDI

SDS-PAGE analysis of the three proteins confirmed their predicted sizes (Figure 3.8), with m151 and m153 migrating at a slightly higher molecular weight, possibly indicating glycosylation of the proteins in the insect cells.

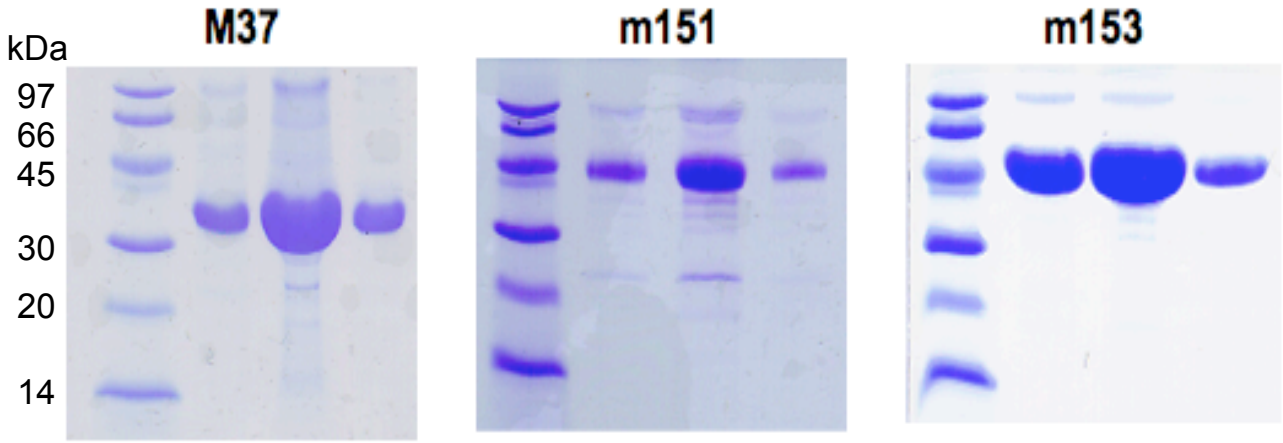

Figure 3.8. SDS-PAGE analysis of insect cell-expressed M37, m151 and m153. The His-tagged MCMV proteins were purified from S2 supernatants on Ni-NTA affinity columns as described in Chapter 2, section 2.12. Fractions eluted from the nickel columns were analyzed on 20% SDS-PAGE gels and visualized by Coomassie staining. The size markers (kDa) are indicated.

M37 and m153 expressed at very high levels in the S2 cells and could easily be purified to homogeneity (Figures 3.9 and 3.10). Although m151 was expressed at appreciable levels, SEC analysis revealed that a significant amount of the protein had formed aggregates (Figure 3.9, upper right panel). Some m151 of the predicted size of 30 kDa could be purified, but the yield was very low and the protein also tended to aggregate

upon storage (data not shown). M37 eluted at the expected retention time during SEC analysis (Figure 3.9). SEC analysis of m153 indicated a larger than expected size for the protein. This result will be addressed in more detail in the following chapter. Final anion-exchange purification yielded highly homogeneous protein suitable for crystallization trials for both M37 and m153 (Figure 3.10).

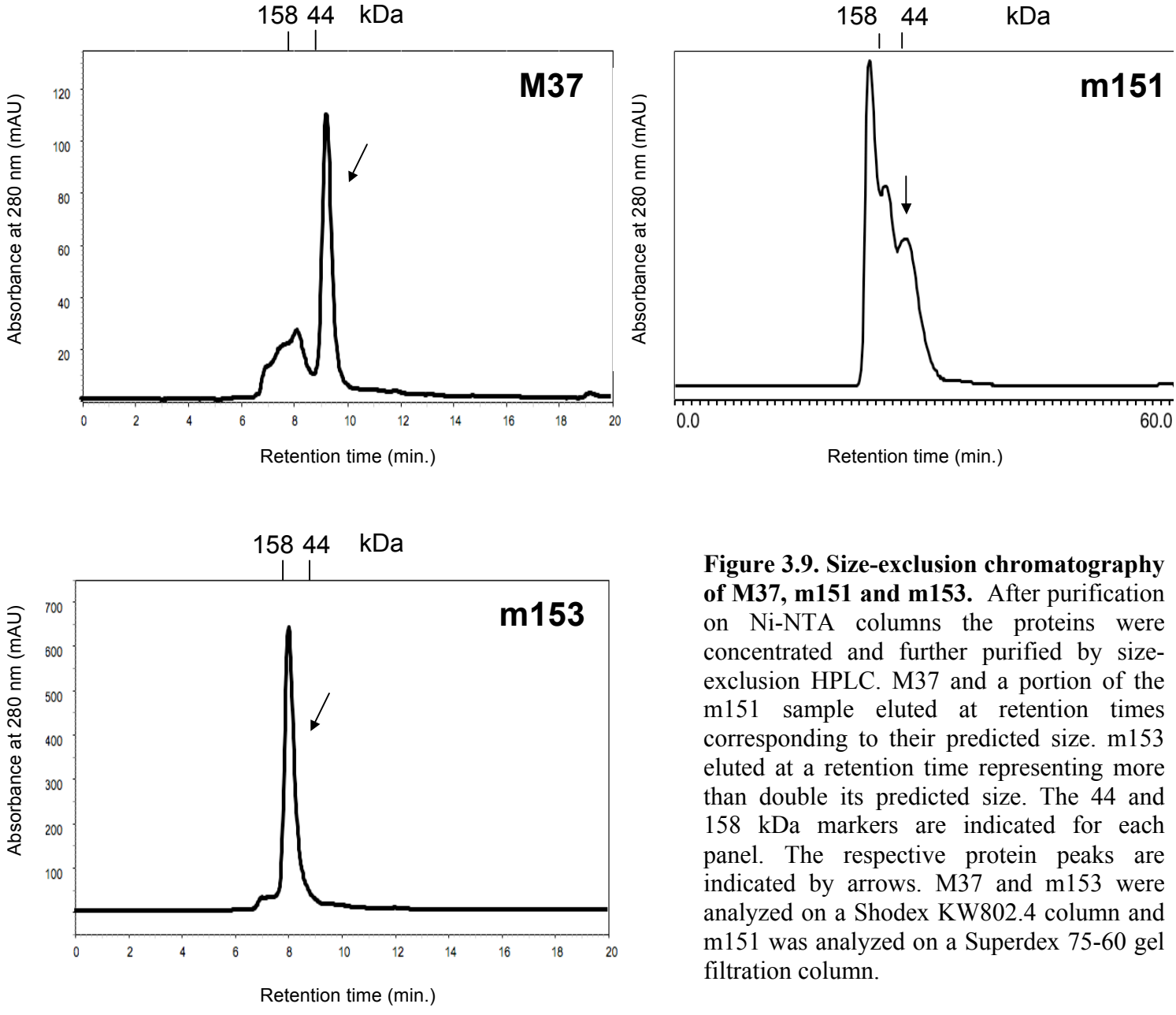

Figure 3.9. Size-exclusion chromatography of M37, m151 and m153. After purification on Ni-NTA columns the proteins were concentrated and further purified by size-exclusion HPLC. M37 and a portion of the m151 sample eluted at retention times corresponding to their predicted size. m153 eluted at a retention time representing more than double its predicted size. The 44 and 158 kDa markers are indicated for each panel. The respective protein peaks are indicated by arrows. M37 and m153 were analyzed on a Shodex KW802.4 column and m151 was analyzed on a Superdex 75-60 gel filtration column.

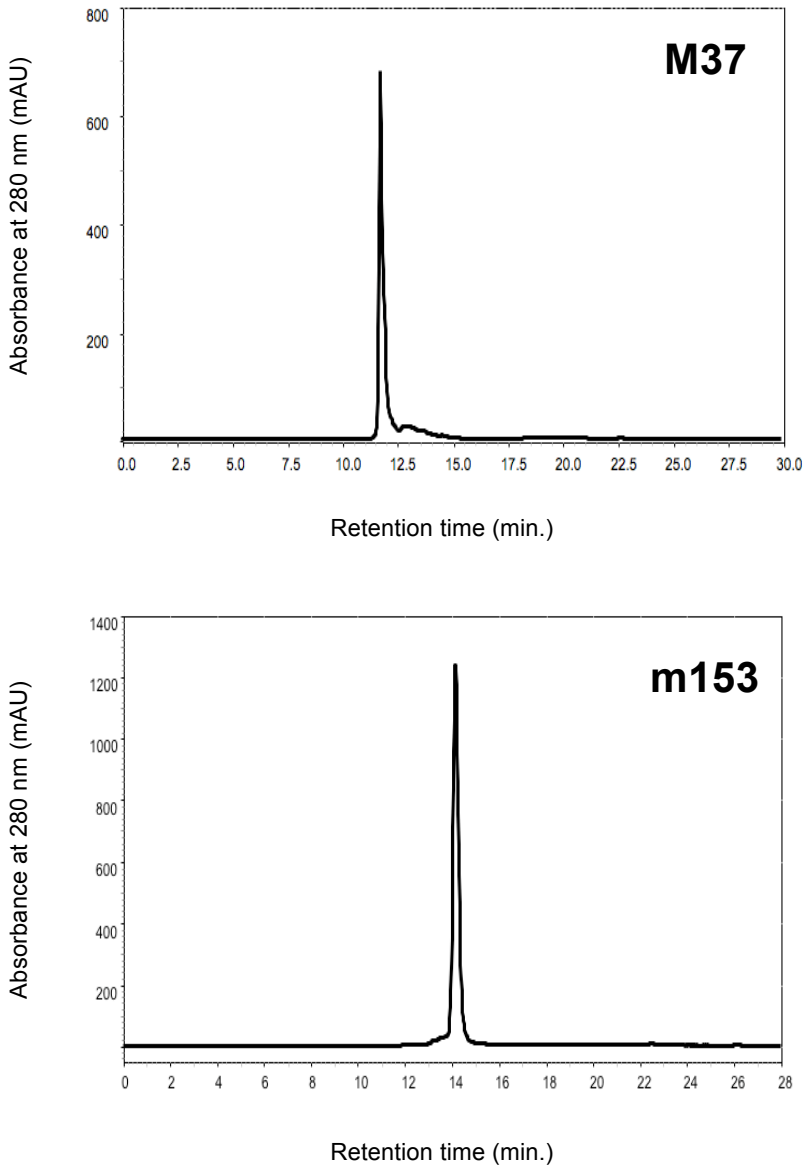

Figure 3.10. Anion-exchange chromatography of M37 and m153. The proteins were eluted from a Mono Q column with a 0-1 M NaCl gradient from 5 to 25 minutes.

Insect cell expression thus seems to be a more successful approach to express the MCMV viral MHC-I molecules than bacterial expression, and we have since also expressed m152 successfully in this system (data not shown).

3.3 Discussion

As a basis for studying the structure and function of the MCMV MHC-I-like proteins we have analyzed their expression and localization in transfected mammalian cells. Our results indicate that of the m145 family, m17, m152 and m155 are predominantly intracellular proteins. In contrast, m145, m151 and m153 are detected at the cell surface in the majority of transfected cells. m157 has been shown to be a GPI-linked, surface-expressed molecule (Tripathy et al., 2006). Apart from the m145 family members, we have also studied M37 and found that it is mostly expressed at the cell surface. The cellular localization of the individual viral proteins to some extent correlates with their known functions. In the case of m152 and m155, their intracellular location is probably linked to the mechanisms they use to retain MHC-I and/or NKG2D ligands in infected cells. The cell surface localization of m145, on the other hand, suggests that it uses a distinct mechanism from the other immunoevasins to downregulate MULT-1 from the cell surface.

We have used cell lines deficient for either β2m or TAP to show that M37, m145, m151 and m153 can be expressed stably at the cell surface in the absence of these molecules. In support of this, it has been reported that m157 cell surface expression is also independent of β2m and TAP expression (Tripathy et al., 2006). So far, m144 is the only MCMV MHC-I-like protein that does associate with β2m and the crystal structure of m144 was determined in complex with β2m. The initial characterization of the MCMV MHC-I-like molecules suggests that they have adapted the MHC-I fold to achieve stability in the absence of β2m and peptide, like several other non-classical MHC-I molecules. We have also tested the effect of transfection of the different MCMV proteins

on endogenous MHC-I surface expression levels in mouse fibroblasts. Apart from the expected substantial downregulation by m152 (Ziegler et al., 1997), the only family member that reduced MHC-I surface expression is m153. The effect is much less pronounced than that of m152 and is only observed in cells expressing very high levels of m153. It is interesting though, because m152 and m153 are most related to each other within the m145 family.

Our first approach to generate protein material for structural studies was to express the viral proteins as insoluble inclusion bodies in bacteria. This strategy proved unsuccessful. Although several proteins could be expressed in the bacterial system, we were unable to refold any of the viral proteins. Since we had established by this time that M37, m151 and m153 are surface expressed proteins we decided to focus on them and tested the expression of these three proteins in *Drosophila* insect cells. The S2 system provides the advantage that disulfide-containing proteins are expressed faithfully. We selected an expression vector that utilizes the signal sequence of the BiP chaperone (Kirkpatrick et al., 1995) and directs the expression of the foreign gene from a copper-inducible promoter (Johansen et al., 1989). One drawback of the system is the long time it takes to generate stable clones that express the protein of interest. In addition, proteins expressed in insect cells are glycosylated, and that could adversely affect crystallization.

All three proteins expressed at significant levels in S2 cells. m151 had a tendency to aggregate and only a small fraction of the correctly folded, soluble protein could be isolated. In contrast, the M37 and m153 preparations consisted mostly of the correct soluble species and could be purified to homogeneity with ease. To our surprise m153 seemed to exist as a dimer, based on SEC analysis. We screened a range of

crystallization conditions with both M37 and m153. Since we identified several promising conditions for m153 we then focused our characterization and structure determination efforts on this MCMV protein. The following chapter details the characterization of both soluble, recombinant m153 and m153 in transfected and MCMV-infected mammalian cells.

CHAPTER 4

BIOCHEMICAL AND CELL BIOLOGICAL CHARACTERIZATION OF MCMV m153

4.1 Introduction

Within the MCMV m145 family, m153 is most closely related to m150, m151 and m152. The proteins are 41-44% similar with respect to amino acid sequence and m152 is the closest relative with 28% amino acid identity to m153. No biological function of m153 has been reported, whereas m152 has two well-defined functions, namely the downregulation of MHC-I and NKG2D ligands of the Rae-1 family, as detailed in the literature overview in Chapter 1. m153 presented a good target for further characterization and structure determination since it expressed in high yields in insect cells and the protein was very stable.

Initial characterization experiments of MCMV m153 indicated that this protein is expressed predominantly at the cell surface of transfected cells, and that this expression is independent of the presence of β2m or the activity of TAP (Chapter 3). In this Chapter we report the analysis of the m153 glycoprotein in both soluble recombinant as well as native form. The localization of m153 was studied by transfecting both native m153 and an m153-EYFP fusion protein in mouse fibroblasts. In addition, we examined the expression timeframe and localization of m153 in MCMV-infected cells. Recombinant m153 was characterized in terms of its size, glycosylation and

multimerization state. Finally we investigate the ability of m153 to homodimerize in transfected mammalian cells.

4.2 Results

4.2.1 Localization of m153 in transfected NIH3T3 cells

The open reading frame of the *m153* gene predicts a type I transmembrane glycoprotein with a core molecular weight of 45 kDa. Initial localization studies of m153 were performed with a FLAG-tagged version of m153 in COS-7 cells of monkey origin. These experiments confirmed that *m153* is a functional gene that directs expression of the m153 protein to the cell surface (Chapter 3). Subsequent generation of a monoclonal antibody to m153 enabled us to study the localization of untagged m153 in transfected mouse fibroblast cells. In Figure 4.1A the localization pattern of m153 in transfected NIH3T3 cells in both surface staining (upper panel) and intracellular staining (lower panel) experiments is shown. These confocal images clearly reveal that m153 is specifically detected at the cell surface. In the intracellular staining experiment m153 exhibits a punctate distribution throughout the cytoplasm. In order to study further the punctate localization of m153 in living cells we fused EYFP to the C-terminal end of full-length m153. In Figure 4.1B the localization pattern of m153-EYFP, detected either with mAb153.16 or by EYFP fluorescence is shown. m153-specific staining (Figure 4.1B, upper left panel), shows surface localization very similar to the native protein in Figure 4.1A. When the fusion protein is visualized only by EYFP fluorescence the outline of the cell is not visualized as by mAb153.16 staining. This

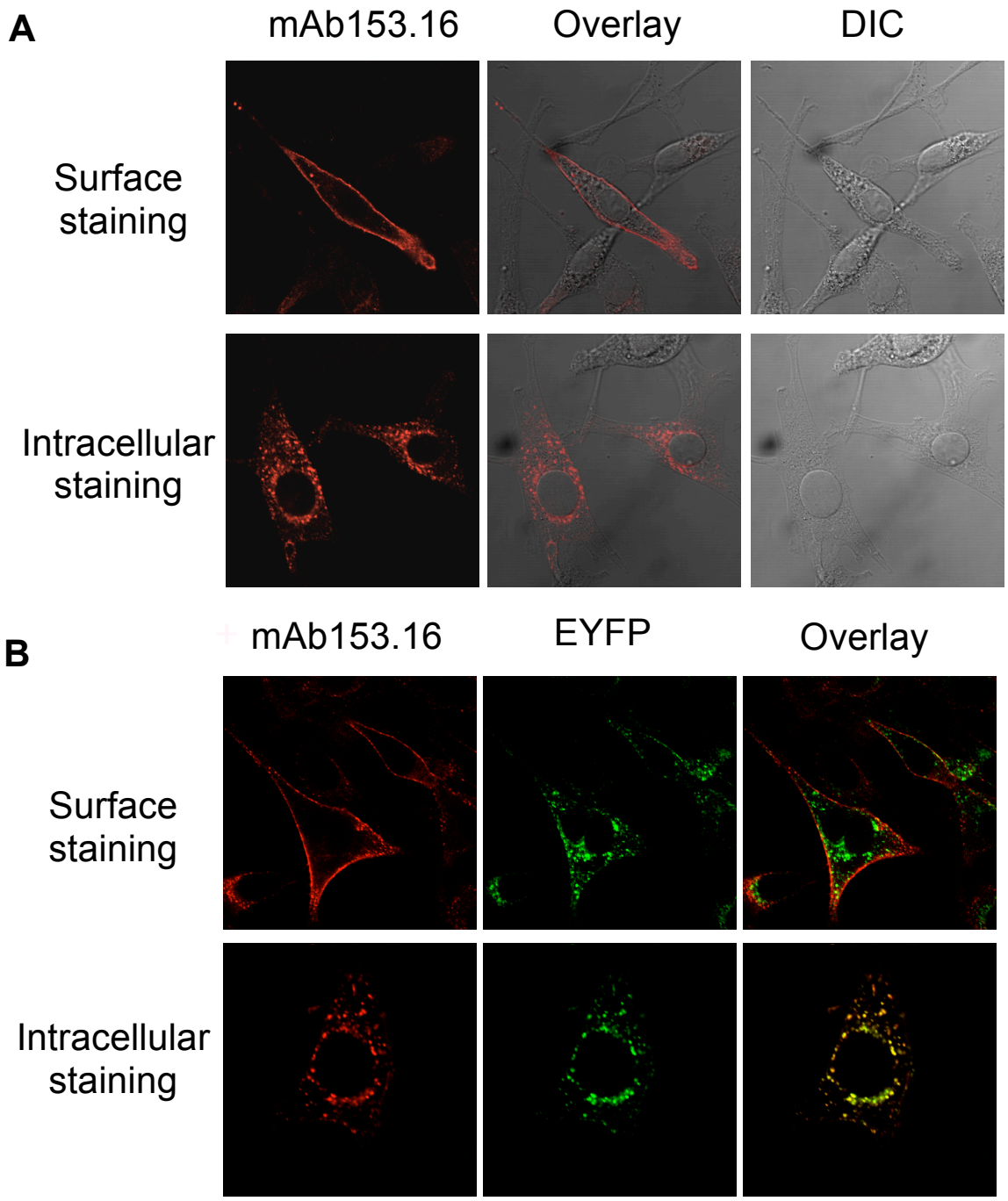

Figure 4.1. Localization of m153 in transfected NIH3T3 cells. NIH3T3 cells transfected with A) full-length m153 or B) m153-EYFP fusion protein, stained with mAb153.16 at 24 h post transfection. Surface staining (*upper panel*) reveals cell surface localization of m153 and intracellular staining (*lower panel*) shows punctate distribution of m153 inside the cell. m153-EYFP displays cellular localization similar to native m153 in both surface and intracellular staining experiments. The experimental details are described in Chapter 2, section 2.9. DIC – differential interference contrast.

observation could be explained if the relative levels of m153 at the surface are lower at the surface than inside the cell, and hence surface m153 is difficult to visualize above the bright cytoplasmic fluorescence. The intracellular staining pattern of m153-EYFP (Figure 4.1B, lower left panel) is almost identical to that of native m153 (Figure 4.1A, lower left panel). Therefore we could use the fusion protein in localization studies of m153.

In NIH3T3 cells transfected with m153-EYFP, the protein displayed punctate cytoplasmic distribution as well as some perinuclear localization in the majority of cells examined. We performed co-localization experiments with either live-cell organelle trackers like Mito- and Lysotracker or antibodies to organelle specific proteins (e.g. anti-Golgin) to determine whether m153 co-localizes with any subcellular organelles. From Figure 4.2 it is evident that m153 does not significantly co-localize with mitochondria, lysosomes, the Golgi-apparatus or early endosomes. The punctate distribution may thus represent m153 in secretory vesicles destined for cell surface expression.

Figure 4.2. Punctate distribution of m153-EYFP fusion protein in transfected NIH3T3 cells. The m153-EYFP fusion construct was transfected in NIH3T3 cells. Different organelle markers were used to establish whether m153 localizes to a specific organelle. Lysosomes – Lysotracker Red, Mitochondria – MitoTracker Red, Nuclei – DAPI, Golgi – anti-Golgin mAb staining, Early Endosomes – anti-EEA1 mAb staining. For details see Chapter 2, section 2.9.

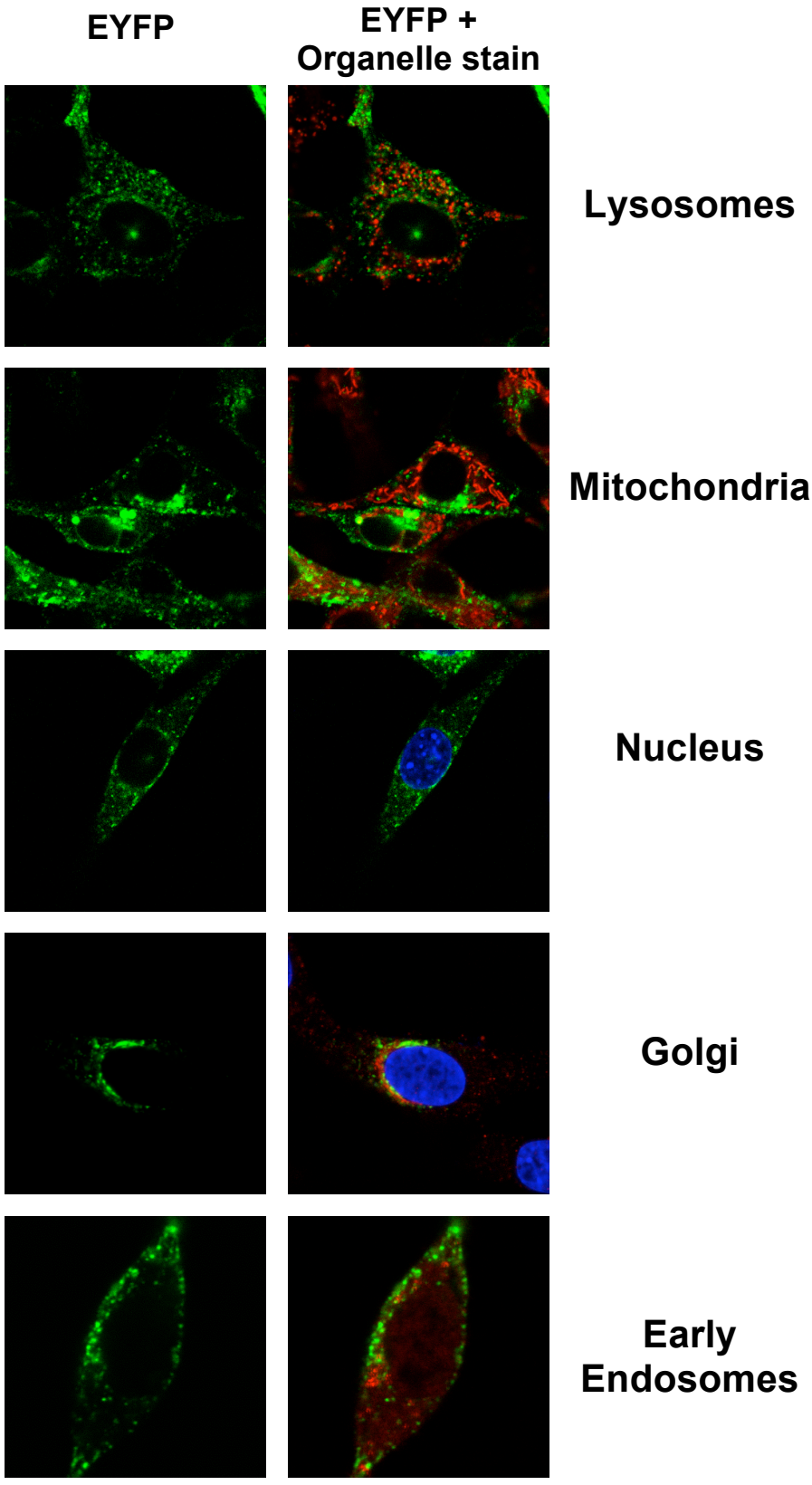
EYFP
EYFP +
Organelle stain
Lysosomes
Mitochondria
Nucleus
Golgi
Early
Endosomes

Figure 4.2.

4.2.2 m153 is expressed on the surface of MCMV-infected fibroblasts

To determine whether our transfection studies reflect the localization of m153 during virus infection, we examined the expression of m153 in MCMV-infected fibroblasts. NIH3T3 cells, infected with MCMV at an m.o.i of 2, expressed readily detectable levels of m153 at the cell surface 24 h post infection (p.i.) as detected by the monoclonal antibody mAb153.16, specific for the extracellular domain of m153 (Figure 4.3A). Uninfected cells did not stain with this antibody. By immunoprecipitation m153 was detected in detergent lysates of infected cells as early as 3 h and up to 48 h after infection with protein levels peaking at 24 h p.i. (Figure 4.3C). Immunoprecipitation of cell lysates followed by SDS-PAGE and Western blot analysis of m153 revealed an unexpectedly high apparent molecular weight of 80 kDa, which is decreased to 45 kDa upon deglycosylation with PNGaseF (Figure 4.3B). Such heavy glycosylation is consistent with six predicted sites for asparaginyl-carbohydrate addition in the extracellular domain of m153. The m153 that was immunoprecipitated from the transfected cells (Figure 4.3B, lane 3) migrated in a broad band, which may represent heterogeneous glycosylation, and the lower part of this band was not completely deglycosylated (Lane 4).

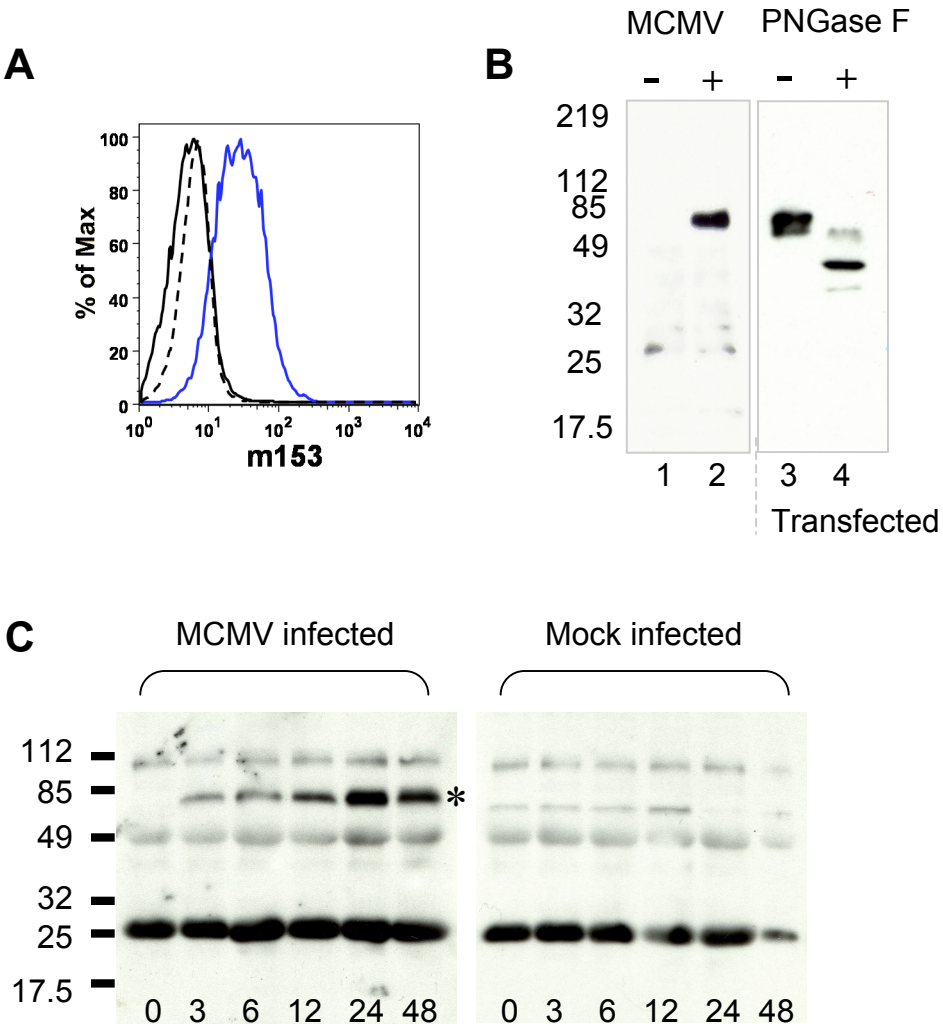

Figure 4.3. m153 expression in MCMV-infected cells. A) m153 is detected at the surface of MCMV-infected NIH3T3 cells. Cells were surface stained for m153 expression at 24 h post infection (p.i.). *Blue*, infected cells + mAb153.16, *Black*, infected cells + control Ab, *Dashed*, uninfected cells + mAb153.16. B) Immunoprecipitation and Western blot analysis of m153 from uninfected (*lane 1*) and MCMV-infected (*lane 2*) NIH3T3 cell lysates at 24 h p.i. Immunoprecipitation of m153 from transfected NIH3T3 cells (Immunoprecipitation-mAb153.16, Western blot-anti-m153 rabbit serum). Samples were mock-treated (*lane 3*) or treated with PNGAse F (*lane 4*) before SDS-PAGE and Western blot. C) Time-course analysis of m153 expression in MCMV-infected NIH3T3 cells. m153 was immunoprecipitated from infected cell lysates with mAb153.16 at the indicated times after infection (0-48 h) and analyzed by Western blot as described in Chapter 2, section 2.10. Mock-infected NIH3T3 cells were harvested at the same time points and served as a negative control. The m153 band (*) migrates just below the 85 kDa marker and is first detected at 3 h p.i. and peaks at 24 h p.i. The bands at 50 and 25 kDa represent detection of the heavy and light chains of the immunoprecipitating antibody. Another non-specific band is observed at ~ 112 kDa.

4.2.3 Glycosylation of m153 in *Drosophila* S2 cells

There are seven possible N-linked glycosylation sites on m153, six of which are predicted to be glycosylated by the NetNGlyc 1.0 server (Table 4.1). m153 expressed in transfected cells is glycosylated (Figure 4.3B). We next analyzed the recombinant version of m153 that was expressed in *Drosophila* cells. PNGaseF cleavage releases most oligomannose, hybrid and complex N-linked glycans and causes the conversion of asparagine to aspartate (Maley et al., 1989). PNGaseF digestion of the soluble ectodomain of m153 resulted in increased mobility on an SDS-PAGE gel, which would be consistent with the removal of carbohydrates from the protein (Figure 4.4).

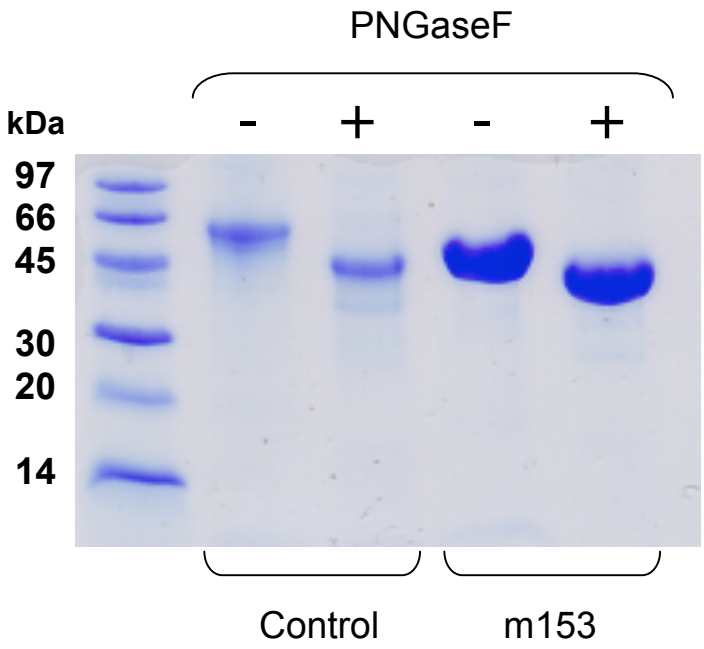

Figure 4.4. Recombinant m153, expressed in S2 insect cells, is glycosylated. Reducing SDS-PAGE analysis of m153 and a glycosylated control protein (bovine fetuin) after mock (-) or PNGaseF (+) digestion overnight. An increase in mobility for both bovine fetuin and m153 treated with the enzyme confirms the presence of carbohydrates on the proteins. The size markers are indicated in kDa.

Mass spectrometry analysis of mass changes induced by the Asn to Asp conversion of deglycosylated tryptic peptides of insect-expressed m153 confirmed glycosylation at five of the six predicted N-linked sugar addition sites on the ectodomain (data not shown). The analysis also revealed glycosylation at a seventh site, which was not predicted by the NetNGlyc 1.0 server, and indicated the types of sugar moieties that were added at the different positions.

Table 4.1. Analysis of glycosylation positions and content of recombinant m153.

Amino acid position	Asn-Xaa-Ser/Thr motif	Predicted N-linked site*	Site occupied	Glycan moieties detected
8	NRT	Yes	No	-
65	NES	Yes	Yes	$(HexNAc)_2(Fuc)_1(Hex)_3$
107	NCT	Yes	Yes	$(HexNAc)_2(Hex)_{1-7}$
152	NVT	Yes	Yes	$(HexNAc)_2(Fuc)_{0,1}(Hex)_{3-5}$
246	NRS	Yes	Yes	not detected
252	NTT	Yes	Yes	$(HexNAc)_2(Hex)_3$
310	NDS	No	Yes	$(HexNAc)_2(Fuc)_1(Hex)_3$

Hex – hexoses, NAc – N-acetylglucosamine, Fuc – fucose
* N-linked sites were predicted using the NetNGlyc 1.0 server (http://www.cbs.dtu.dk/services/NetNGlyc)

4.2.4 Recombinant m153 forms a stable, non-covalent dimer

The extracellular domain of m153 that was expressed in S2 insect cells has a predicted mass of 37.4 kDa. SEC analysis of m153 revealed that the protein eluted earlier than expected from the column. m153 eluted with a retention time of 8.2 min. which corresponds to a molecular weight between 158 kDa and 44 kDa (Figure 4.5A). This result suggested that m153 is expressed as a homodimer. SDS-PAGE analysis of insect-expressed m153 under both reducing and non-reducing conditions showed protein bands migrating between the 30 and 45 kDa markers (Figure 4.5B). The faster migration of non-reduced m153 implies that the protein contains intrasubunit disulfide bonds and has a more compact conformation in the unreduced state. These results also indicate that the m153 homodimer is non-covalent, since treatment with SDS-PAGE sample buffer breaks up the dimer and the protein migrates at its monomeric size.

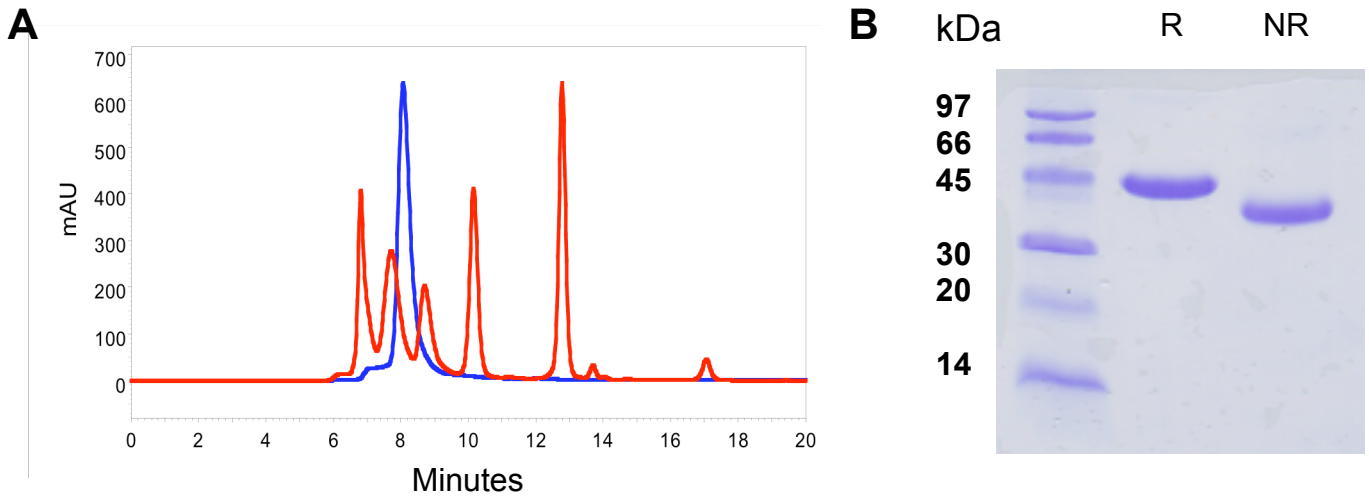

Figure 4.5. m153 is a non-covalent dimer when expressed in S2 insect cells. A) Size exclusion chromatography analysis of insect cell expressed m153 (extracellular domain – 1-314). The protein elutes between the 158 kDa and 44 kDa markers, whereas its predicted molecular weight is 37.4 kDa. B) SDS-PAGE analysis of recombinant m153 under reducing (R) and non-reducing (NR) conditions indicates that m153 contains intrasubunit disulfide bonds.

To confirm that m153 exists as a multimer in solution we performed sedimentation velocity analytical ultracentrifugation. In Figure 4.6A the results of a sedimentation velocity run performed with m153 at a concentration of 0.2 mg/ml are shown. The sigmoid shaped curves that migrate with time to increasing distances from the center of rotation are called sedimentation boundaries. The displacement with time of the boundary midpoints determines the *s*-value. The sedimentation data can be described by a differential sedimentation coefficient distribution *c(s)*. The distribution describes the superposition of boundaries of many species with different *s*-values. The SEDFIT program was used to calculate *c(s)* (Schuck, 2000)-
http://www.analyticalultracentrifugation.com.

The sedimentation coefficient distribution *c(s)* displays one main peak at 4.2 S. This indicated that the majority of m153 exists as a single species. (Figure 4.6C). The magnitudes of deviation of the model from the data points are shown in Figure 4.6B. Since the *c(s)* distribution contains one major peak it can be transformed to a molar mass distribution *c(M)*. The estimated molar mass of m153 is 78 800 Da (Figure 4.6D), thus confirming the observation that m153 forms a homodimer. Similar *s* values and molar mass estimations were obtained in four different sedimentation velocity experiments at different protein concentrations (Figure 4.7).

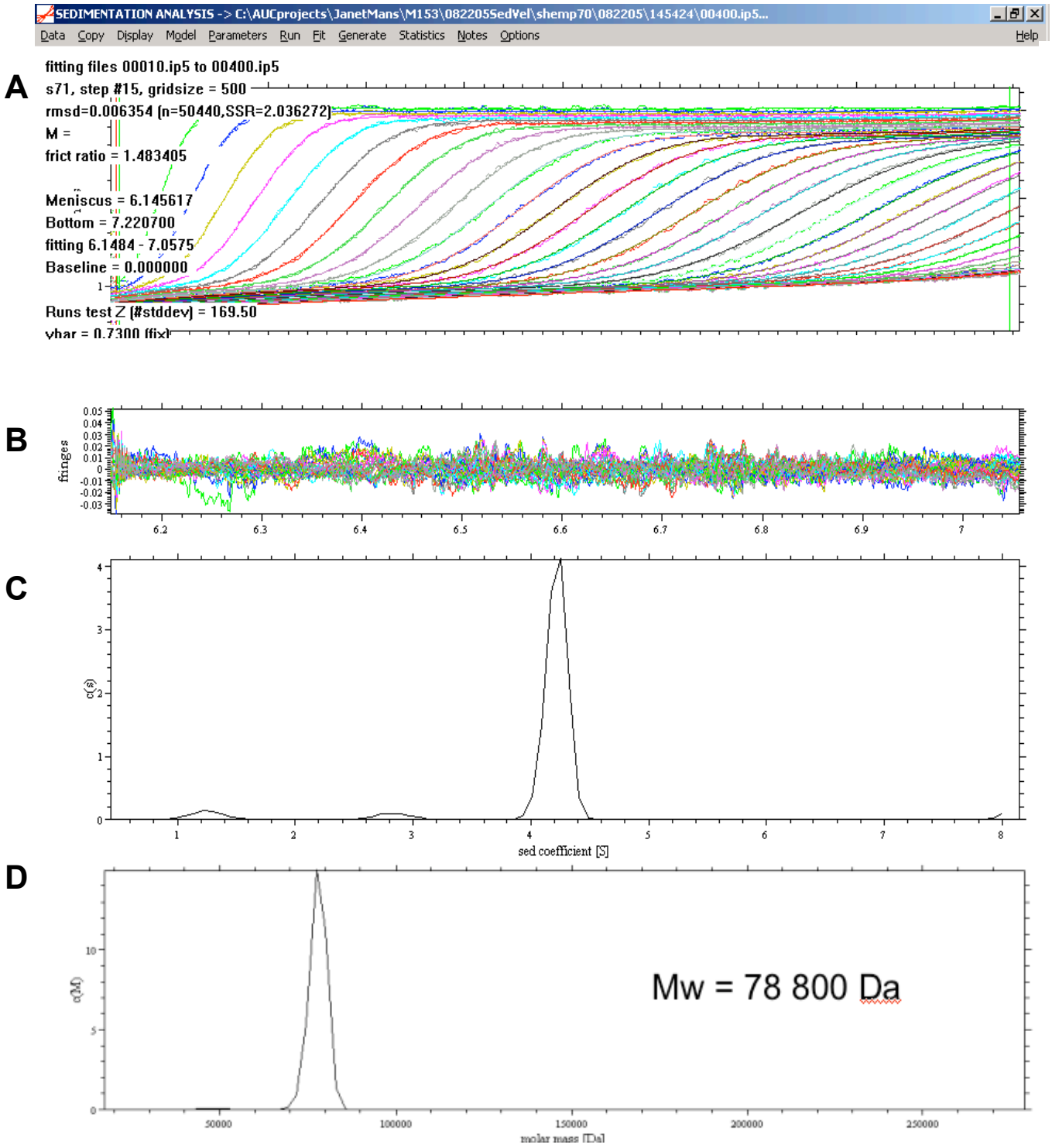

Figure 4.6. SEDFIT analysis of m153 sedimentation velocity data. A) Concentration profiles that change over time as the protein migrates away from the center of rotation. B) Superimposed radial residuals representing the deviation of the model from the original data. C) Sedimentation coefficient distribution *c(s)* from the analysis of the data shown in A. The distribution displays one main peak at ~ 4.2 S. D) The molar mass distribution *c(M)* of the peak obtained in C. The estimated molar mass of the single major peak (m153) is 78 800 Da. Experimental details are described in Chapter 2, section 2.15.

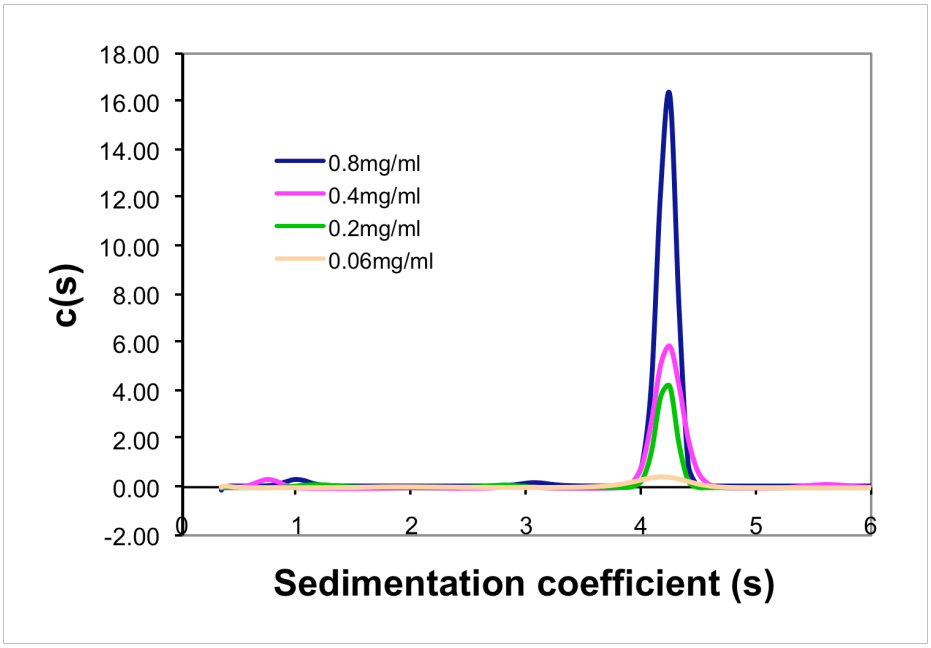

Figure 4.7. Sedimentation coefficient distribution *c(s)* derived from sedimentation velocity experiments at four different concentrations of m153.

4.2.5 Full-length m153 is dimeric in mammalian cells

To investigate the possibility that dimerization is a result of the engineering of soluble m153, we used two approaches to examine m153 in mammalian cells. Bimolecular fluorescence complementation (BiFC) can be used to visualize protein-protein interactions in cells. The N- and C-terminal domains of a fluorescent protein (e.g. YFP) are fused to the target proteins. The constructs are co-transfected and if the target proteins interact, the association brings the portions of the fluorescent protein together and fluorescence is observed (Hu et al., 2002; Kerppola, 2008). We fused full-length m153 to either N- or C-terminal segments of YFP. While transfectants of either construct alone did not show fluorescence, co-transfection of m153-N-YFP and m153-C-YFP resulted in the complementation of YFP fluorescence in transfected cells, indicating that m153 does form dimers. Cells transfected with YFP fusion constructs of m144, a

monomeric MHC-Iv protein, showed fewer than 1% YFP positive cells (Figures 4.8A and B). In a second approach we co-transfected N-terminal FLAG- and HA-tagged m153 in NIH3T3 cells. Successful immunoprecipitation of m153 with anti-FLAG antibodies and Western blot detection with anti-HA antibodies confirmed that m153 dimerizes in transfected fibroblasts (Figure 4.8C). Together these results provide strong evidence that m153 is a dimer when expressed as the full-length protein in mammalian cells.

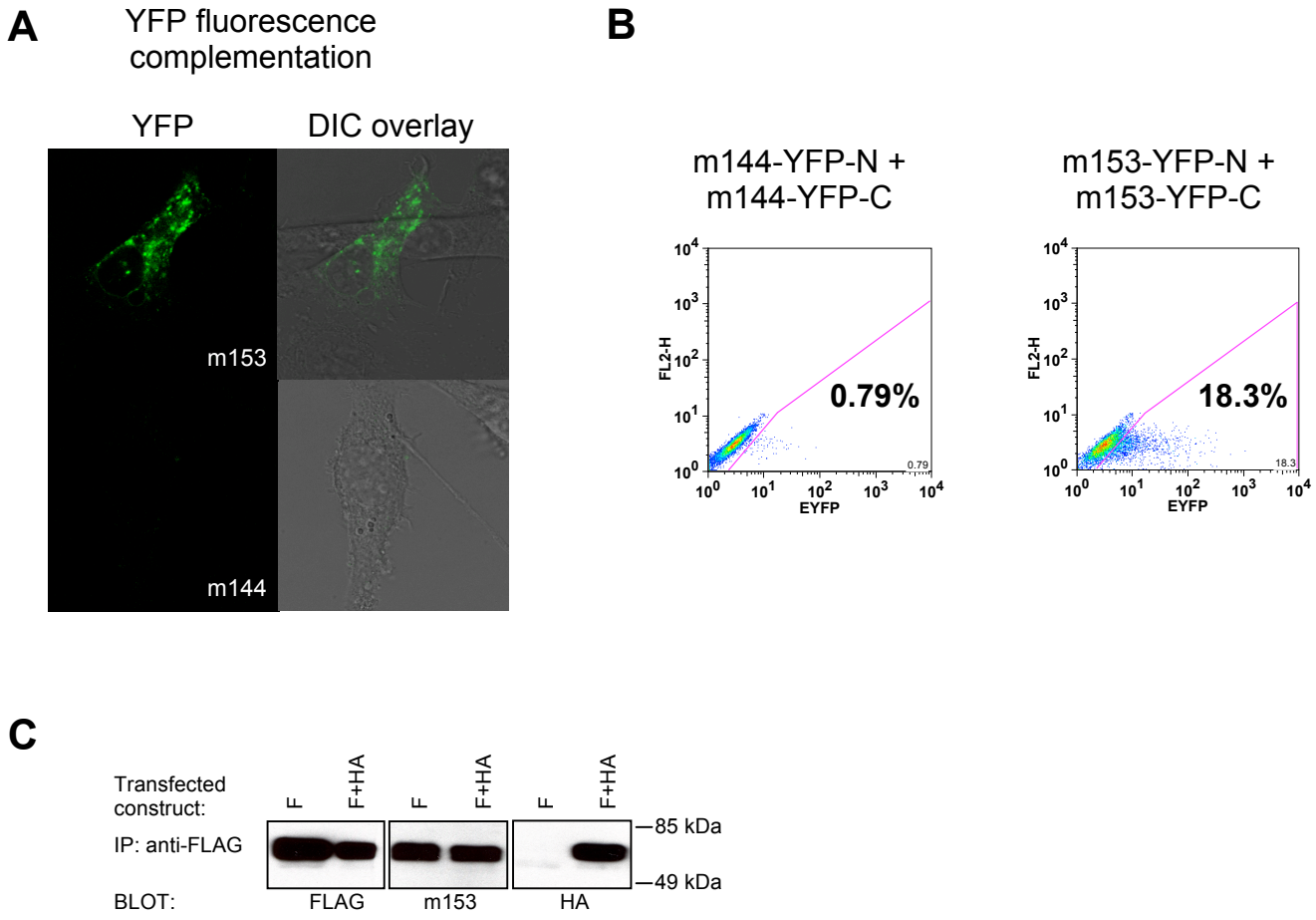

Figure 4.8. m153 forms a homodimer in mammalian cells. A) Bimolecular fluorescence complementation analysis. m153 constructs, fused to the N-terminal or C-terminal portions of YFP, were cotransfected in NIH3T3 cells and the live cells were examined by confocal microscopy for fluorescence complementation after 48 h. As a negative control YFP-fusion constructs of MCMV m144 were cotransfected. YFP channel (*left*), overlay of the YFP on the differential interference contrast (DIC) channel (*right*). B) Quantification of the number of YFP positive cells. After confocal microscopy the YFP-fluorescent cells were detached from the coverslips and counted by

FACS. YFP fluorescence was visible in 18% of m153-transfected cells but only in 0.8% of m144 transfected cells. C) Co-immunoprecipitation of differentially tagged m153. FLAG-m153 (F) or F + HA-m153 (F+HA) constructs were transfected in NIH3T3 cells. 24 h post transfection post-nuclear cell lysates were immunoprecipitated with anti-FLAG antibodies and detected on a Western blot with anti-FLAG (*left*), anti-m153 rabbit antibodies (*middle*) or HA-specific antibodies (*right*). Experimental details are described in Chapter 2, sections 2.8 and 2.10.

4.3 Discussion

The characterization of m153 has revealed several interesting features of this protein. First, we have shown that m153 is expressed in MCMV-infected cells starting at early times after infection and that the protein can be detected at the cell surface at 24 h post infection. Localization studies in transfected cells have also confirmed surface expression of m153 and further revealed that m153 is concentrated in punctate spots throughout the cytoplasm. This punctate distribution does not represent localization to lysosomes, early endosomes or the Golgi-apparatus. m153 is highly glycosylated when expressed in mammalian cells and mass spectrometry analyses confirmed that the recombinant ectodomain of m153, which was produced in insect cells, is also glycosylated at six of seven possible sites. Surprisingly, recombinant m153 forms a stable, non-covalent homodimer. The putative homodimer size estimate, obtained from gel filtration results, was clearly confirmed by analytical ultracentrifugation studies. These results showed that m153 exists only as a dimer species with an estimated molecular weight 78.8 kDa. The dimerization of m153 in transfected mammalian cells was studied by both bimolecular fluorescence complementation and co-immunoprecipitation experiments. Both approaches confirmed that m153 chains dimerize in mammalian cells. The functional significance of m153 dimer formation is not known at this time. But homodimerization may afford stability to the protein in the

absence of β2m and peptide association. In BiFC studies of m152, the m145 family member most related to m153, we did not observe any complementation (data not shown), therefore m152 does not dimerize in transfected cells.

In general MHC-I molecules do not dimerize, however disulfide linked dimers of classical MHC-I molecules have been reported for both human and mouse proteins as early as 1973 (Cresswell and Dawson, 1975; Schwartz et al., 1973). More recent work on H-2L^{d}, H-2D^{b} and H-2D^{d} suggested that the dimerization occurs in the absence of β2m and that the disulfide linkage is dependent on a cysteine present in the cytoplasmic domain of the class I heavy chain (Capps et al., 1993). The physiological significance of such dimers is not known. HLA-B27 is an example of a human class I molecule that forms disulfide-linked homodimers *in vivo*. The HLA-B27 allele has been associated with ankylosing spondylitis (Brewerton et al., 1973). The mechanism by which HLA-B27 is involved in disease pathogenesis remains unknown, however it is possible that the tendency of the heavy chain to form β2m-free homodimers via a disulfide linkage at cysteine 67 may underlie its effects (Bowness, 2002; Colbert, 2004). m153 would seem to form a distinct type of dimer, since no disulfide bonds are involved.

The high yields of recombinant m153, and the stability of the homodimer made this protein an ideal candidate for crystallization and structure determination. The following chapter describes the crystal structure of m153, explains the mode of dimer formation and highlights implications from this structure for other m145 family members.

CHAPTER 5

CRYSTAL STRUCTURE OF THE MOUSE CYTOMEGALOVIRUS GLYCOPROTEIN, m153

5.1 Introduction

The viral MHC-I homologs encoded by HCMV (UL18) (Beck and Barrell, 1988) and MCMV (m144) are clearly related to MHC-I based on amino acid sequence similarity (Farrell et al., 1997). UL18 resembles MHC-I the most, since it binds peptide and associates with β2m. A structural model of UL18, based on HLA-A2, has been proposed (Cerboni et al., 2006). The secondary structure of UL18 is very similar to MHC-I, but there are some regions with structural variations, two of which have been implicated in interactions of UL18 with its receptor LIR-1 (Cerboni et al., 2006; Wagner et al., 2007). The model also predicts a second disulfide bond in the α3 domain that is absent in classical MHC-I molecules. Mutation of the cysteines involved in this bond abolished binding of UL18 to β2m (Wagner et al., 2007) confirming the importance of this novel bond.

m144 is less related to classical MHC-I than UL18, since it does not require peptide for cell surface expression but it does associate with β2m (Chapman and Bjorkman, 1998; Natarajan et al., 2006). The crystal structure of m144 showed an MHC-I-like protein, bound to β2m but not associated with peptide, confirming predictions based on sequence comparison. The molecule is characterized by a large angle between α1α2 and α3, a

unique stabilizing disulfide bond in α1α2, and relatively loose association of the heavy chain with β2m (Natarajan et al., 2006).

The crystal structure of m157, one of the eight m145 family members with a predicted MHC-I fold, was reported recently (Adams et al., 2007). m157 expression does not require either β2m or peptide (Arase et al., 2002). Its crystal structure revealed several deviations from the MHC-Ia fold: an extended, helical N-terminus, designated α0, that precedes the canonical α1 helix and imparts a three-helix structure to the amino terminal α1α2 domain; a long α2 helix that extends into the α3 domain; short interhelical distances and close interactions of the α1α2 domain with α3 resulting in a molecule significantly more compact than classical MHC-I; and an α3 domain whose Ig fold is less twisted than typical Ig folds (Adams et al., 2007).

We have determined the crystal structure of MCMV m153. In contrast to any other MHC-I molecules, the soluble ectodomain of m153 forms a stable, non-covalent dimer. The crystal structure of m153 reveals the mode of dimerization in addition to other distinguishing features, including an extended N-terminus, different from that of m157. Thus, although prediction algorithms group members of the m145 family together within the broad MHC-I structural family, the details of the individual structures show wide variation from MHC-I and demonstrate the robustness and adaptability of the MHC-I fold in the service of diverse biological functions.

5.2 Results

5.2.1 The MHC-I fold of m153

To elucidate the structure of m153, a selenomethionine (SeMet) derivative was prepared by biosynthetic labeling of the protein expressed in *Drosophila* S2 cells. Size exclusion chromatography indicated that soluble m153 was a dimer (Chapter 4, Figure 4.5). Diffraction data from a single crystal were collected, the structure was solved by single anomalous dispersion (SAD) phasing, and the model was refined at 2.4 Å resolution to final R_{cryst} and R_{free} of 23% and 27.9% respectively (Table 5.1). Analysis of the psi/phi angles of the m153 backbone was performed with both Procheck (Table 5.1) and Molprobity (Figure 5.1).

There is a single dimer in the asymmetric unit with chains designated A and B. We observed continuous electron density for residues 2-230 and 238-277 of chain A and residues 5-277 of chain B. No electron density was observed for the C-terminal residues 278-314 of either chain and these were omitted from the model. The average B-factor was 42 $Å^2$ for chain A and 32 $Å^2$ for chain B. We selected chain B to describe the structural features of the monomer as they relate to the MHC-I fold, because it is more complete and has lower B-factor values.

Table 5.1. Data collection, refinement and validation statistics.

Data Collection	
Space Group	$P2_1$
Unit cell dimensions	
a, b, c	61.7, 78.2, 62.7
α, β, γ	90.0, 90.4, 90.0
Molecules per asymmetric unit	2
Resolution (Å)	2.3
Total observations	335, 101
Unique reflections	26, 191
Completeness (%)[a]	97.5 (80.6)
$I/\sigma I$ [a]	9.7 (1.54)
R_{sym} [a/b]	0.081 (0.40)
Refinement	
Resolution range	62.75 - 2.4
Reflections	
Working set	23443
Test set	1183
R_{cryst} (%)[c]	23.0
R_{free} (%)[c]	27.9
Number of non-H protein atoms	4393
Number of water molecules	57
Carbohydrate chains	3
r.m.s deviations from ideality	
Bond lengths (Å)	0.01
Bond angles (deg.)	1.318
Average B values ($Å^2$)	A , B
Main-chain	42.2 , 32.2
Side-chain	42.5 , 32.7
Whole chain	42.4 , 32.4
Overall	37.6
Model Validation	
Ramachandran plot statistics (%)	
Procheck	
Most favored	87.8
Allowed	12.2
Generous	0
Disallowed	0

[a]Values in parentheses are statistics for the highest resolution shell (2.48–2.38 Å). [b]$R_{sym}(I) = \sum | Ij - \langle I \rangle | / \sum Ij$, where Ij is the intensity of the jth observation of a reflection and <I> is the mean intensity from multiple measurements of that reflection. [c]$R_{cryst} = \sum ||F_o| - |F_c|| / \sum |F_o|$, where F_o and F_c are the observed and calculated structure factor amplitudes, respectively. R_{free} is as for R_{cryst} but calculated for a randomly selected 5.0% of reflections not included in the refinement.

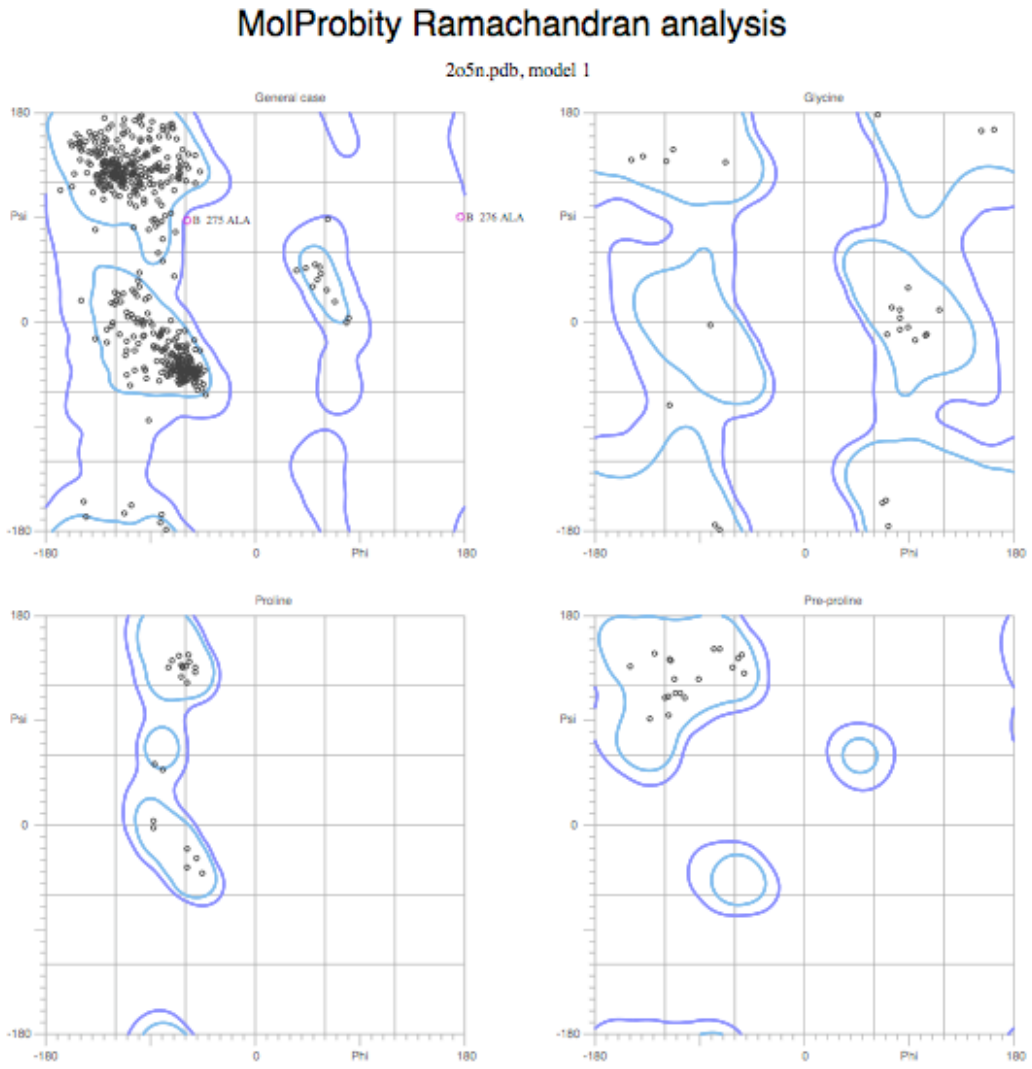

95.9% (517/539) of all residues were in favored (98%) regions.
99.6% (537/539) of all residues were in allowed (>99.8%) regions.

There were 2 outliers (phi, psi):
B 275 ALA (-59.3, 88.4)
B 276 ALA (176.1, 91.3)

Figure 5.1. Ramachandran analysis of the m153 model with the Molprobity server (http://kinemage.biochem.duke.edu, (Davis et al., 2007)).

The structure of m153 (Figure 5.2) reveals basic structural elements of the MHC-I fold. The m153 α1α2 domain consists of a unit in which the α1 helix and a discontinuous α2 helix rest atop a platform of seven β-strands. Three of the strands derive from the α1 domain and four from α2. The fourth β–strand of the α1 domain, commonly found in MHC-Ia and Ib molecules, is not observed in m153. Unlike either MHC-Ia or Ib molecules the C-terminal end of the α2-helix extends downwards into a third helix (H2b) that connects the α1α2 domain with the Ig-like α3 domain (Figure 5.2A).

Several structural features of the m153 monomer differ substantially from classical MHC-I molecules. Most striking is the N-terminus, extended by 20 residues, that starts adjacent to the G strand of the α3 domain, forming a short β strand. From there it extends upwards alongside the H2b helix and continues as the first strand of the platform beginning at residue 21 (Figure 5.2A). This feature is absent in all MHC-I molecules described thus far and differs substantially from m157, whose extended N-terminus forms instead a third, short helix adjacent to the α2 helix (Figure 5.2C). A unique disulfide between C16 and C171 anchors the extended N-terminus of m153 to the H2b helix (Figure 5.2D). In addition, there are several hydrogen bonds between the extended N-terminal strand (residues 6-15) and the loop connecting platform strands β2 and β3. Other hydrogen bonds link the extended N-terminus to the H2b helix and the α3 F-G loop and serve to further stabilize the structure (Figure 5.2C). The α1 and α2 helices are shorter than those observed in MHC-Ia proteins and are closely juxtaposed above the β sheet floor. Close interactions between these helices preclude the binding of peptide or other ligand (Figure 5.2B), in agreement with cellular expression studies indicating that

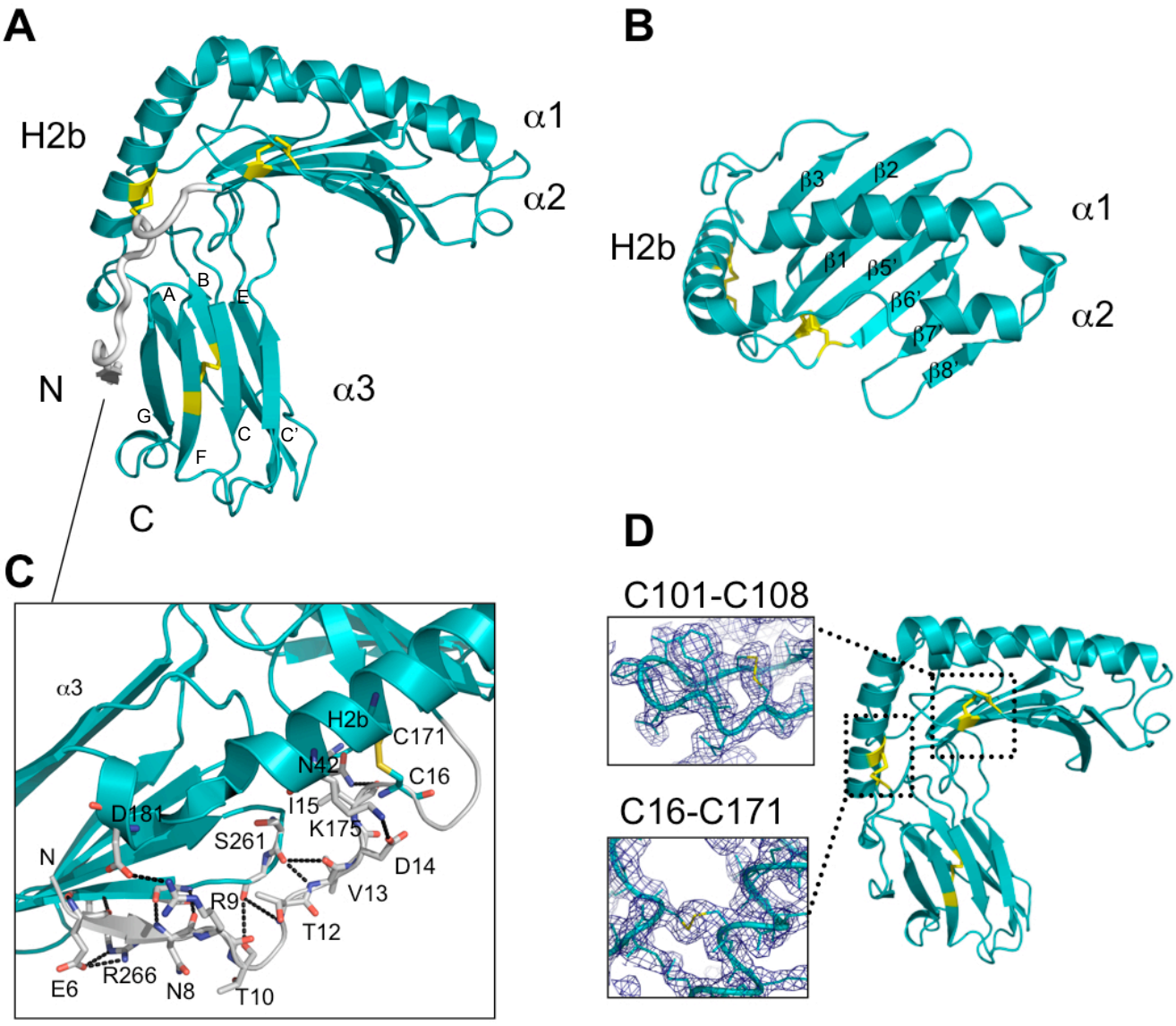

Figure 5.2. Conserved and unique features of the m153 monomer. A) Side view of m153 chain B. The α1, α2 and H2b helices, the α3 domain, N- and C-termini are labeled and the disulfide bonds are in *yellow*. N-terminal residues 2-20 are colored *gray*. B) Top view of the 7 β-strand platform and α1α2 helixes of m153. C) Extended N-terminus of m153. Extensive interactions between the N-terminus (*gray*) and H2b helix, loops in the α1α2 domain and the G strand of the α3 domain (*cyan*). Hydrogen bonds are in *black*. D) Side view of m153 monomer. Two unique disulfide bonds link the N-terminal fragment to the H2b helix (C16-C171) and the β5' platform strand to the loop connecting the β5' and β6' strands (C101-C108). Electron density around the unique disulfides is contoured at 1.25σ. The conserved disulfide bond (C203-C255) is located in the Ig-like α3 domain.

m153 does not depend on bound peptide for stability (Chapter 3, Figure 3.3). The platform is stabilized by a second unusual disulfide (C101-C108) which connects strands β5' and β6' of the floor (Figure 5.2D). A similar bond is seen in m157 (C103-C112) but MHC-Ia molecules preserve a disulfide bond in the same region which links β-strand 5 of the platform to the α2 helix (C101-C164) (Bjorkman et al., 1987). We examined m153 by mass spectrometry to confirm the presence of the unusual disulfide bonds.

Desalted and PNGaseF treated MCMV-m153 was digested with trypsin and nano electrosprayed. FT-MS/MS spectra were recorded after electron capture dissociation (ECD) fragmentation of indicative peptides to selectively reduce Cys-Cys bonds between two tryptic peptides. Alternatively TCEP was added to the solution to obtain mass shift experiments of FT-MS survey scans for identification of e.g. internal Cys-Cys bonds in one and the same tryptic peptide. Figure 5.3 shows the selective Cys-Cys reduction using ECD fragmentation of the quadruply charged m/z=708.097 (tryptic peptides TGTVDIC*QGPMELIFSVSR and WTEIC*K), whereas Figure 5.4 shows the mass shift of 1.005 at the doubly charged m/z= 757.851 caused by TCEP induced reduction of the internal Cys-Cys bond of tryptic peptide C*PVPQFNC*TITHR.

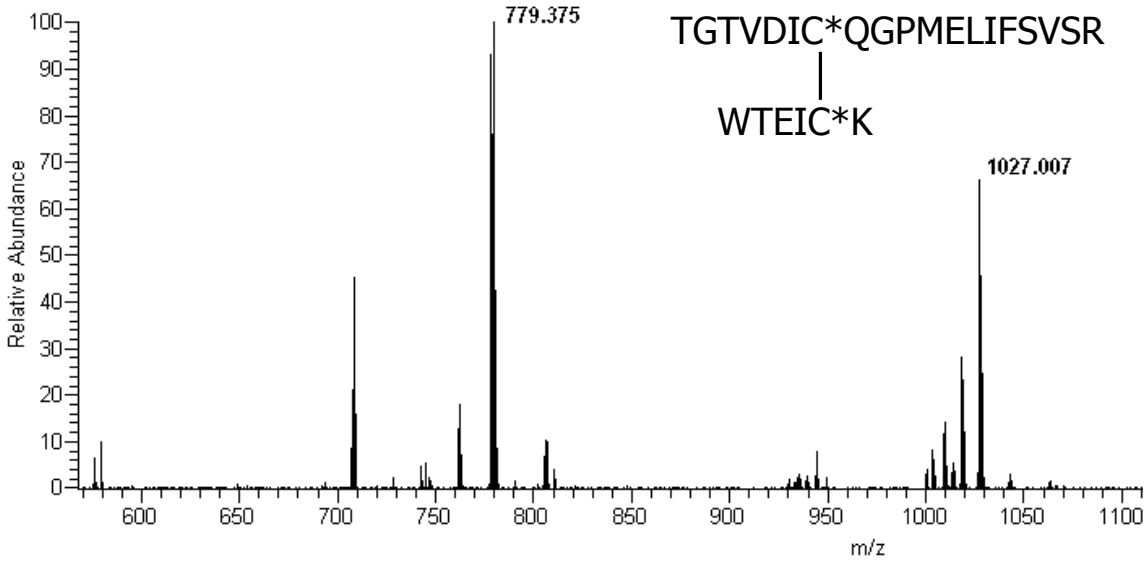

Figure 5.3. Mass spectrum of a disulfide-linked tryptic peptide confirms the C16-C171 disulfide bond. FT-MS/MS spectrum after electron capture dissociation (ECD) fragmentation of the quadruply charged m/z=708.097. ECD induced a fragmentation of the disulfide bond yielding the singly charged fragment m/z=779.375 and the doubly charged fragment m/z=1027.007, corresponding to the tryptic peptides TGTVDICQGPMELIFSVSR and WTEICK, respectively. ECD also resulted in further peptide fragmentation revealing the sequence tag FSVS.

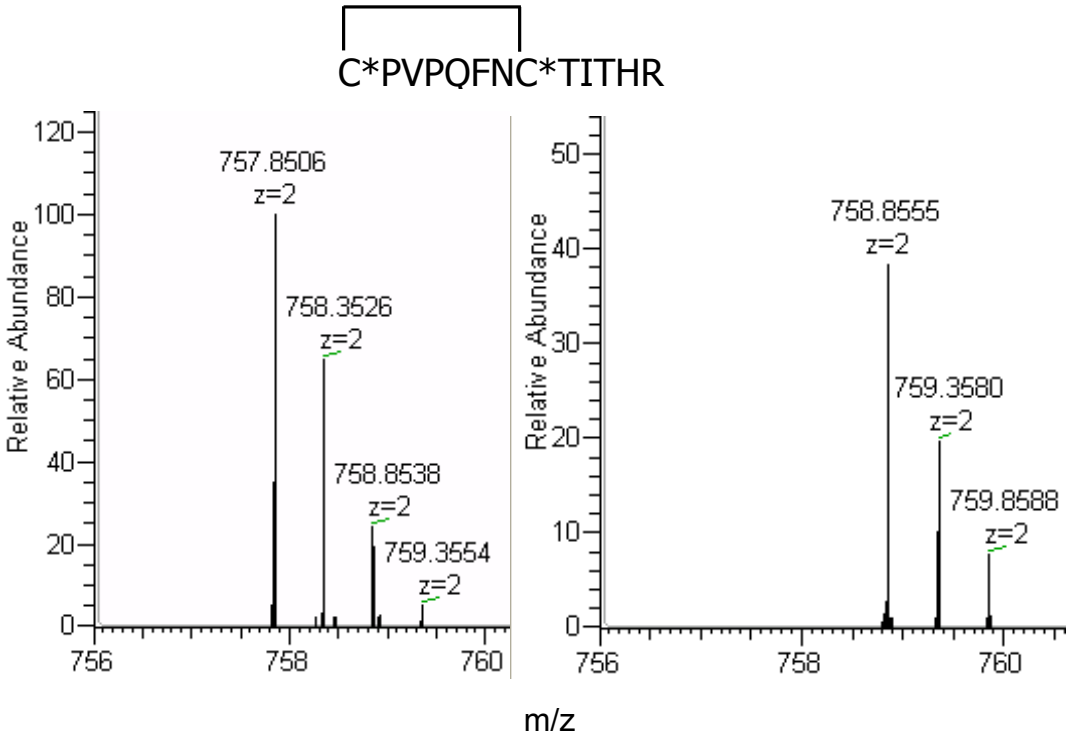

Figure 5.4. Mass spectra of C*PVPQFNC*TITHR peptide before and after reduction with TCEP confirmed the C101-C108 disulfide bond. Mass shift of 1.005 at the doubly charged peptide m/z=757.851 indicated addition of two protons after reduction of internal Cys-Cys bond in tryptic peptide CPVPQFNCTITHR.

The α3 domain of m153 has a C2 type Ig-fold, which is characterized by a more compact domain and shorter intercysteine spacing than the C1 or V type fold (Halaby and Mornon, 1998). The A, B and E strands make up one sheet of the domain and the C, C', F and G strands make up the opposite sheet (Figure 5.2A). The canonical Ig-domain disulfide bond (C203-C255) connects strands B and F. Searches against the DALI database (Holm and Sander, 1996) identified m144, also with a C2 type Ig-fold, and CD1d as proteins with α3 domains that are structurally most closely related to m153. The difference between the strand dispositions in the α3 domains of m153 and m157 is indicated by the relatively high r.m.s.d. of 2.3 Å for the superposition of 67 Cα atoms. The α3 domain of m153 has longer β-strands that exhibit the characteristic β-sandwich twist, whereas the m157 α3 domain has strands that are shorter and form flatter sheets (Figure 5.5C). The terminal residues that were modeled in both structures adopt different conformations, in m153 they form a short α-helix, whereas in m157 the C-terminal strand forms a circular loop that contacts both sheets of the α3 domain (Adams et al., 2007).

In Figure 5.5 we compare the α1α2 domain of m153 chain B to that of m157, H-2K^b (Fremont et al., 1992), rat FcRn (Burmeister et al., 1994a), and the NKG2D ligand Rae-1β (Li et al., 2002). The α1 and H2b helices of m153 and m157 are in equivalent positions, whereas their α2 helices differ. The N-terminal end of the m157 α2 helix was not modeled due to lack of electron density (Adams et al., 2007). The m153 α2 helix starts with two full turns (residues 140-146), followed by an extended region that stretches along the platform ending in two turns of helix before bending sharply downward to continue as the H2b helix.

The maximal distance between the α1 and α2 helices of m153 is 8.1 Å compared to 16.8 Å in H-2K^b (Figure 5.5A). Surface representations of the α1α2 domains of m153 and H-2K^b (Figure 5.5B) illustrate the lack of a peptide-binding groove in m153. The groove region of m153 is comparable to that of Rae-1β and FcRn, two molecules that also do not bind peptide. The maximal distance between Cα atoms of the α1 and α2 helices of Rae-1β and FcRn are 8.2 Å and 9.2 Å respectively. The α1 helices of m153, Rae-1β, and FcRn have a similar arrangement on the platform but the m153 helix is shorter. The m153 platform has seven strands compared to the eight found in classical MHC-I proteins (Figure 5.5A).

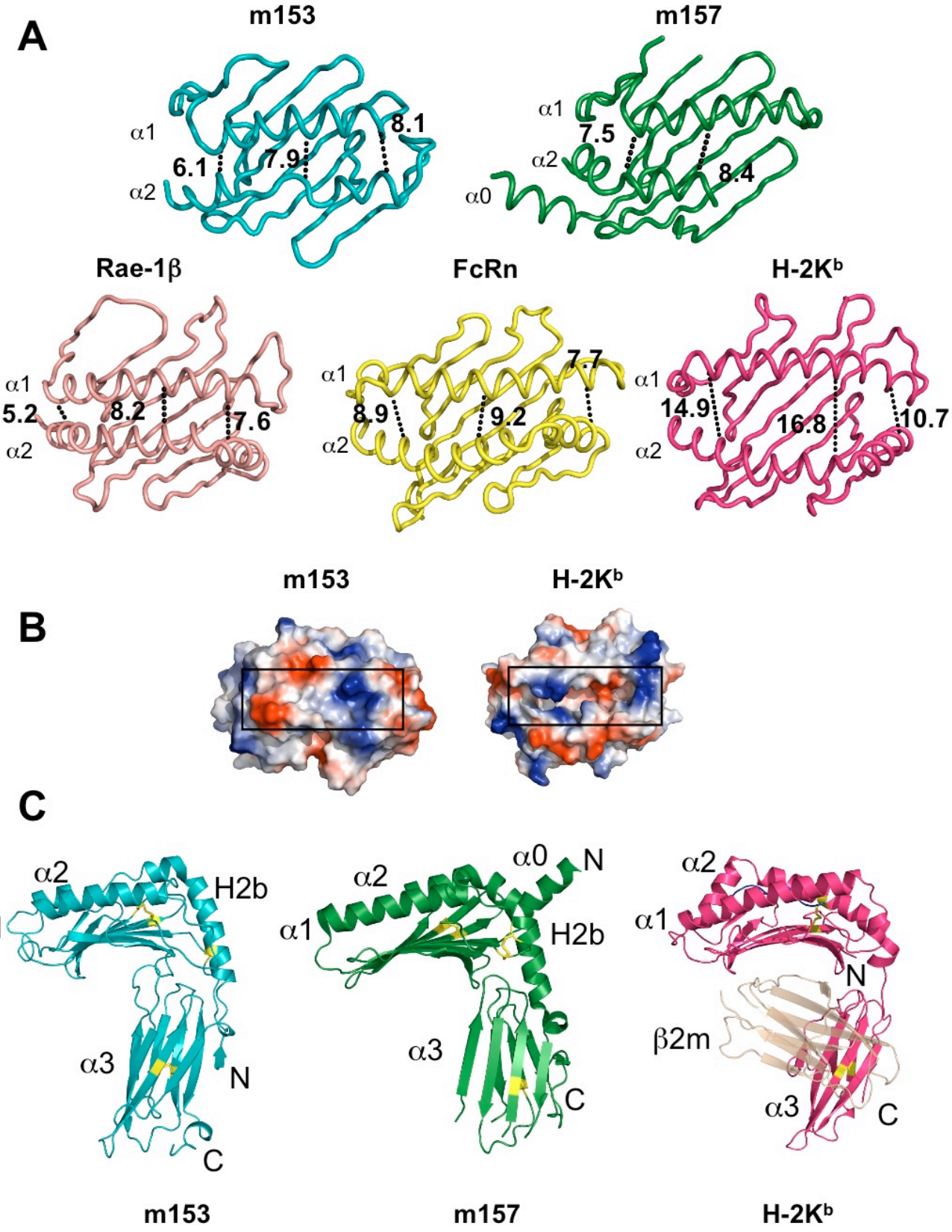
A
m153
α1
α2
6.1
7.9
8.1
m157
α1
α2
α0
7.5
8.4
Rae-1β
α1
α2
5.2
8.2
7.6
FcRn
α1
α2
8.9
9.2
7.7
H-2K^b
α1
α2
14.9
16.8
10.7
B
m153
H-2K^b
C
α2
α1
H2b
α3
N
C
α0
N
α2
α1
H2b
α3
C
α2
α1
N
β2m
α3
C
m153
m157
H-2K^b

Figure 5.5. Comparison of m153 with m157, H-2K^b, Rae-1β and rat neonatal FcR. A) Ribbon diagrams of the platform domains of m153, m157, Rae-1β, FcRn and H-2K^b. The width of the groove of each molecule is indicated in Å and was measured at both ends and in the middle at comparable residues of the α-helices. B) Surface representation of the peptide-binding domain of H-2K^b (groove shown without any peptide) and the corresponding region of m153. Black rectangles indicate the groove. C) Comparison of m153 chain B with m157 and H-2K^b. The α1α2 and H2b-helices, α3-domain, and N- and C-termini are labeled. PDB accession codes: 2NYK, 2VAA, 1JFM and 3FRU for m157, H-2K^b, Rae-1β and rat FcRn, respectively.

The hinge angle between α1α2 and α3 of m153 chain B is 76º, which is within the range of the MHC-I molecules H-2K^b, CD1d and T22 (71-74º), but is smaller than that of m157 (81º), MICA (116º) and m144 (98º) (Table 5.2). The m153 α3 domain makes extensive contacts with the H2b helix, with the loop connecting strands β2 and β3 of the platform as well as with the loop connecting β3 and α1. The buried surface area between α1α2 and α3 of m153 is 1777 Å^2, which is considerably larger than the analogous interfaces in m157 (1265 Å^2) and H-2K^b (455 Å^2).

Table 5.2. Hinge angle between the α1α2 and α3 domains of viral, MHC-Ia and MHC-Ib molecules.

Protein	PDB code	Angle (degrees)	Associated subunits
m153	2O5N	76	m153
m157	2NYK	81	None
m144	1U58	98	β2m
H-2K^b	2VAA	71	β2m, peptide
CD1d	1ZHN	75	β2m, lipid
T22	1C16	72	β2m
ZAG	1TW7	90	β2m
MICA	1B3J	116	β2m

Hinge angles were calculated with the HINGE program as described in Chapter 2, section 2.14.

5.2.2 The m153 dimer

Size exclusion chromatography (SEC) of the insect cell expressed extracellular portion of m153 indicated that the molecule formed a stable non-covalent homodimer (Chapter 4, Figure 4.5), an observation confirmed by velocity sedimentation (Chapter 4, Figures 4.6 and 4.7). The crystal structure reveals the details of the mode of dimerization. Two MHC-I-like chains of m153 are organized in a head-to-tail arrangement forming a compact dimer (Figure 5.6A). The two chains are almost identical (r.m.s.d. of 0.624 Å for superposition over 268 Cα atoms). The interaction of the platform domain of one subunit with the α3 domain of the other imparts a coronal shape forming a central cavity with a volume of about 9500 $Å^3$. The conical cavity measures 46 Å x 35 Å at the top narrowing down to 22 Å x 18 Å. It is closed off at the bottom where the K115 sidechains of each subunit are only 4 Å apart. We propose an orientation of the m153 dimer with respect to the plasma membrane shown in Figure 5.6B. The subunits lie with their long axes parallel to the membrane and with the α1 helices closest to the membrane. In this orientation the C-termini of both chains point towards the membrane (Figure 5.6B – lower). The 37 C-terminal residues for which no electron density was observed in either chain may form a flexible stalk connecting the ectodomain to the transmembrane region. m153 conserves only two of the 31 β2m-contacting residues present in H-$2K^b$. It is evident from the dimer orientation of m153 that association with β2m would be sterically hindered, an observation consistent with the β2m independence of m153 expression (Chapter 3, Figure 3.2).

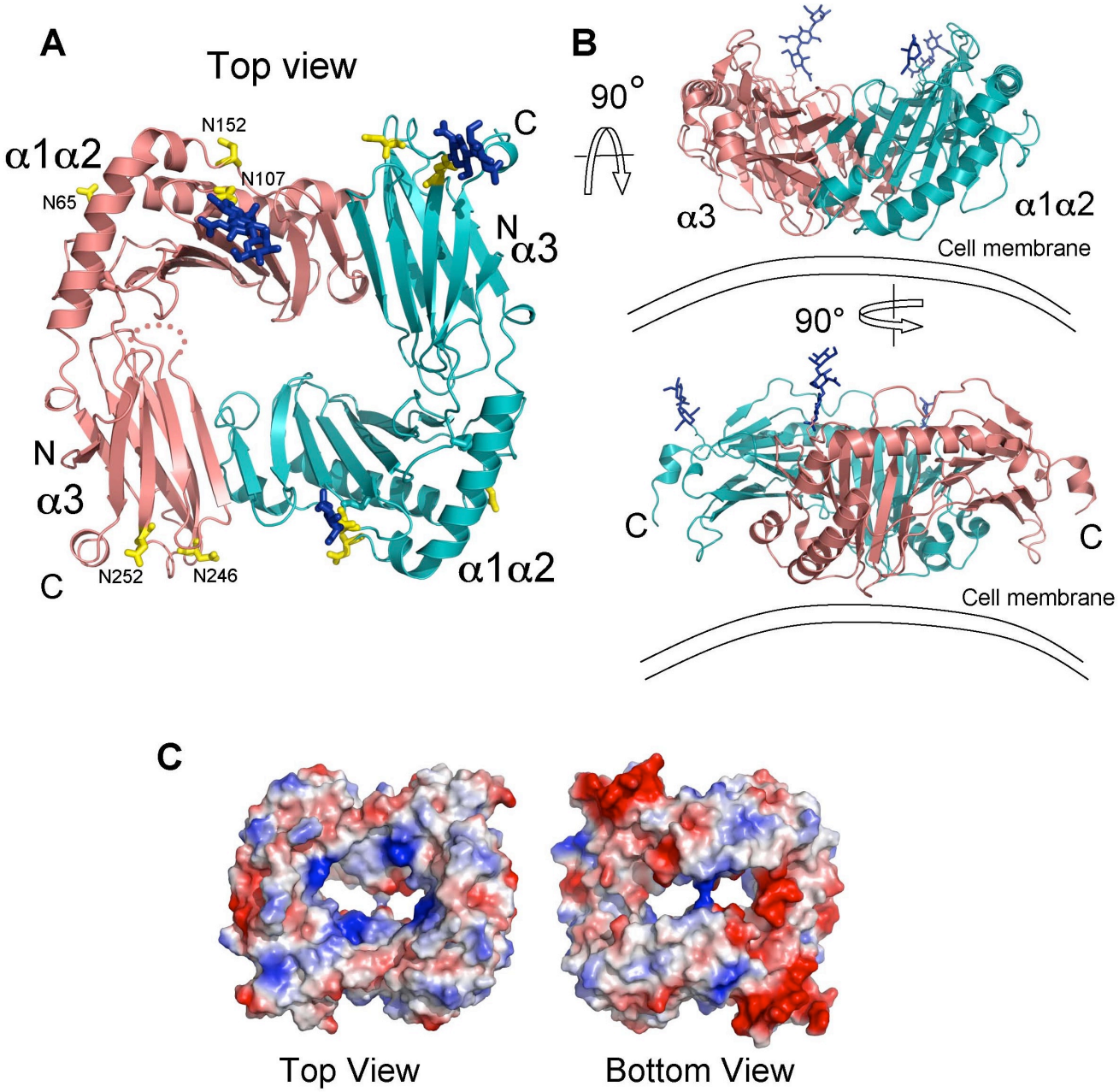

Figure 5.6. Overall structure of the m153 dimer. A) Ribbon diagram of the m153 dimer as viewed from the top. Chain A - *salmon*, Chain B - *cyan*. The α1α2 helices, the α3 Ig-like domains and N- and C-termini are labeled. Dashed line in chain A indicates a disordered loop. *Blue sticks* - carbohydrates observed in the crystal structure, *Yellow sticks* - N-linked glycosylation sites confirmed by mass spectrometry. B) Two 90º rotations reveal different side views of the m153 dimer, and its proposed orientation on the cell membrane. C) Top and bottom views of the electrostatic surface representation of the m153 dimer (*red* – acidic; *blue* – basic).

Three sugar moieties were modeled in the m153 structure (at N107 in chains A and B and N252 in chain B). These all point upward from the dimer away from the cell surface. Mass spectrometry indicated glycosylation at five of the six predicted N-linked carbohydrate addition sites and one additional site (Chapter 4, Table 4.1). These sites occur in both α1α2 and α3, and are distributed around the periphery of the m153 dimer, with none in the central cavity or at the proposed membrane proximal face of the molecule (Figure 5.6A). The electrostatic surface of the m153 dimer reveals four nearly symmetrical basic patches inside the central cavity, and two highly acidic regions on the bottom surface that are formed by the loop that connects the A and B strands of the α3 domain and the C-terminal α-helical fragment (Figure 5.6C).

The m153 dimer interface is formed by parallel β-strand interactions between the platform (β8' strand) of one subunit and the α3 domain (C' strand) of the second subunit (Figure 5.7A), resulting in two extended, twisted β-sheets of 12 strands each that form the core of the dimer. The two interfaces are not perfectly symmetrical as 21 residues of chain A and 22 residues of chain B are involved in dimerization. There are 16 hydrogen bonds at the interface, most of which represent backbone interactions (Figure 5.7B). In addition there are 114 non-bonded contacts. The area buried at the dimer interface is 1088 $Å^2$ (Figure 5.7C), which is larger than that observed in HLA-G (676 $Å^2$), which forms a disulfide-linked MHC-Ib dimer. The shape complementarity (Sc) index of the dimer was calculated as 0.72, which is higher than that of most antibody-antigen interfaces (0.62-0.68), consistent with the stability of the homodimer (Sc=1 represents a perfect fit, (Lawrence and Colman, 1993)).

To confirm the observed interface we tested the effects of mutating four interface residues T128, S131, R225, and S241, all of which form side-chain/side-chain hydrogen bonds, to alanine (Figure 5.7C). In a second mutant we introduced an alanine mutation at a site distant from the interface (D194A) as a control. Wild-type (wt) m153 and the respective mutants were expressed in insect cells and analyzed by chromatography. SEC indicated a smaller size for the quadruple interface m153 mutant, whereas the control mutant migrated with wt m153 (Figure 5.8A). Analytical ultracentrifugation analysis of wt and interface mutant m153 showed that the mutant protein had a smaller sedimentation coefficient indicating disruption of the dimer (Figure 5.8B). Thus the four mutations destabilized the m153 dimer and confirm the mode of dimerization visualized in the structure.

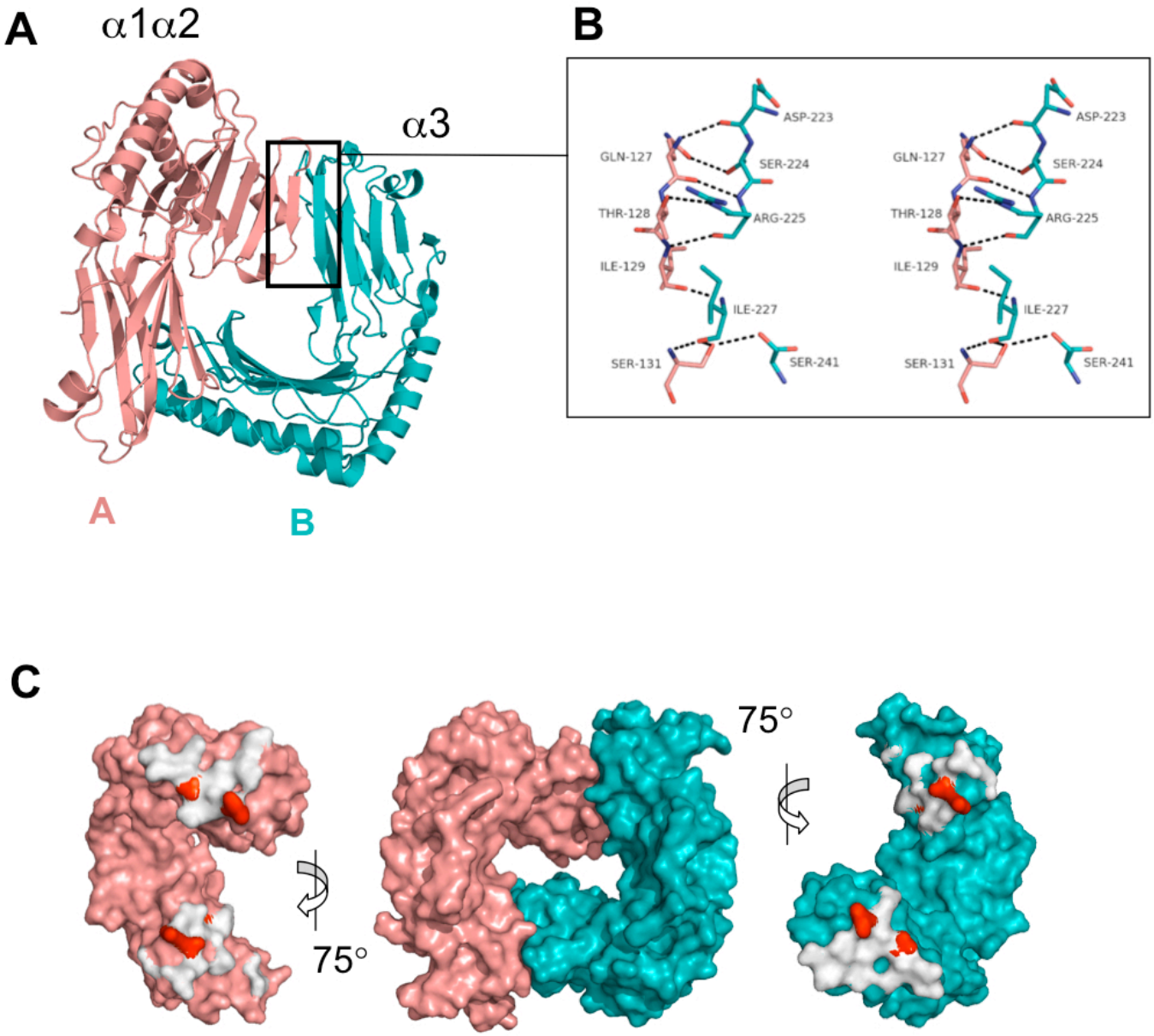

Figure 5.7. Dimer interface of m153. A) Chain A-platform/Chain B-α3 interface indicated by *boxed region*. B) Stereo view of the parallel β strand interactions between the β8' strand of chain A (*salmon*) and the G strand of chain B (*cyan*). The nine hydrogen bonds are shown as *black dashes*. Oxygen-*red*, Nitrogen-*blue*. C) Molecular surface representation of m153 dimer (*center*). At the left and right the two chains were rotated 75º out of the plane of the paper to display the buried interaction surfaces (*white*). The positions of the interface residues that were mutated to alanine (T128A, S131A, R225A, S241A) are shown in *red*.

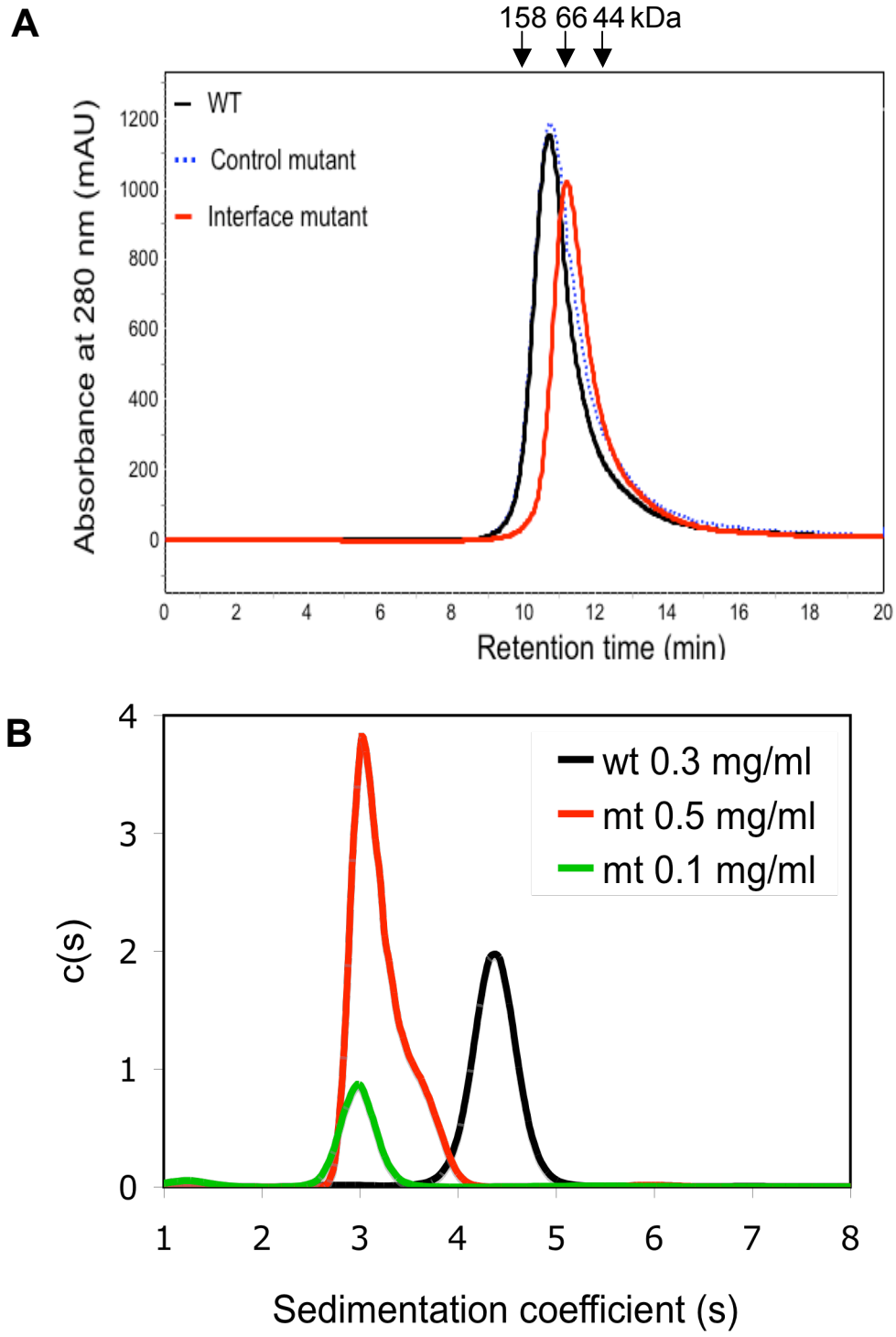

Figure 5.8. Mutations at the interface destabilize the m153 dimer. A) Size exclusion chromatography analysis of wild type (*black*), 4-alanine interface mutant (*red*) and control mutant (*dashed blue*) m153 purified from SF9 insect cells. The interface mutant migrates at a slower rate through the column, indicating a smaller size compared to wt m153 and the control mutant. B) Sedimentation coefficients of wild type m153 (*black* – 0.3 mg/ml) and quadruple mutant m153 (T128A, S131A, R225A, S241A, *red* – 0.5 mg/ml, *green* 0.1 mg/ml) as determined by sedimentation velocity ultracentrifugation. For experimental details see Chapter 2, section 2.15.

5.2.3 Comparison of m153 to the m145 family

m153 is related by sequence to proteins of the mouse and rat CMV 145 families but has no direct homolog in the rat virus (Rawlinson et al., 1996; Vink et al., 2000). The m153 protein is most closely related to m152 (28% identity), a known regulator of MHC-I and NKG2D ligands in MCMV-infected cells (Lodoen et al., 2003; Ziegler et al., 1997). Figure 5.9 shows a sequence alignment of the m145 family highlighting shared structural features. Based on comparison of m153 and m157 we suggest that the core of the viral MHC-I-like fold of the m145 family is comprised of the α1α2 domain, the extended H2b helix and an Ig-like α3 domain. The number of platform strands, the length of α2 on top of the platform and the position of some disulfide bonds may vary. A crucial stabilizing interaction for this MHC-I-like fold is that between E70 (α1 helix), R166 and W167 (H2b helix) (Figure 5.10). Apart from a cysteine in the α3 domain, these three residues are the only amino acids that are conserved throughout the mouse and rat 145 families, emphasizing the importance of this salt-bridge. Stretches of similarities are found in α helix and β sheet regions, whereas loop regions and the α3 domain show less conservation. The m153 residues involved in dimerization are not conserved in the rest of the family consistent with our observation that m151 and m152 do not dimerize in solution (unpublished). Thus dimerization may be unique to m153. Four family members (m17, m151, m152 and m155) contain cysteines that align with those of the unusual m153 C16-C171 disulfide. The C101-C108 and C203-C255 disulfides are also conserved among some of the family members. The limited sequence similarity of the N- and C-terminal regions of the extracellular domains of the m145 family members likely indicate a structural divergence in these parts of these molecules.

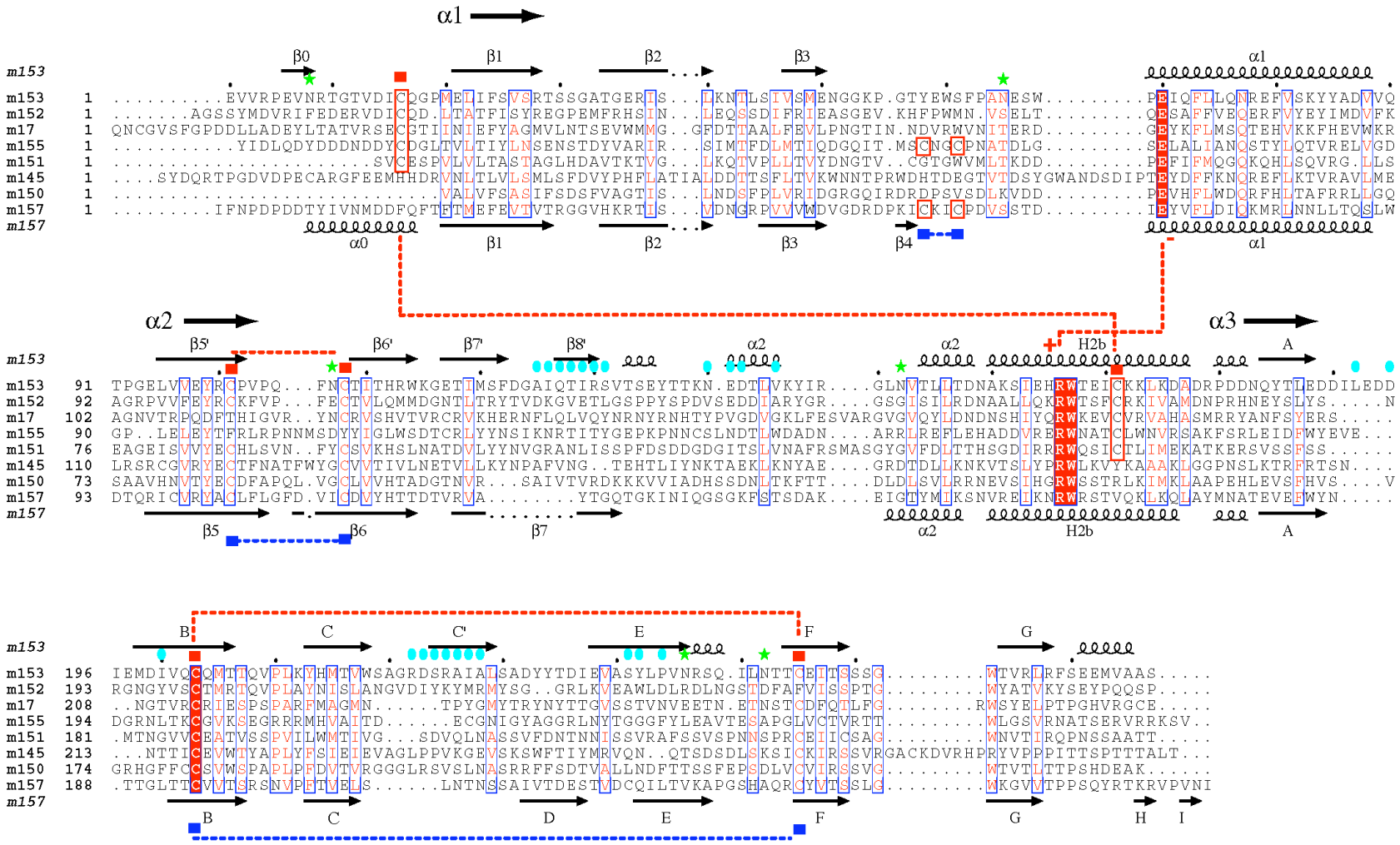
α1
β0
β1
β2
β3
α1
m153
m153 1 .....EVVRPEVNRTGTVDICQGPMELIFSVSRTSSGATGERISLKNTLSIVSMENGGKP.GTYEWSFPANESW.....PEIQFLLQNREFVSKYYADVVQ
m152 1 .....AGSSYMDVRIFEDERVDICQD.LTATFISYREGPEMFRHSINLEQSSDIFRIEASGEV.KHFPWMN.VSELT.....QESAFFVEQERFVYEYIMDVFK
m17 1 QNCGVSFGPDDLLADEYLTATVRSECGTIINIEFYAGMVLNTSEVWMMGGFDTTAALFEVLPNGTIN.NDVRWVNITERD.....GEYKFLMSQTEHVKKFHEVWKR
m155 1 .....YIDLQDYDDDNDDYCDGLTVLTIYLNSENSTDYVARIRSIMTFDLMTIQDGQIT.MSCNGCPNATDLG.....SELALIANQSTYLQTVRELVGD
m151 1 .....SVCESPVLVLTASTAGLHDAVTKTVGLKQTVPLLTVYDNGTV..CGTGWVMLTKDD.....PEFIFMQGQKQHLSQVRG.LLS
m145 1 ....SYDQRTPGDVDPECARGFEEMHHDRVNLTLVLSMLSFDVYPHFLATIALDDTTSFLTVKWNNTPRWDHTDEGTVTDSYGWANDSDIPTEYDFFKNQREFLKTVRAVLME
m150 1 .....VALVFSASIFSDSFVAGTISLNDSFPLVRIDGRGQIRDRDPSVSDLKVDD.....PEVHFLWDQRFHLTAFRRLLGQ
m157 1 .....IFNPDPDDTYIVNMDDFQFTFTMEFEVTVTRGGVHKRTISVDNGRPVVVWDVGDRDPKICKICPDVSSTD.....IEYVFLDIQKMRLNNLLTQSLW
m157
α0
β1
β2
β3
β4
α1
α2
β5'
β6'
β7'
β8'
α2
α2
H2b
α3
A
m153
m153 91 TPGELVVEYRCPVPQ...FNCTITHRWKGETIMSFDGAIQTIRSVTSEYTTKN.EDTLVKYIR....GLNVTLLTDNAKSIEHRWTEICKKLKDADRPDDNQYTLEDDILEDD
m152 92 AGRPVVFEYRCKFVP...FECTVLQMMDGNTLTRYTVDKGVETLGSPPYSPDVSEDDIARYGR....GSGISILRDNAALLQKRWTSFCRKIVAMDNPRHNEYSLYS.....N
m17 102 AGNVTRPQDFTHIGVR..YNCRVSHVTVRCRVKHERNFLQLVQYNRNYRNHTYPVGDVGKLFESVARGVGVQYLDNDNSHIYQRWKEVCVRVAHASMRRYANFSYERS.....
m155 90 GP..LELEYTFRLRPNNMSDYYIGLWSDTCRLYYNSIKNRTITYGEPKPNNCSLNDTLWDADN....ARRLREFLEHADDVRERWNATCLWNVRSAKFSRLEIDFWYEVE...
m151 76 EAGEISVVYECHLSVN..FYCSVKHSLNATDVLYYNVGRANLISSPFDSDDGDGITSLVNAFRSMASGYGVFDLTTHSGDIRRRWQSICTLIMEKATKERSVSSFSS.....
m145 110 LRSRCGVRYECTFNATFWYGCVVTIVLNETVLLKYNPAFVNG..TEHTLIYNKTAEKLKNYAE....GRDTDLLKNKVTSLYPRWLKVYKAAAKLGGPNSLKTRFRTSN....
m150 73 SAAVHNVTYECDFAPQL.VGCLVVHTADGTNVR...SAIVTVRDKKKVVIADHSSDNLTKFTT....DLDLSVLRRNEVSIHGRWSSTRLKIMKLAAPEHLEVSFHVS....V
m157 93 DTQRICVRYACLFLGFD.VICDVYHTTDTVRVA.....YTGQTGKINIQGSGKFSTSDAK....EIGTYMIKSNVREIKNRWRSTVQKLKQLAYMNATEVEFWYN.....
m157
β5
β6
β7
α2
H2b
A
B
C
C'
E
F
G
m153
m153 196 IEMDIVQCQMTTQVPLKYHMTVWSAGRDSRAIALSADYYTDIEVASYLPVNRSQ.ILNTTCEITSSSG.....WTVRLRFSEEMVAAS.....
m152 193 RGNGYVSCTMRTQVPLAYNISLANGVDIYKYMRMYSG..GRLKVEAWLDLRDLNGSTDFAFVISSPTG.....WYATVKYSEYPQQSP.....
m17 208 ..NGTVRCRIESPSPARFMAGMN.....TPYGMYTRYNYTTGVSSTVNVEETN.ETNSTCDFQTLFG.....RWSYELPTPGHVRGCE.....
m155 194 DGRNLTKCGVKSEGRRRMHVAITD.....ECGNIGYAGGRLNYTGGGFYLEAVTESAPGLVCTVRTT.....WLGSVRNATSERVRRKSV..
m151 181 .MTNGVVCEATVSSPVILWMTIVG...SDVQLNASSVFDNTNNISSVRAFSSVSPNNSPRCEIICSAG.....WNVTIRQPNSSAATT.....
m145 213 ...NTTICEVWTYAPLYFSIEIEVAGLPPVKGEVSKSWFTIYMRVQN..QTSDSDLSKSICKIRSSVRGACKDVRHPRYVPPPITTSPTTTALT...
m150 174 GRHGFFCCSVWSPAPLPFDVTVRGGGLRSVSLNASRRFFSDTVALLNDFTTSSFEPSDLVCVIRSSVG.....WTVTLTTPSHDEAK.....
m157 188 .TTGLTTCVVTSRSNVPFTVELS.....LNTNSSAIVTDESTVDCQILTVKAPGSHAQRCYVTSSLG.....WKGVVTPPSQYRTKRVPVNI
m157
B
C
D
E
F
G
H
I

Figure 5.9. Amino acid sequence alignment of the m145 family. The predicted extracellular domains of all m145 family members (Refseq: NC_004065 (Rawlinson et al., 1996)) were aligned using ClustalW (Chenna et al., 2003) and optimized based on m153 and m157 structure. Secondary structure elements of m153 are shown above and those of m157 shown below the alignment. Cysteines involved in disulfide bonds are indicated by *red* (m153) and *blue* (m157) *squares*, and the respective pairs are indicated. Cysteines that are not conserved throughout the family, but are predicted to form disulfide bonds are *boxed in red*. Residues involved in a salt bridge (E70 and R166) are also indicated. N-linked glycosylation sites are indicated by *green stars*. The residues involved in m153 dimer interface contacts are indicated by *blue ovals*. The figure was generated with ESPRIPT (Gouet et al., 1999).

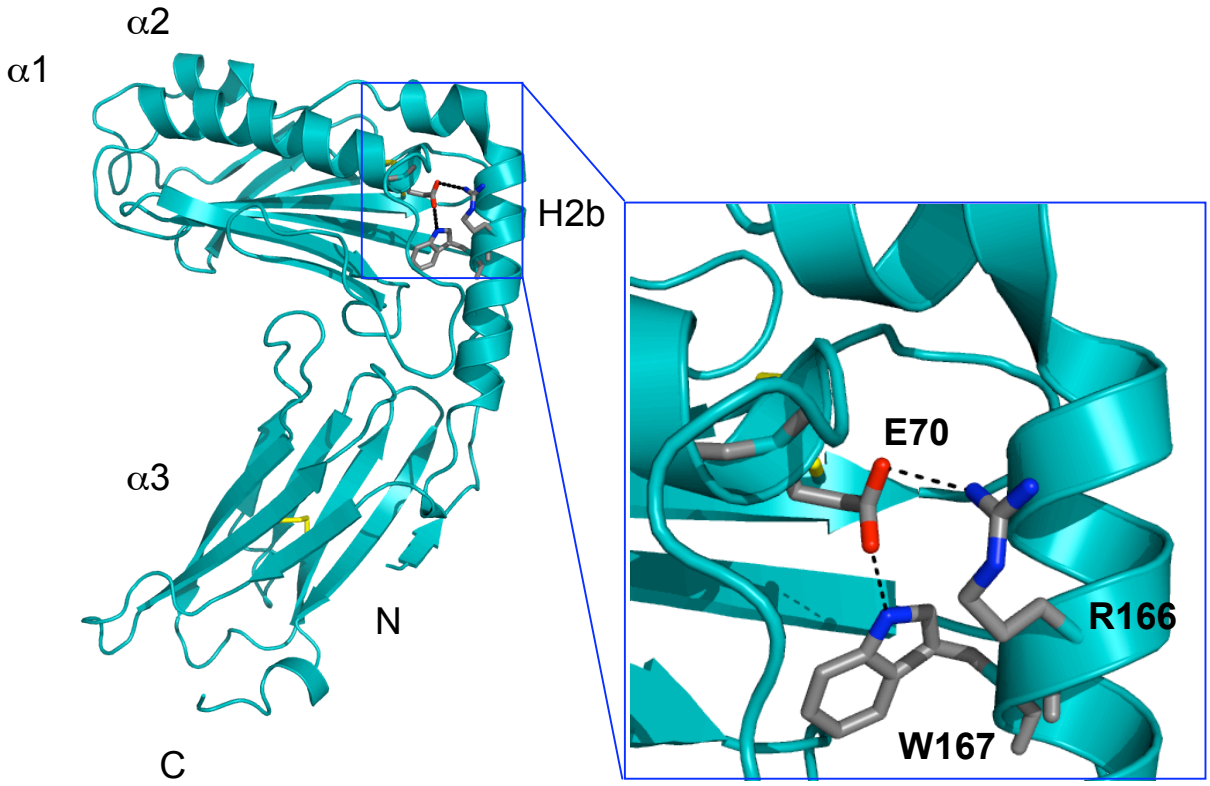

Figure 5.10. Conserved interaction between E70, R166 and W167 connects α1 and H2b helices. B chain of m153 (*cyan*), disulfides (*yellow*). Inset, E70, R166 and W167 are labeled, hydrogen bonds shown in *black*.

5.3 Discussion

MHC-I molecules play a crucial role in the protection of the host against virus infection. Not only are MHC-I molecules essential for the detection of infection and priming of the cytotoxic $CD8^+$ T cell response, but their presence on the cell surface protects healthy cells from attack by natural killer cells. Viral molecules with an MHC-I-like structure are likely to be excellent decoys for inhibitory natural killer receptors and may be able to interact with numerous molecules involved in the immune response. It is therefore not surprising that herpesviruses have incorporated MHC-I-like molecules in their arsenal of immunoevasins. Human, mouse and rat CMV encode MHC-I-like molecules that exhibit different levels of similarity to MHC-Ia molecules (Rawlinson et al., 1996; Vink et al., 2000). HCMV encodes the MHC-I homolog UL18 which binds both β2m and peptide and engages the inhibitory receptor LIR-1 (Cosman et al., 1997). It also encodes UL142, which functions to inhibit NK cell lysis, has less sequence similarity to MHC-I and is predicted to consist of only the MHC-I α1α2 domain (Wills et al., 2005). MCMV encodes proteins like m144 that can associate with β2m, and others like m153 and m157, members of the m145 family, that are expressed without β2m. It is likely that several host genes have been captured by viruses during the course of coevolution (Alcami and Koszinowski, 2000). In the case of the MHC-I viral homologs it is probable that the closely related MHC-I genes like *m144* and *r144* were originally acquired from the host and that the distantly related m145 and r145 families arose via gene duplication and expansion of an ancestral *144* gene shaped by the selective pressures of the host immune response.

The crystal structure of MCMV m153 provides an example of the versatility of the MHC-I fold and is the first report of an obligate non-covalent dimer composed of two MHC-I-like chains. Together with the recently reported m157 structure, it highlights both the conserved and divergent features of the m145 family. The m153 monomer retains the core MHC-I characteristics, a β-sheet platform that supports two α-helices and an Ig-like α3 domain, but it exploits several structural adaptations to yield a stable molecule in the absence of peptide and β2m. Three main features combine to stabilize the m153 monomer: 1) the closely spaced α1 and α2 helices on the platform do not form a groove and alleviate the need for peptide binding; 2) the extended H2b helix bridges the α1α2 domain to the α3 domain; and 3) numerous interdomain contacts and two unique disulfide bonds (C16-C171 and C101-C108) stabilize the structure. Some of these features are shared among the other members of the m145 family. Whereas m157 is GPI-linked and functions as a monomer (Arase et al., 2002), m153 has a bona fide transmembrane region and a large (47 amino acid) intracellular domain. We have shown that m153 is a stable dimer when expressed in mammalian cells, and the crystal structure of the soluble ectodomain reveals the mode of dimerization.

Dimerization is unusual for MHC-I molecules. Although dimers of some classical MHC-I molecules have been reported i.e., HLA-B27 (Bowness, 2002) and HLA-G (Shiroishi et al., 2006), these are disulfide-linked and their physiological relevance remains unclear. A non-disulfide linked dimer has been observed in crystals of the rat FcRn. Unlike m153, the two MHC-I molecules of the FcRn interact via their α3 and β2m domains, utilizing extensive protein-protein and protein carbohydrate interactions at the interface (Burmeister et al., 1994a). In the m157 crystal, a dimer of the same orientation as m153 is formed with one of the symmetry related molecules. In m157 this dimer interface is

formed by anti-parallel beta strand interactions between the β6 strand of the platform and the D strand of the α3 domain. Thus the same chain orientation but an opposite sheet of the α3 domain (ABED) is utilized in the observed crystal packing.

To gain insight into possible ligand binding sites on m153 we have examined regions corresponding to known interaction sites on murine MHC-I like molecules. These include the CD8αα binding site (α3 domain residues 220-228 and residues of the α1α2 domain platform), the Ly49A NK receptor binding site ("site 2" including residues from the α3 domain, the α1α2 domain platform, and key residues of β2m), and the region of the FcRn-Fc interaction site (N-terminal portions of the α2 domain and of β2m) (Margulies et al., 2007). The compact nature of the m153 dimer, its lack of β2m association, and the regions that are masked by dimerization make it unlikely that any of the above mentioned sites are available for ligand binding.

Since m153 is clearly related to other immunoevasins by both amino acid sequence and structure, it may be expected also to function to subvert the host immune response. Several features strongly indicate that m153 has a significant role in the viral life cycle. 1) Several regions of the m153 sequence are conserved among related molecules with known immunoregulatory function. m152 and m155 conserve the C16-C171 disulfide, and m152 and m145, as well as m157, conserve the β5'-β6' C101-C108 disulfide. 2) This is a readily expressed viral glycoprotein easily detected both intracellularly and at the cell surface in MCMV-infected fibroblasts. 3) Heteroduplex mobility assay (HMA) and DNA sequence analysis have been used to examine the levels of sequence variation of a number of MCMV genes of isolates from wild mice and laboratory strains. The MHC-Iv immunoevasins m144, m155 and m157 have significant variation, while m152

is highly conserved (Smith et al., 2006; Voigt et al., 2003). m153, like m152, is highly conserved among many strains showing little variation by both HMA and sequencing (Personal communication: Lee Smith and Alec Redwood, University of Western Australia). Such conservation implies not only a role in viral survival, but suggests that m153, like m152, may interact with an invariant site on a host molecule (Smith et al., 2006).

The following chapter presents our approach to the identification of ligands for m153 and describes the identification of mouse spleen cells that express a putative m153 ligand.

CHAPTER 6

IDENTIFICATION OF SPLEEN CELL SUBPOPULATIONS THAT ENCODE A PUTATIVE LIGAND FOR MCMV m153

6.1 Introduction

Virus-encoded proteins that are expressed at the surface of infected cells may serve a variety of different functions. Some are incorporated in the mature virus particles of enveloped viruses and facilitate adhesion and entry of viruses into uninfected cells and thereby enable the virus to spread. Other surface expressed viral proteins interact with and manipulate cells of the host immune response to create a favorable environment for virus survival. m153 forms part of a family of glycoproteins of which four have described immunevasion functions. The functions of m145, m152 and m155 are related in terms of their interaction with three different MHC-I-like NKG2D ligands. m152 also downregulates host MHC-I and m157 interacts with activating and inhibitory NK cell receptors. The MHC-I fold that was predicted for the m145 family has been proven for m153 (Chapter 5, (Mans et al., 2007)) and m157 (Adams et al., 2007). Thus it seems likely that the m145 family members share a similar MHC-I-like fold. The members with established function all interact with molecules that are either structurally related to MHC-I or interact with MHC-I molecules under normal physiologic circumstances. Since there are many examples of proteins with the MHC-I fold that have functions other than antigen presentation to T cells, just having a structure similar to MHC-I does not suggest an obvious function for any given protein. Since we have shown that m153 does not bind peptide or β2m it is clear that it would not function like traditional MHC-I

molecules. To evaluate whether m153 could have the same function as other m145 family members we have tested the effect of transfected m153 on the cell surface levels of MHC-I, and have observed only a small effect on MHC-I surface levels at very high overexpression levels of m153 (Chapter 3). Immunoprecipitation studies of m153 in metabolically labeled MCMV-infected cells did not detect any binding partner (data not shown). To elucidate the function of MCMV m153 one can approach the problem in several different ways. An *m153* deletion mutant can be constructed and the effect of the deletion evaluated in different mouse models of MCMV infection. Should a clear phenotype be observed, the organ and cell types in which the deletion has its greatest effect can be studied. In another approach, the viral molecule can be generated in recombinant form and used as "bait" to identify cell lines or cell types that express a ligand. Once a target population is identified, cDNA expression cloning can be used to find the ligand. The C-type lectin-related ligands for the NKRP1 family of NK cell receptors have been identified by a similar approach using NKRP1 reporter cells to screen tumor cells for ligands (Iizuka et al., 2003).

We have used the reporter cell strategy to initiate the search for ligands of MCMV m153. In this chapter we will describe the generation of an m153-reporter cell line and the identification of mouse spleen cell populations that specifically stimulate the reporter cells.

6.2 Results

6.2.1 Generation of m153z_43.1 and m144z_43.1 reporter cell lines

In order to follow a reporter cell strategy to identify a ligand for m153, we generated an m153-reporter cell line using the 43.1 T cell line. The 43.1 cell line was established by Ohtsuka and colleagues (Ohtsuka et al., 2004). They transfected an NFAT-GFP cassette in the 2B4 T cell hybridoma and selected a clone that produced GFP upon crosslinking of the TCR. We fused the extracellular domain of m153 to the transmembrane and intracellular domains of the human zeta chain. This fusion protein construct was then introduced in 43.1 cells using a retrovirus. Approximately 71% of the 43.1 cells were infected and expressed detectable m153-zeta fusion protein at the cell surface (Figure 6.1). We constructed a control m144-43.1 reporter cell line using the same strategy. We observed lower infection efficiency with the m144-zeta fusion protein virus and obtained a reporter cell population in which 45% of the cells express the m144-zeta fusion protein (Figure 6.1).

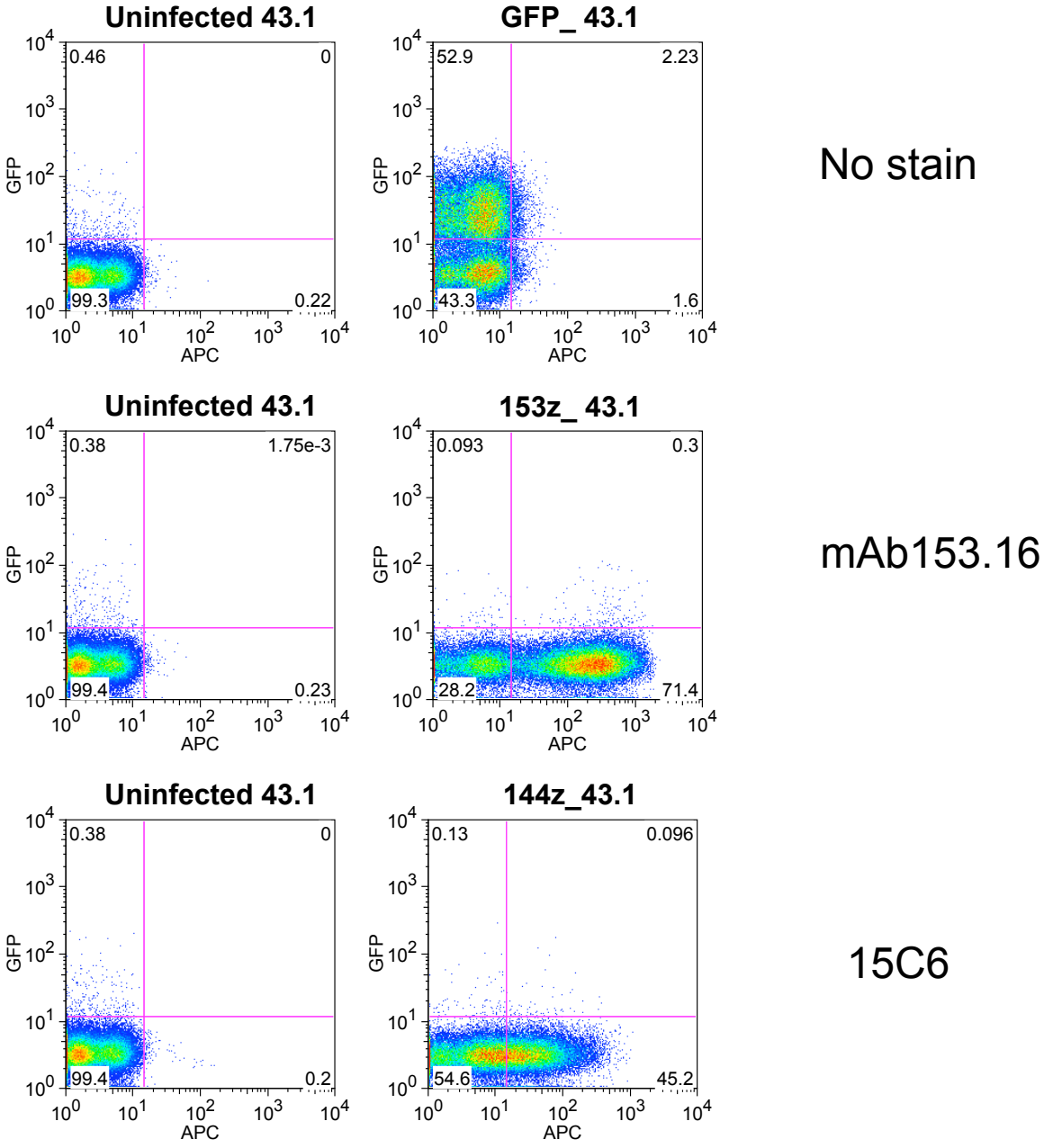

Figure 6.1. Infection of 43.1 reporter cells with GFP-, 153z- and 144z-retroviruses. *Upper panel* – Unstained uninfected 43.1 cells (*left*), unstained control GFP-virus infected 43.1 cells (*right*) 55% of cells express GFP. *Middle panel* – Uninfected 43.1 cells (*left*) and 153z-virus infected 43.1 cells (*right*) stained for m153 expression with mAb153.16 and anti-mouse IgG-APC. Seventy-one percent of 43.1 cells were infected with m153z. *Lower panel* – Uninfected 43.1 cells (*left*) and 144z-virus infected 43.1 cells (*right*) stained for m144 expression with mAb 15C6 and anti-mouse IgG-APC. Forty-five percent of 43.1 cells were infected with 144z. For experimental details see Chapter 2, section 2.17.

To establish whether the 153z_43.1 and 144z_43.1 reporter cell lines could produce GFP in response to crosslinking of m144 or m153, we cultured the reporter lines and the parental 43.1 cells on plates coated with monoclonal antibodies to the TCR (H57), m144 (15C6) and m153 (mAb153.16). The 153z_43.1 cells responded very weakly to antibody coated at 1 μg/ml on plates. Therefore we titrated the m153.16 antibody (Figure 6.2) and found that 4 μg/ml is the optimal concentration for plate-bound antibody stimulation of 153z_43.1. The 43.1 and 144z_43.1 cell lines could be triggered to produce GFP by antibody concentrations of 1 μg/ml (Figure 6.3).

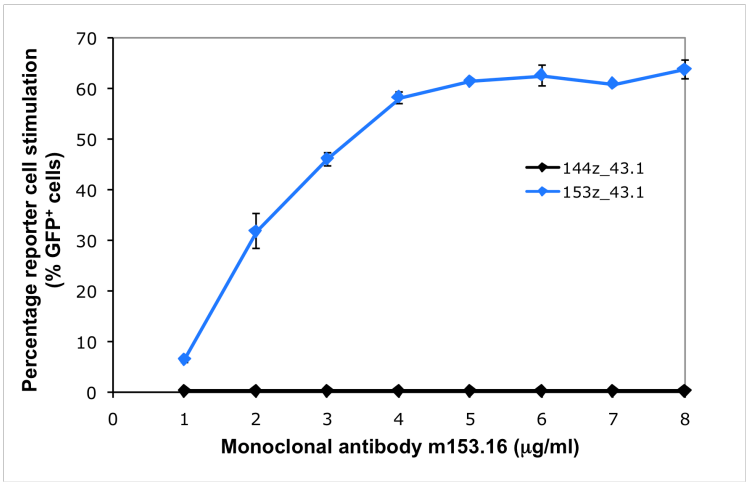

Figure 6.2. Titration of mAb153.16 in a plate-bound 153z_43.1 stimulation assay. 144z_43.1 and 153z_43.1 were cultured overnight on plates coated with increasing concentrations of m153 specific monoclonal antibody mAb153.16. The number of GFP positive cells was measured by FACS and represents the percentage reporter cell stimulation. Experimental details are described in Chapter 2, section 2.18.

Between 80-90% of all three reporter cell types produced GFP in response to plate-bound H57 anti-Vβ5. The numbers of 144z_43.1 cells that produced GFP corresponded to the proportion of cells that express m144 (45%) at the cell surface (Figures 6.1 and 6.3). The 153z_43.1 cells were slightly less responsive and between 50 and 60% of the cells produced GFP, although 70% of the cells express the 153-zeta fusion protein (Figures 6.1 and 6.3). This response was specific since both reporter lines did not produce significant levels of GFP after culture on the non-specific antibodies (Figure 6.3).

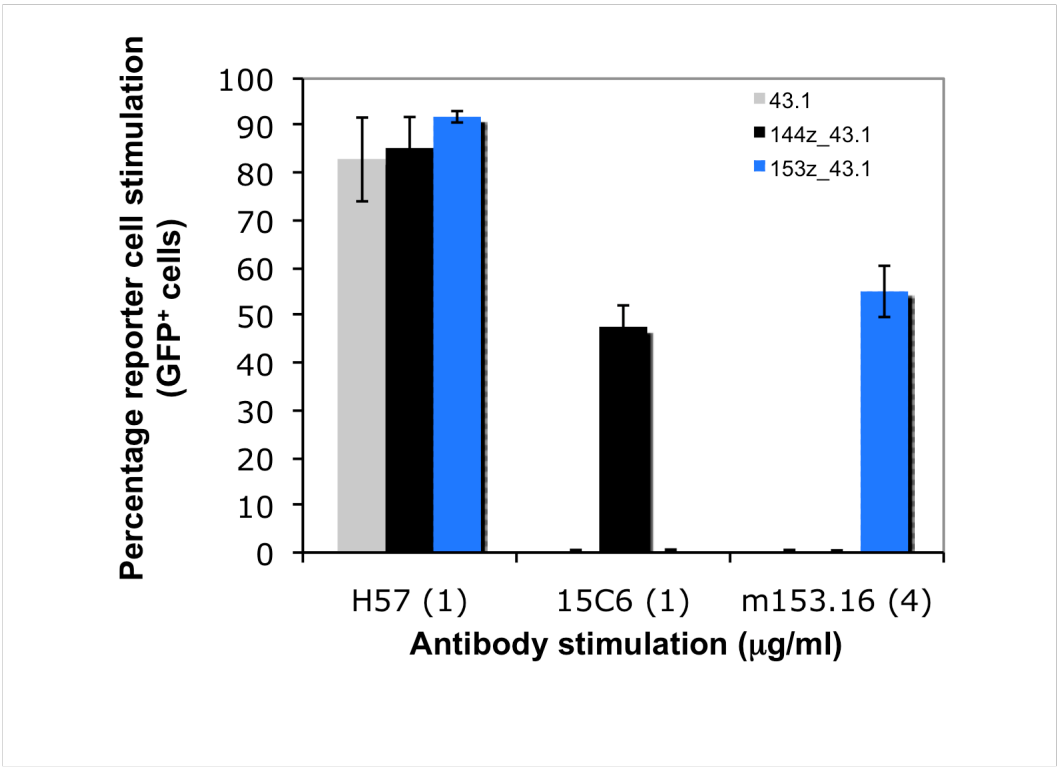

Figure 6.3. Antibody-specific triggering of GFP production in 43.1, 144z_43.1 and 153z_43.1 reporter cells. Reporter cells (1 x 10^5) were stimulated overnight with plate-bound H57 (1μg/ml), 15C6 (1 μg/ml) or mAb153.16 (4 μg/ml). The percentage of GFP^+ cells was determined by FACS and represents the reporter cell stimulation. For more details see Chapter 2, section 2.18.

6.2.2 Freshly isolated mouse splenocytes stimulate GFP production in 153z_43.1 cells

We performed overnight co-culture assays to screen several mouse cell lines of different tissue origin for reporter cell stimulation. None of the cell lines tested stimulated significant GFP production in 153z_43.1, 144z_43.1 or 43.1 cells (Figure 6.4). However, when we tested freshly isolated total spleen cells from B6 mice we observed GFP production in 10% of the 153z_43.1 reporter cells, whereas only 0.85% of the parental 43.1 and 1% of the 144z_43.1 cells respectively produced GFP.

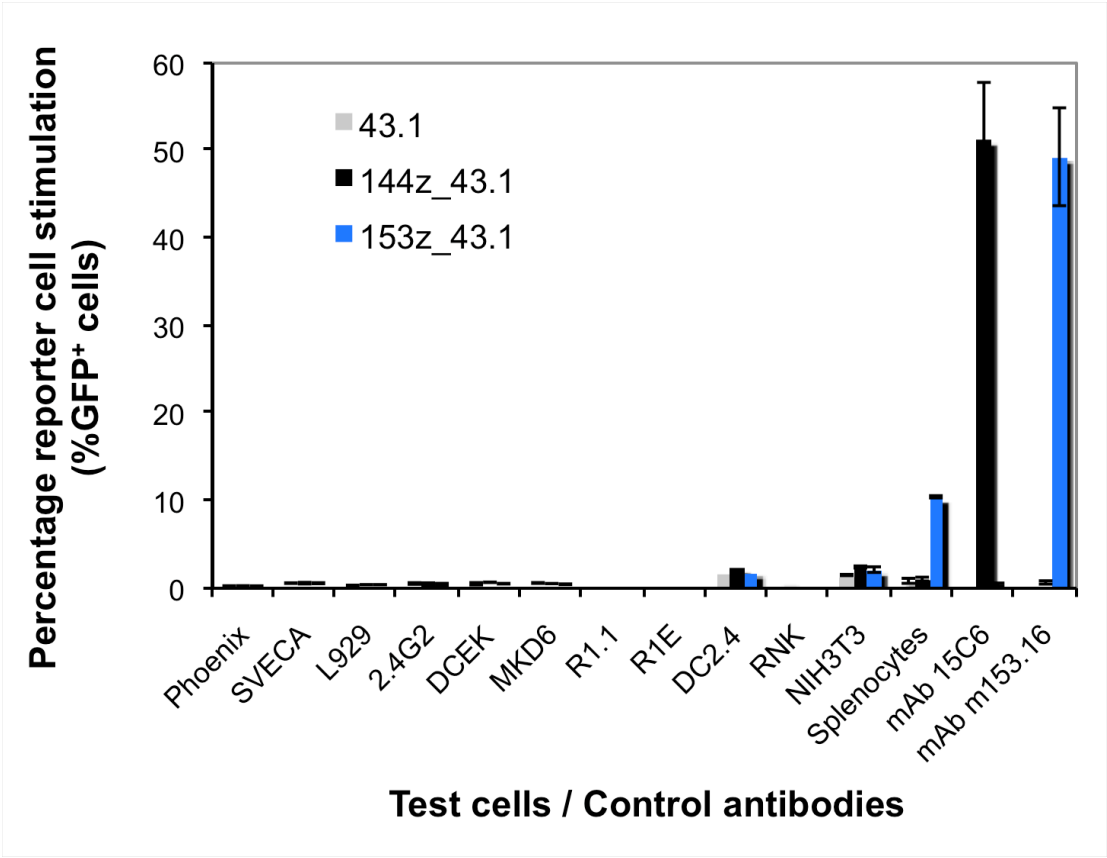

Figure 6.4. Mouse spleen cells stimulate GFP production in 153z_43.1 reporter cells. Coculture assays of 43.1, 144z_43.1 and 153z_43.1 reporter cells with a panel of cell lines and freshly isolated spleen cells. Reporter cells (1 x 10^5) were cocultured overnight with 1x10^6 test cells. The number of GFP^+ cells was determined by FACS. Reporter cells were discriminated from stimulator cells by forward and side scatter gating. Freshly isolated spleen cells from C57BL6 mice induced GFP expression in 10% of 153z_43.1 cells. Control stimulation was performed with plate-bound mAb 15C6 (144z_43.1) or mAb m153.16 (153z_43.1). Experimental details can be found in Chapter 2, sections 2.19-2.20.

To determine whether the stimulation we observed with freshly isolated spleen cells was dose responsive we titrated the number of spleen cells in a coculture assay. The stimulation of the 153z_43.1 reporter cells by mouse spleen cells was clearly dose-dependent (Figure 6.5). Both the parental 43.1 and control 144z_43.1 cells did not respond significantly to stimulation with total spleen cells.

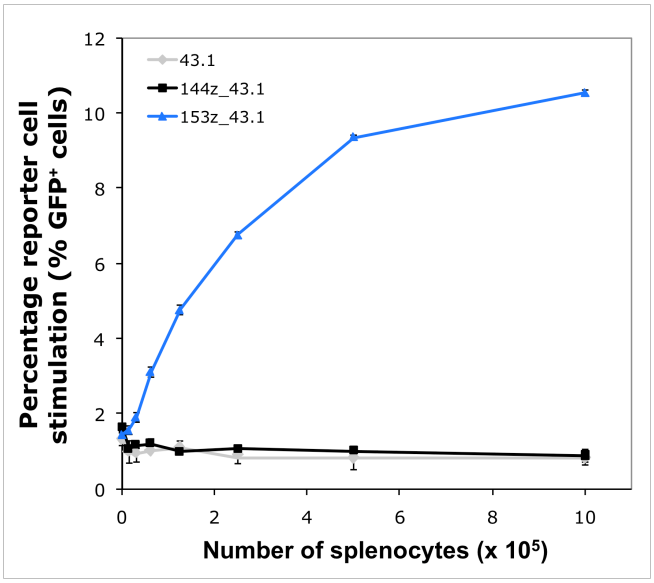

Figure 6.5. Dose response curve of spleen cell stimulation of 153z_43.1 reporter cells. The different reporter cells were cultured overnight with B6 splenocytes at a 1:10 reporter to stimulator ratio. The percentage GFP^+ cells was determined by FACS. Experimental details can be found in Chapter 2, section 2.19.

Addition of the soluble ectodomain of m153, expressed in insect cells, to spleen cell/153z_43.1 cocultures blocked reporter cell stimulation by 40% (Figures 6.6 and 6.7). Thus the stimulation of 153z_43.1 by mouse spleen cells is dose dependent and can be partially blocked by soluble m153.

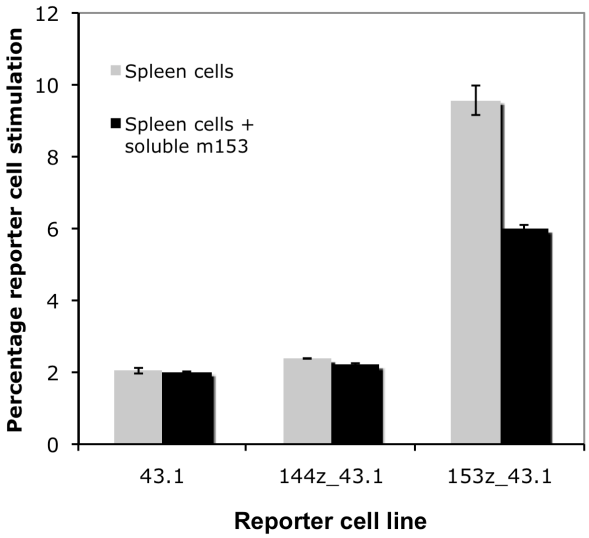

Figure 6.6. Soluble m153 partially blocks stimulation of 153z_43.1 reporter cells by mouse splenocytes. Mouse splenocytes (B6) were cocultured overnight with 43.1, 153z_43.1 or 144z_43.1 reporter cells at a ratio of 1:10 reporter to stimulator. The soluble extracellular domain of m153 was added to the cultures at a concentration of 128 μg/ml. Experimental procedures are detailed in Chapter 2, section 2.19.

In a first attempt to identify the spleen cell population/s that stimulate 153z_43.1 reporter cells, we depleted mouse spleen cells with beads specific for MHC class II, DX5 and CD11c. Although the depletion was incomplete (data not shown), we observed that depletion of $CD11c^+$ cells reduced the number of GFP^+ cells obtained by total spleen cell stimulation from 9.86% to 5.69%. Depletion of MHC II or DX5 positive cells had a smaller effect and reduced the percentage of GFP^+ cells to between 7.3-7.4%. When we tested the $CD11c^+$ enriched population in a coculture assay with 153z_43.1 (at a ratio of 1 : 4 reporter to stimulator) we observed a significant increase in GFP^+ cells (9.86% to 22.6%). These results suggested that the stimulating population might be $CD11c^+$ cells.

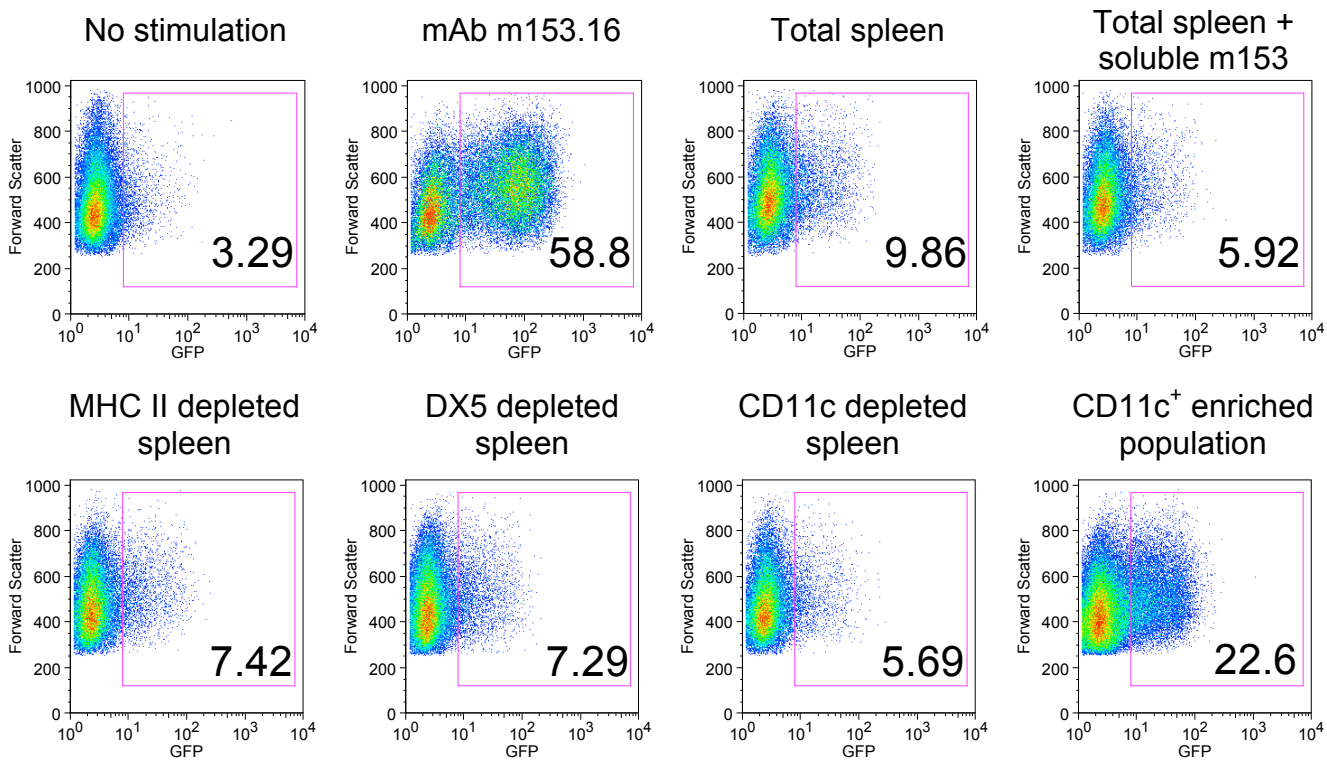

Figure 6.7. $CD11c^+$ enriched spleen cells increases 153z_43.1 reporter cell stimulation. 153z_43.1 cells (1 x 10^5) were cocultured with no stimulation, positive control mAb153.16 or 1 x 10^6 total mouse (B6) spleen cells, total spleen cells + soluble m153, MHC II depleted spleen cells, NK cell (DX5) depleted spleen cells, CD11c depleted spleen cells or 4 x 10^5 $CD11c^+$ enriched cells. After overnight culture the number of GFP^+ cells was determined by flow cytometry (the percentage GFP^+ cells is indicated in each gate). $CD11c^+$ cell depletion reduced 153z_43.1 stimulation from 9.9% to 5.7% and the $CD11c^+$ enriched population increased the number of GFP-expressing reporter cells to 22.6%. Experimental details are described in Chapter 2, section 2.19.

6.2.3 Generation of reporter cell lines 153z_43.1_H and 144z_43.1_H

Since the number of reporter cells that were stimulated by total spleen cells was relatively low, we wanted to increase the sensitivity of the coculture assay. The original m144- and m153-specific 43.1 reporter cell lines did not express the viral proteins on all cells in the respective populations (Figure 6.1). Therefore, we attempted to isolate reporter cell populations in which the majority of the cells expressed the m144- or m153-zeta fusion proteins. We performed limiting dilution experiments and were able to generate new cell lines with higher and more homogeneous expression of the viral fusion proteins. The new cell lines were designated 153z_43.1_H and 144z_43.1_H. Surface staining of these cell lines indicated that approximately 90% of 144z_43.1_H cells expressed m144-zeta and 98% of 153z_43.1_H cells expressed m153-zeta. (Figure 6.8A and C). When tested in a stimulation coculture assay, the capacity of the 153z_43.1_H cells to produce GFP in response to total spleen cell stimulation (1:10 reporter : stimulator) increased approximately two-fold (Figure 6.8B). The new reporter cell lines were used in all subsequent stimulation assays.

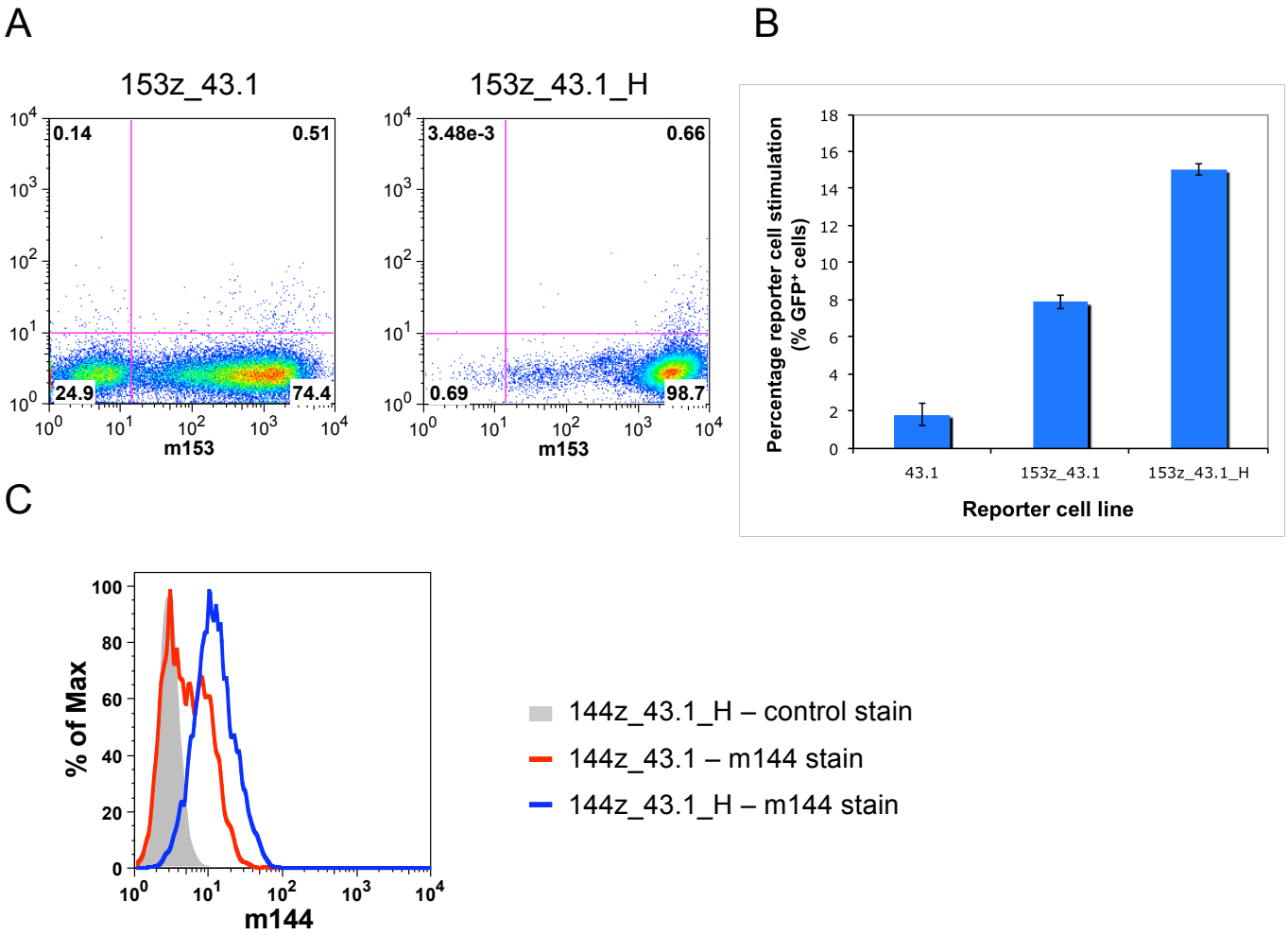

Figure 6.8. 144z_43.1_H and 153z_43.1_H reporter cells. A) m153-zeta surface expression on the original 153z_43.1 reporter cell population (*left*, 74% m153$^+$) and the 153z_43.1_H cells (*right*, 98% m153$^+$). Cells were surface stained with mAb153.16 and anti-mouse IgG-APC. B) Comparison of GFP production in 153z_43.1 and 153z_43.1_H cells. The respective reporter cells (1 x 10^5) were cultured overnight with 1 x 10^6 total spleen cells from BALB/c mice. The number of GFP positive cells was determined by FACS. C) Surface expression of m144-zeta on the original 144z_43.1 and the new 144z_43.1_H cells. Cells were stained with m144 specific mAb 15C6 and anti-mouse-PE. Experimental details are described in Chapter 2, sections 2.17 and 2.19.

6.2.4 Dendritic cells are the major population in mouse spleen that stimulates 153z_43.1_H reporter cells

Based on the initial results of the $CD11c^+$ depletion experiments, we isolated $CD11c^+$ cells by positive selection and tested these cells in a coculture assay with 153z_43.1_H and 144z_43.1_H. To obtain the highest numbers of dendritic cells from spleen the single cell suspensions were prepared by enzymatic disaggregation. This resulted in increased yields of $CD11c^+$ cells. The results in Figure 6.9A show that total spleen cells prepared by this method showed increased stimulation of 153z_43.1_H cells of ~ 30%. This represents a two-fold increase in the stimulation that was observed with mechanically aggregated spleen cells (Figure 6.8B). Purified $CD11c^+$ cells induced GFP production in approximately 70% of 153-specific reporter cells but did not cause significant GFP production in the control 144z_43.1_H cells (Figure 6.9A). Spleen cells that were depleted of about half of the original number of $CD11c^+$ cells had a reduced capacity to stimulate the 153z_43.1_H cells when compared to total spleen cells (18% versus 30%). Taken together these results show that $CD11c^+$ cells are potent and specific stimulators of 153z_43.1_H cells and therefore could encode a ligand for m153.

To establish whether additional spleen cell populations have the ability to stimulate 153z_43.1_H reporter cells we isolated $CD11b^+$ (monocytes/macrophages), $DX5^+$ (NK) and $CD19^+$ (B) cells by positive selection and $CD4^+$ and $CD8^+$ T cells by negative selection and tested them in coculture assays. In Figure 6.9B the percentage reporter cell stimulation relative to $CD11c^+$ stimulation (which was set to 100%) is shown.

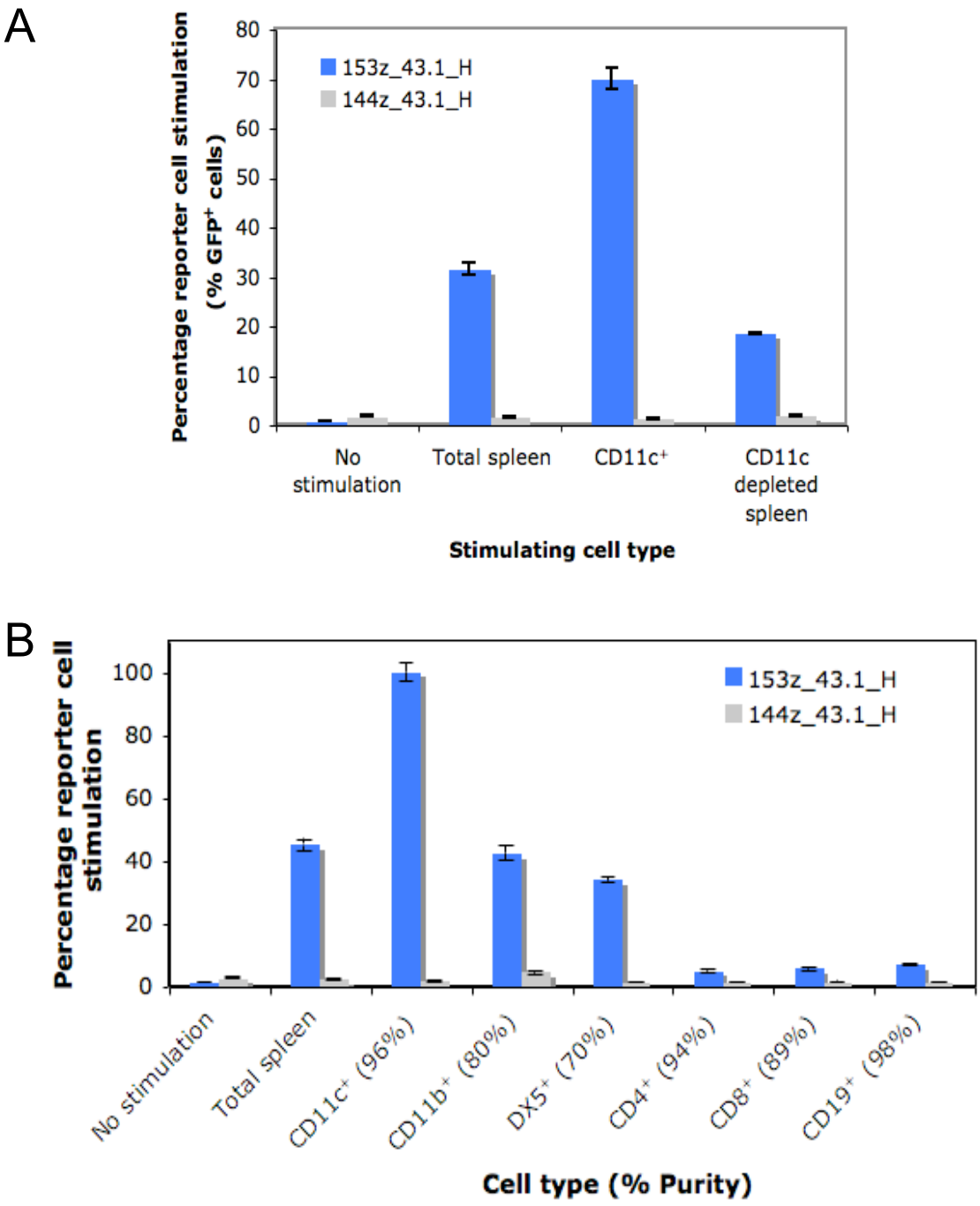

Figure 6.9. CD11c$^+$ cells are the most potent stimulators of 153z_43.1_H reporter cells. A) Total BALB/c spleen cells, CD11c$^+$ cells or CD11c$^+$-depleted spleen cells were cocultured overnight with 153z_43.1_H or 144z_43.1_H at a 1:10 ratio of reporter to stimulator. B) 144z_43.1_H or 153z_43.1_H cells were stimulated overnight with CD11c$^+$ cells, CD11b$^+$ cells (monocytes/macrophages), NK cells (DX5), B cells (CD19) or T cells (CD4 or CD8) (1:10 ratio reporter to stimulator). The purity of the respective stimulator populations is indicated in parentheses. In both A) and B) the reporter cells were stained with an anti-Vβ3-PE antibody, to facilitate discrimination between the reporter and stimulator cells. The number of Vβ3 and GFP double positive cells was determined by FACS and represents the percentage reporter cell stimulation. In B) the

stimulation observed by $CD11c^+$ cells was set at 100% and the other values normalized to that level. Details on the isolation of the spleen cell populations and the coculture assay can be found in Chapter 2, sections 2.19 and 2.21.

Compared to $CD11c^+$ cells, only $CD11b^+$ cells and NK cells caused significant stimulation of GFP production in 153z_43.1_H cells (Figure 6.9B). In mice, CD11b is expressed on monocytes/macrophages and is present at lower levels on granulocytes, NK cells and subsets of DCs. The CD11b population that was isolated for testing against the 153z_43.1_H reporter cells was 80% positive for CD11b. Sixteen percent of this population expressed both CD11b and CD11c and represents DCs. Thus the stimulation observed could in part be due to contaminating DCs. The purity of the NK cells was 70% based on DX5 expression. There was a substantial amount of $CD11c^+$ cell contamination (data not shown) in the NK cell preparation. To obtain a purer NK cell isolation we isolated NK cells by first performing negative selection and then enriching that population for $DX5^+$ cells using positive selection. Using this combination we obtained 91% pure $DX5^+$ NK cells (1-2% $CD11c^+$ DC contamination). When compared to $CD11c^+$ cells in a stimulation assay these NK cells could induce GFP production in 20% of the reporter cells, whereas 76% of the 153z_43.1_H cells responded to $CD11c^+$ cell stimulation (Figure 6.10). The low level of DC contamination in the NK preparation could not account for this stimulation, therefore it is likely that a ligand for m153 is present at low levels or only on a subset of NK cells. It is clear however, that B and T cells do not encode a ligand for m153, since even cell populations of high purity could not induce substantial GFP production in the 153z_43.1_H reporter cells.

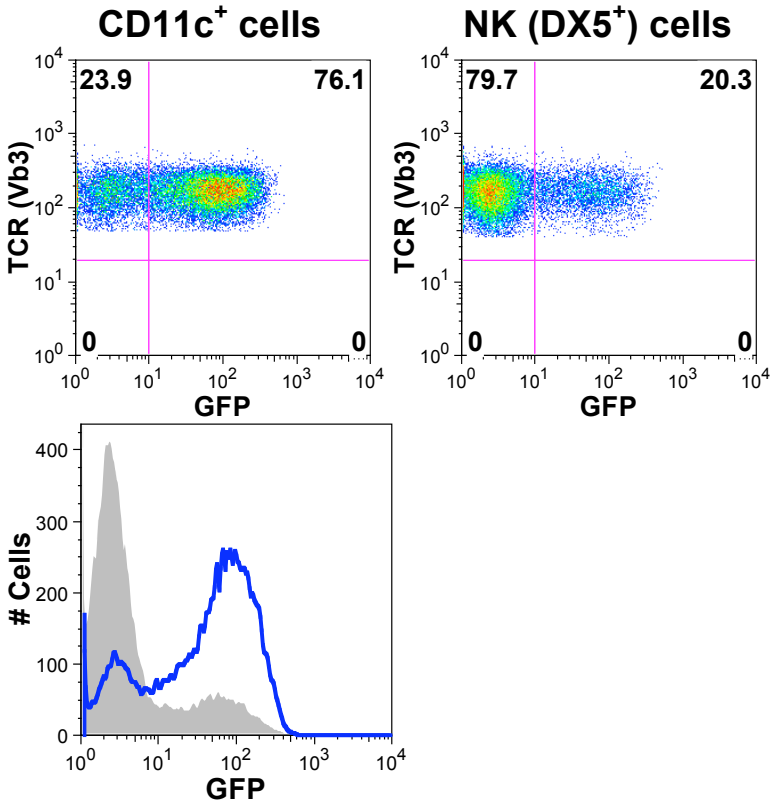

Figure 6.10. Comparison of 153z_43.1_H reporter cell stimulation by CD11c$^+$ DCs and DX5$^+$ NK cells. 153z_43.1_H reporter cells (1 x 10^5) were cocultured overnight with 9 x 10^5 DCs or NK cells. The cells were analyzed by FACS as described in the legend to Figure 6.9. *Filled grey histogram* – NK cells + 153z_43.1_H, *blue line* – DCs + 153z_43.1_H.

Another dendritic cell type that occurs at a low frequency in the spleen is the plasmacytoid dendritic cell (pDC). Since conventional dendritic cells were strong stimulators of m153-specific reporter cells, we isolated pDCs from mouse spleens and tested them for stimulation of the 153z_43.1_H cells. Our results in Figure 6.11 reveal that pDC are even more potent stimulators of 153z_43.1_H reporter cells. Compared to the ~ 70% GFP$^+$ cells induced by conventional CD11c$^+$ DCs, ~ 89% of the reporter cells produced GFP after overnight coculture with pDCs (Figure 6.11A). The control 144z_43.1_H cells did not produce any GFP in response to coculture with pDCs, confirming the specificity of the stimulation (Figure 6.11B). In summary, only cells of the innate immune system are capable of stimulating 153z_43.1_H cells. cDC and pDC

are the most potent stimulators, macrophages and NK cells provide much weaker stimulation and B and T cells no significant stimulation at all.

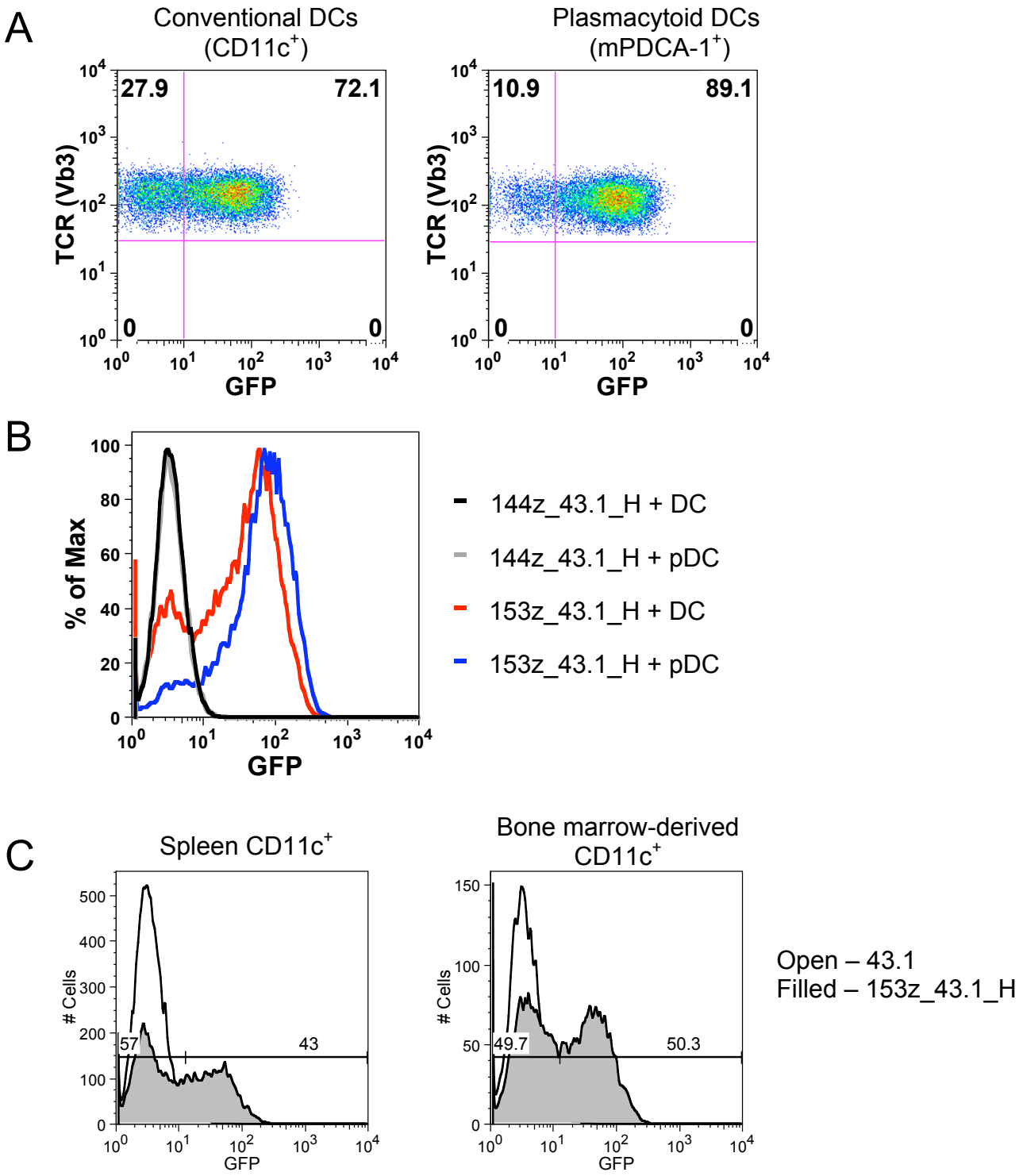

Figure 6.11. Plasmacytoid DC and bone marrow-derived CD11c$^+$ DC stimulate 153z_43.1_H reporter cells. A) GFP production in 153z_43.1_H reporter cells cocultured overnight with BALB/c CD11c$^+$ DCs (*left*) or pDCs (*right*) at a 1 : 7 ratio of reporter to stimulator cell. Reporter cells were stained for Vβ3 and analyzed for GFP

expression by FACS. Double positive cells (Vβ3+GFP) represent the number of stimulated cells. B) Histogram representation of GFP production in A with addition of the control cells 144z_43.1_H. C) GFP production in parental 43.1 and 153z_43.1_H reporter cells in response to overnight stimulation with splenic $CD11c^+$ cells (*left*) and BM-derived $CD11c^+$ cells (*right*). The cells were gated on Vβ3 expression and the percentage of GFP^+ cells was determined by FACS. Experimental details in Chapter 2, sections 2.21.2 and 2.22.

To establish whether dendritic cells derived from bone marrow cultures could stimulate 153z_43.1_H reporter cells we cocultured reporter cells with $CD11c^+$ cells isolated from six- day old bone marrow (BM)-GM-CSF cultures. BM-derived $CD11c^+$ cells stimulated 153z_43.1_H reporter cells as potently as $CD11c^+$ cells isolated from the spleen (Figure 6.11C).

We next titrated the number of spleen $CD11c^+$ cells in a coculture assay and determined that the stimulation we observed resembled a specific interaction and could be saturated. Maximal stimulation of the 153z_43.1_H reporter cells was observed with 5×10^5 $CD11c^+$ cells (Figure 6.12A). To ascertain that the reporter cell stimulation we observed was due to a specific interaction of MCMV m153 with a ligand/ligands on dendritic cells we pre-incubated splenic $CD11c^+$ cells with increasing concentrations of soluble m153, and soluble m152 as a negative control, and then performed the overnight coculture assay. Soluble m153, but not soluble m152, reduced the reporter cell stimulation from 56% to 29% (Figure 6.12B) indicating that the stimulation is m153 specific. In addition we show that the stimulation of 153z_43.1_H reporter cells by spleen $CD11c^+$ cells is cell contact dependent (Figure 6.12C). In a standard 24 well coculture assay, 52% of 153z_43.1_H cells produce GFP in response to $CD11c^+$ cells, whereas less that 1% parental 43.1 cells produce GFP. When the cocultures are performed using transwell inserts (0.4 μm membrane) that separate the stimulator cells from the reporter cells, the

reporter cell stimulation is abolished. Thus, CD11c^{+} cells stimulate 153z_43.1_H reporter cells in a dose-, m153-specific and cell contact-dependent fashion. We conclude that both conventional and plasmacytoid DC potently and specifically stimulate 153z_43.1_H reporter cells and thus express a ligand for MCMV m153.

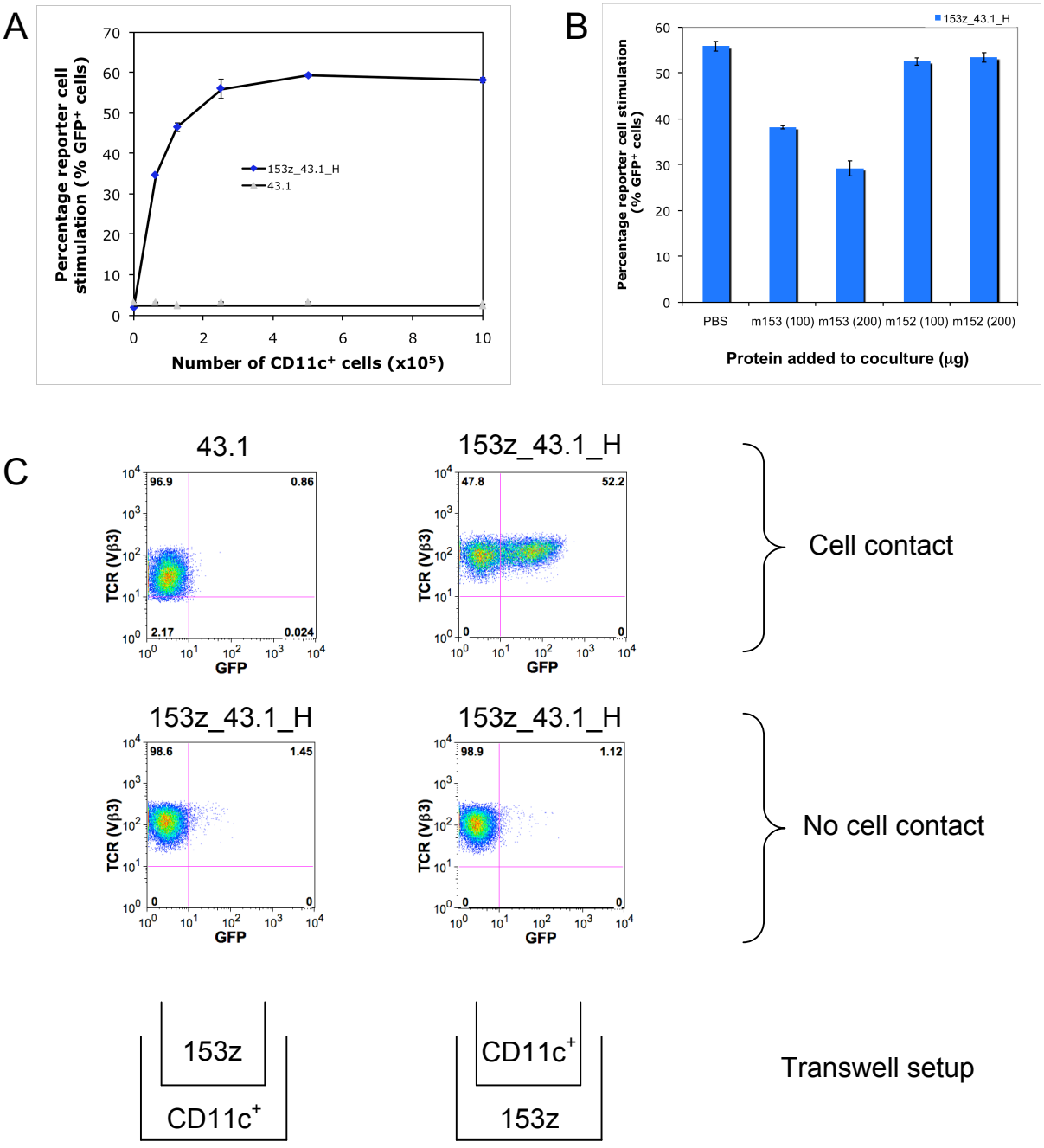

Figure 6.12. The stimulation of 153z_43.1_H reporter cells by CD11c$^+$ cells is m153-specific and dose- and cell contact-dependent. A) Percentage reporter cell stimulation after overnight coculture of parental 43.1 cells or 153z_43.1_H reporter cells (1x10^5) with increasing numbers of BALB/c spleen-derived CD11c$^+$ cells (0.625 – 10 x 10^5). Reporter cells were stained for TCR (Vβ3) expression and the percentage of TCR/GFP double positive cells represents stimulation. B) BALB/c CD11c$^+$ cells (5 x 10^5) were pre-incubated with either 100 or 200 μg soluble MCMV m152 or m153 for 30 min. at 37 °C before addition of 1 x 10^5 153z_43.1_H reporter cells and overnight coculture. Reporter cell stimulation was decreased from 56% in the PBS control to 38% (100 μg) and 29% (200 μg) after m153 pre-incubation. m152 pre-incubation did not affect reporter cell stimulation significantly (around 53% stimulation at both concentrations). C) Coculture of 1.2 x 10^6 BALB/c CD11c$^+$ cells with 5 x 10^5 43.1 or 153z_43.1_H reporter cells (*upper panels*) and transwell cocultures of 1.2 x 10^6 CD11c$^+$ cells with 5 x 10^5 153z_43.1_H reporter cells (*lower panels*). Reporter cells were stained for TCR expression to facilitate discrimination from stimulator cells. TCR/GFP double positive cells represent the fraction of activated reporter cells. The cell-cell contact assay is described in Chapter 2, section 2.23.

6.2.5 Dendritic cells from a variety of mouse strains stimulate 153z_43.1_H reporter cells

We have screened several mouse strains to establish how widely the m153 ligand is expressed. Total spleen cell populations and purified CD11c$^+$ cells from eight different strains were tested. DCs from all strains were able to stimulate the 153z_43.1_H reporter cells specifically although some strains were more potent than others (Figure 6.13). Further experiments were performed with cells isolated from BALB/c mice, since cells from this strain caused strong stimulation of the 153z_43.1_H reporter cells.

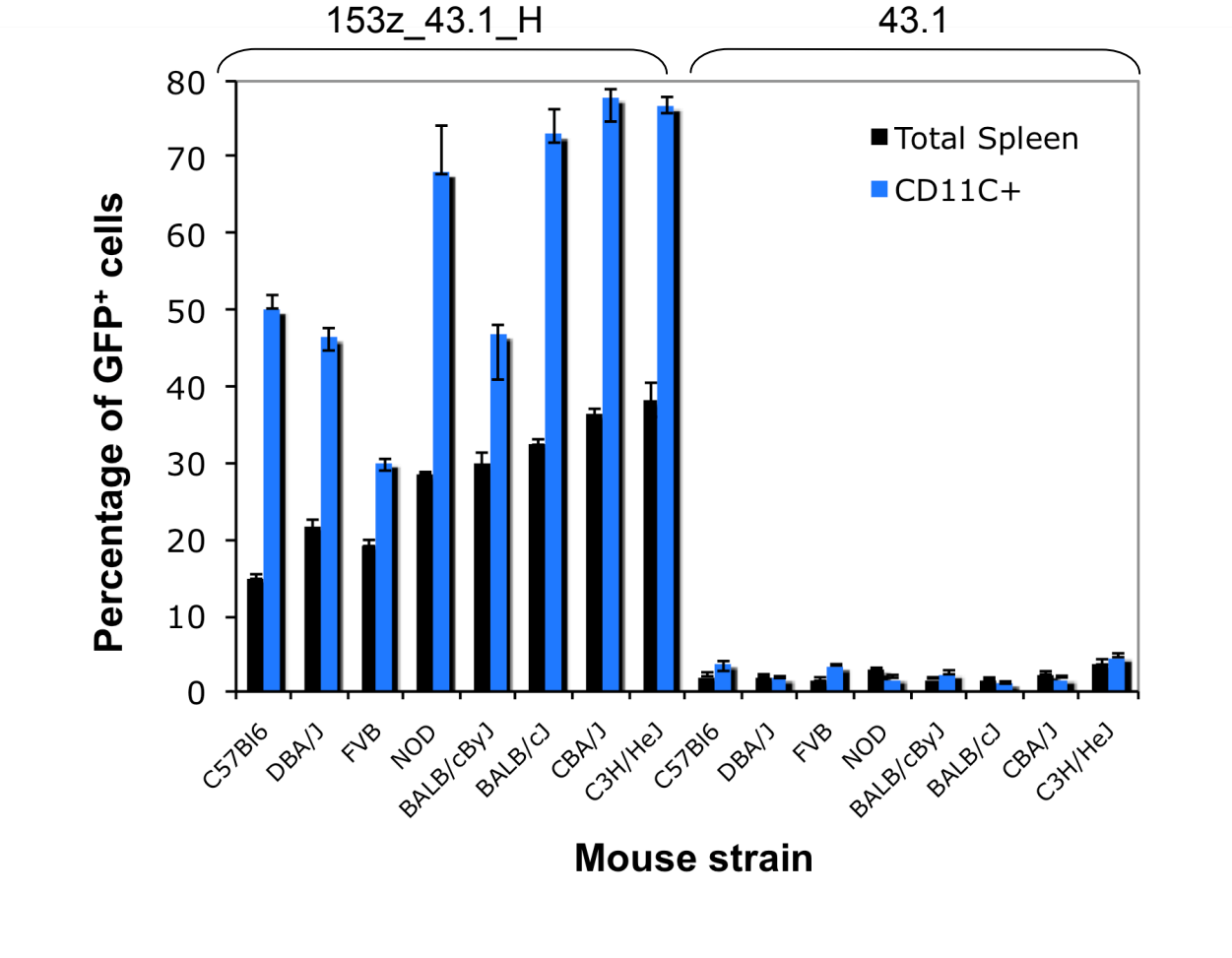

Figure 6.13. Splenocytes and CD11c$^+$ cells from eight mouse strains stimulate 153z_43.1_H reporter cells. Total spleen cells (1 x 10^6) or positively selected CD11c$^+$ cells (1 x 10^6) from each strain were cocultured overnight with 1 x 10^5 153z_43.1_H reporter cells or parental 43.1 cells as a control. The reporter cells were stained for TCR (Vβ3) and analyzed by FACS. The TCR/GFP double positive cells represent stimulated reporter cells. Details on the isolation of total spleen and CD11c$^+$ cells as well as the coculture protocol can be found in Chapter 2, sections 2.19-2.21.

We also tested total splenocytes and splenic OX62$^+$ dendritic cells isolated from Wistar rats for stimulation of the 153z_43.1_H reporter cells (Figure 6.14) but observed no significant GFP production. These results indicate that the m153 ligand is expressed in a range of mouse strains but not in the rat.

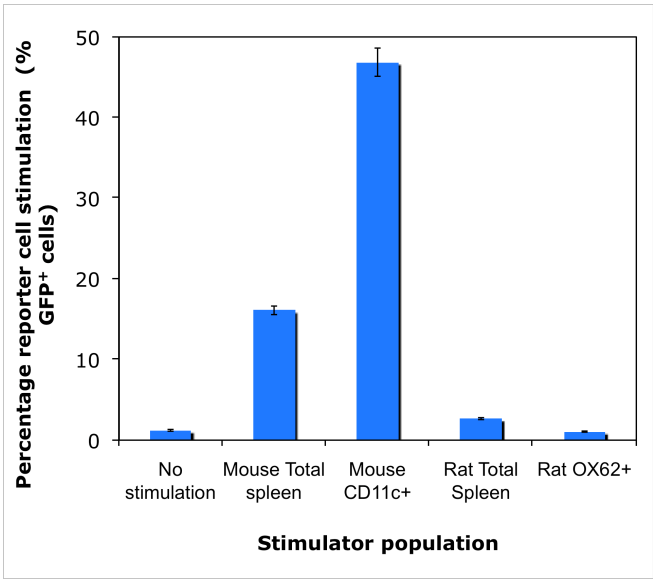

Figure 6.14. Rat OX62$^+$ dendritic cells do not stimulate the 153z_43.1_H reporter cells. Total spleen and dendritic cells were isolated from mice or rats and cocultured overnight with 153z_43.1_H reporter cells. The reporter cells were stained for TCR (Vβ3) expression and analyzed by FACS. The percentage of Vβ3 cells that express GFP represent the stimulated fraction. Details on the cell isolation and cocultures can be found in Chapter 2, sections 2.19-2.21.

6.2.6 Analysis of the surface phenotype and migration of CD11c$^+$ DCs after exposure to 153z_43.1_H reporter cells or plate-bound m153

We have shown that coculture of CD11c$^+$ DCs and 153z_43.1_H can induce GFP production in the m153-specific reporter cell line. These results imply an interaction of m153 with one or several unknown ligands on the surface of mouse DCs. Dendritic cells undergo rapid phenotypic changes linked to their maturation and function. We have examined whether the interaction of CD11c$^+$ DCs with 153z_43.1_H reporter cells specifically affects the expression levels of the DC surface markers CD40, CD80, CD86 and MHC class II. Dendritic cells were either cultured alone, with control 43.1 cells or with 153z_43.1_H reporter cells at a 1 : 1 ratio to optimize cell-cell interactions. The cell cultures were then stained for CD11c and the respective cell surface markers as shown in Figure 6.15.

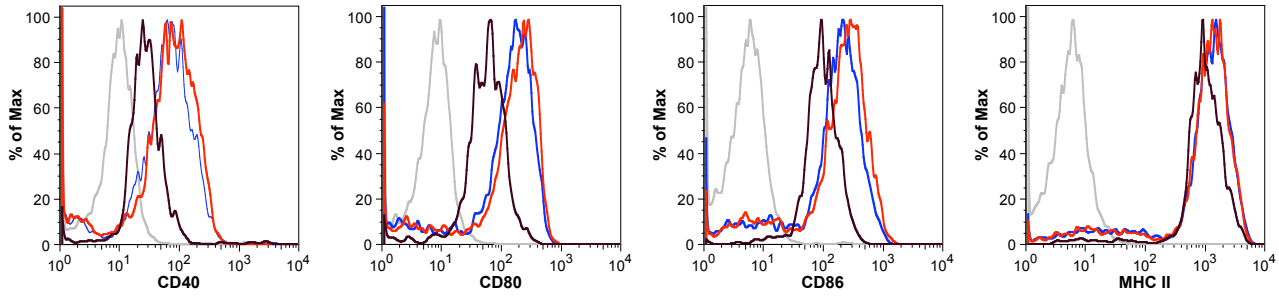

Figure 6.15. CD11c$^+$ surface phenotype is not specifically affected by coculture with 153z_43.1_H cells. The levels of CD40, CD80, CD86 and MHC II on the surface of BALB/c CD11c$^+$ cells were determined after overnight culture of CD11c$^+$ cells alone or with 43.1 or 153z_43.1_H reporter cells (at a 1:1 ratio). *Grey* – isotype control, *black* – CD11c$^+$ cells alone, *blue* – CD11c$^+$ + 43.1, *red* – CD11c$^+$ + 153z_43.1_H. Cells were stained for CD11c and gated on this population before analysis of the surface marker staining. Experimental details in Chapter 2, section 2.25.

Coculture of dendritic cells with the control 43.1 cells or 153z_43.1_H cells caused significant upregulation of CD40, CD80 and CD86 and slight upregulation of MHC class II in both cultures. Since the parental control cell line and 153z_43.1_H cells induced comparable upregulation in DC surface markers the effect is not specific to m153. Therefore the m153/DC interaction does not seem to specifically affect the surface levels of CD40, CD80, CD86 and MHC class II on dendritic cells.

Next we examined the effect of m153 on the migration capacity of CD11c$^+$ cells. Purified CD11c$^+$ cells were cultured overnight on plates coated with recombinant m153 or m152 as a negative control. The cells were then transferred to transwell chambers with 5 μm polycarbonate membranes in wells containing the chemokine MIP-3β (CCL19). The number of cells that had migrated was quantified by FACS after 5 hours of incubation.

In comparison to the PBS treated control DCs, the cells that were grown on plate-bound m152 or m153 exhibited a reduced capacity to migrate in response to MIP-3β (Figure 6.16). Therefore this effect was not specific to MCMV m153. DCs treated overnight with LPS showed only a slight decrease in migration.

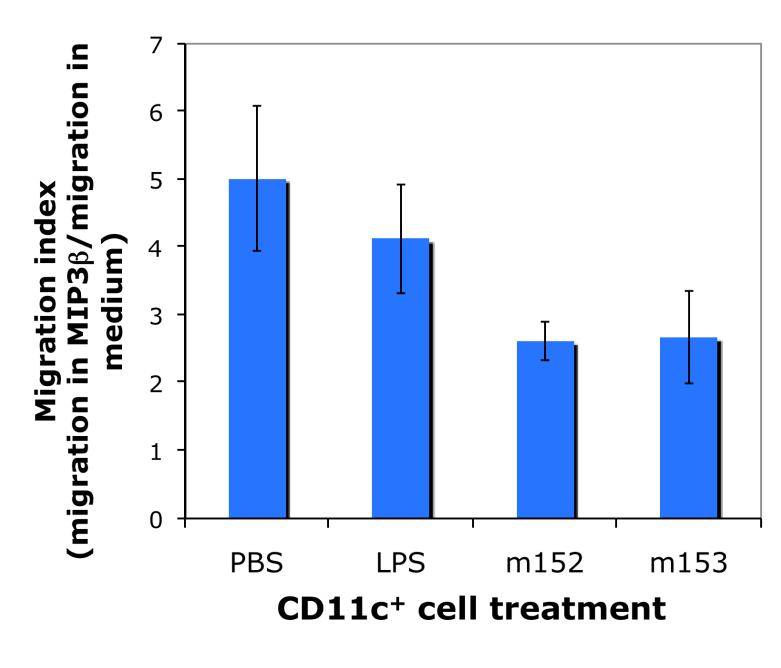

Figure 6.16 Migration of dendritic cells in response to MIP-3β (CCL19) is not affected by MCMV m153. BALB/c CD11c$^+$ cells were cultured overnight on plates coated with PBS, PBS + 1μg/ml LPS in the medium, m152 or m153 (10 μg/ml). The migration of the control and treated DCs was assessed in a migration assay in 5 μm transwell plates as described in Chapter 2, section 2.24. The migration index represents the ratio of number of cells migrating in chemokine (MIP-3β)/ number of cell migrating in medium.

6.3 Discussion

We have identified dendritic cells as a cell type that encodes a potential ligand for MCMV m153. By using the recombinant extracellular domain of m153 fused to the transmembrane and signaling chains of human zeta, we have created a reporter cell line (153z_43.1_H) that expresses GFP upon cross-linking of the m153-zeta fusion protein.

$CD11c^+$ dendritic cells derived both from the spleen and the bone marrow, as well as splenic plasmacytoid DCs, potently stimulate GFP production in the 153z_43.1_H cell line. The stimulation was shown to require cell-cell contact and increased in a dose dependent manner with increasing numbers of purified $CD11c^+$ DCs. The specificity of the interaction was confirmed by two different controls. An m144-specific reporter cell line, 144z_43.1_H, constructed in the same way as the m153-specific reporter line, did not produce GFP in response to coculture with dendritic cells. In addition, the stimulation of 153z_43.1_H cells could be blocked partially by addition of soluble m153. These results strongly suggest that an interaction between m153 and one or more molecules on DCs triggers GFP production in the m153-specific reporter cells. We were however, unable to stain DCs with either the dimer or tetramer of soluble m153 (data not shown). This could indicate that it is a low affinity interaction that can occur between molecules on the surfaces of interacting cells, but is not strong enough to be detected by surface staining.

Dendritic cells from a variety of mouse strains were able to stimulate the 153z_43.1_H reporter cells in a specific manner. We also tested rat dendritic cells for reporter cell stimulation. These cells were unable to induce GFP expression in the m153 reporter

cells. This correlates with the absence of a direct homolog of MCMV m153 in the rat CMV (Vink et al., 2000). Different dendritic cell subsets play pivotal roles in orchestrating the immune response to virus infections. Therefore it would not be surprising if MCMV targets this specific cell type via m153. In our experiments, pDCs induced nearly 20% more GFP positive cells than the same number of conventional $CD11c^+$ DCs. This could either indicate that the ligand is present at higher concentrations on pDCs, or that only a subset of $CD11c^+$ cells express the ligand at levels comparable to pDCs. This remains to be investigated. Since a target population has now been identified, a viable approach to identify the ligand for m153 is to construct a dendritic cell-specific cDNA library and screen this library with the reporter cell line. The success of this approach depends on the assumption that the ligand is a single molecule.

We have assessed the functional effect of m153 on dendritic cell surface phenotype and the ability of the cells to migrate in response to the chemokine MIP3β. Neither the surface phenotype nor the migration capacity of $CD11c^+$ dendritic cells was altered specifically due to interaction with 153z_43.1_H reporter cells. In contrast to the other members of the MCMV m145 family with defined functions, which all target NK cell related ligands, our data suggests that m153 targets dendritic cells of various subsets. The identification of the ligand for m153 and further functional characterization of the interaction should shed light on the mechanism that MCMV uses to manipulate these antigen presenting cells to its own advantage.

CHAPTER 7

CONCLUDING DISCUSSION

In this study we set out to characterize the m145 glycoprotein family encoded by MCMV and test the prediction that these proteins are structurally similar to MHC class I molecules, despite very low amino acid similarity between the viral proteins and MHC-I. The first MHC-I structure was determined twenty-one years ago (Bjorkman et al., 1987). At that time the mechanism of antigen presentation by MHC-I molecules was not well understood. The structure revealed the nature of the antigen-binding site and the authors correctly predicted that the unidentified electron density in the groove represented peptide antigen bound to the heavy chain. The classical role of MHC-I molecules in antigen presentation to CD8 T cells has been studied extensively in the past decades. However, more recently several examples of MHC-I related molecules with functions unrelated to peptide binding and presentation have been described. The neonatal rat Fc receptor structure was the first structure of a non-classical MHC-I molecule to be determined. The structure revealed a peptide-free, β2m-associated heavy chain in which the α1 and α2 helices are situated close together (Burmeister et al., 1994a). The structure of the FcRn in complex with Fc showed that a site distinct from the antigen binding groove (N-terminal end of α2 helix and β2m) is utilized in binding to Fc (Burmeister et al., 1994b). This study illustrated for the first time that the MHC-I fold is utilized for functions other than antigen presentation.

Human and mouse CD1 molecules present lipid antigens to NKT cells (Brigl and Brenner, 2004). The crystal structure of mouse CD1d revealed an MHC-I-like heavy

chain associated with β2m (Zeng et al., 1997). The helices that form the groove are longer than in classical MHC-I molecules and closer together and form a deep groove lined with hydrophobic residues, which is consistent with binding of lipid antigens. Further examples of proteins that have the MHC-I fold but perform functions unrelated to antigen presentation are the hemochromatosis gene product (HFE), which plays a role in the regulation of iron metabolism (Adams and Barton, 2007), the zinc-α2-glycoprotein (ZAG), a soluble lipid mobilizing factor involved in the regulation of body weight (Gohda et al., 2003) and the mouse M10 proteins, which are pheromone receptor-associated MHC-like proteins (Olson et al., 2006) that are expressed in the mouse vomeronasal organ. Both HFE and M10.5, an M10 family member, associate with β2m. Whereas HFE does not have a functional groove (Lebron et al., 1998), M10.5 has a groove region that resembles that of classical class I molecules but that was unoccupied in the crystal structure (Olson et al., 2005). The M10.5 structure is the first of an MHC-I-like molecule with an empty, open groove. M10.5 however is thermally unstable, which suggests that the groove is normally occupied by an unknown ligand (Olson et al., 2005). ZAG does not associate with β2m or peptide but binds a yet unidentified ligand with hydrophobic character (McDermott et al., 2006).

The stress-induced ligands Rae-1 (α-γ), MICA, and the viral MHC-I homolog m144 are proteins that exhibit more drastic deviations from the classical MHC-I fold. None of these molecules bind peptide, Rae-1β consists only of an α1α2 domain (Li et al., 2002), MICA and m144 conserve the full-length heavy chain but MICA does not associate with β2m (Li et al., 2001) whereas m144 crystallized in complex with β2m, but is also stable in recombinant form without β2m (Natarajan et al., 2006). To explore the similarities

between classical MHC-I proteins and the members of the MCMV m145 family we studied the proteins in transfected mammalian cells.

Initial experiments indicated that some members (m145, m151, m153) localize predominantly to the cell surface while others (m17, m152, m155) remain inside the cell. The cellular localization possibly reflects the site of action of the viral proteins, although not in all cases since m145 is detected readily at the cell surface in spite of the fact that it downregulates the NKG2D ligand, MULT-1, from the surface of MCMV-infected cells. Experiments in β2m- and TAP-deficient cell lines provided evidence that the surface expression of m145, m151 and m153 as well as M37 is independent of β2m or TAP activity. These results imply that the MCMV proteins have a modified MHC-I fold.

To generate protein for structural characterization we evaluated recombinant expression in bacteria. We were unable to refold any of the MHC-Iv proteins from bacterial inclusion bodies. Classical MHC-I proteins are generally refolded easily when the denatured heavy chain is added to folded β2m and peptide, which presumably act as nuclei for the heavy chain to fold properly. The non-classical MHC-I molecule Rae-1β was refolded successfully from *E. coli* inclusion bodies (Li et al., 2002), probably since it only consists of the α1α2 MHC-I domain. MICA, in contrast, was expressed in insect cells (*Trichoplusia ni*) to obtain protein for crystallization (Li et al., 2001). We expressed M37, m151 and m153 successfully in *Drosophila* insect cells and we have determined the crystal structure of m153. The structure of m157 was also reported recently (Adams et al., 2007).

The MHC-I fold (α1α2 and α3 domains) is clearly recognizable in both structures and the overall shape of the heavy chain is similar for m153 and m157. A most unusual feature of m153 is that it forms a stable, non-covalent dimer. In this dimer the two m153 heavy chains are arranged "head-to-tail" with the platform of one monomer contacting the α3 domain of the other. The β8' strand of the platform domain forms a parallel β strand interaction with the C' strand of the α3 domain. Mutation of four residues that contribute to the dimer interface to alanine, abolished the dimerization of m153.

In both m153 and m157 the α1 and α2 helices are positioned close together on the platform and no peptide binding groove is formed, reminiscent of Rae-1β and HFE. The most distinctive feature of these viral molecules is an extended α2 helix, designated H2b, which bends down at the edge of the platform sheet and extends towards the α3 domain. The upper part of the H2b helix is tethered to the α1 helix via interactions between three highly conserved residues (E70, R166, W167).

m153 and m157 exhibit the biggest differences at their termini. The N-terminus of m153 is elongated compared to other MHC-I molecules and starts adjacent the α3 domain and stretches upwards along the H2b helix until it forms the first strand of the platform sheet. A unique disulfide bond links the extended N-terminus to the H2b helix. m157 also has an extended N-terminus, but this region folds into a short α-helix, designated α0 that lies almost parallel to the α1 and α2 helices. The C-termini of both proteins could not be modeled due to a lack of electron density, suggesting flexibility in those parts of the proteins. The other members of the m145 family are likely to adopt the same basic fold as m153 and m157, with variations at the N- and C-termini. m17, m151, m152 and m155

all conserve Cys16 and Cys171, that are involved in the bond stabilizing the extended N-terminus of m153, suggesting that they have similar N-termini.

m152 and m153 share the largest number of identical amino acids within the m145 family. An interesting feature of m152 is that it lacks the second conserved cysteine in the α3 domain, which is present in all the other m145 and r145 family members. Examples of proteins with Ig-like domains lacking the conserved disulfide bond include CD2 (Jones et al., 1992) and CD4 (Brady et al., 1993). In domain 1 of CD2 the positions of the β strands are not affected by the lack of a disulfide bond and the domain superimposes well on domain 1 of CD4, which has a disulfide bond. In domain 3 of rat CD4 the absence of the disulfide bond causes expansion of the domain, with greater separation between the β sheets. The α3 domain disulfide bond is preserved in the rat homolog of m152, which suggests that the MCMV protein may not display a significant displacement of the strands. A molecular model of m152, based on the structure of m153, could be useful in exploring the interactions of m152 with its cellular ligands.

In conclusion, the structure of m153 reveals yet another adaptation of the MHC-I fold, displays a novel mode of dimer formation for β2m-free heavy chains and together with the m157 structure it allows the prediction of shared structural features for the other m145 family glycoproteins.

The immune modulatory functions of the m145 family members have been discussed in detail in previous chapters. We have shown that m153 is expressed on the surface of MCMV-infected cells. It is likely that m153 functions by engaging a receptor on host cells. To identify host cell populations that express ligands for m153 we constructed a

153-reporter cell line that can express GFP in response to cross-linking of an m153-human zeta fusion protein. Mouse splenocytes stimulated these reporter cells specifically. We subsequently isolated different cell types from the spleen and tested them for stimulation of the m153-reporter cells. Our results show that cells of the innate immune system most likely express a ligand or ligands for MCMV m153. Whilst B and T cells were unable to stimulate the m153-reporter cells, $CD11c^+$ and plasmacytoid dendritic cells and to a lesser extent $CD11b^+$ cells and NK cells specifically stimulated GFP production in the m153-reporter cells. Dendritic cells derived from the spleen as well as bone marrow cultures could stimulate the reporter cells. The stimulation was dependent on cell-cell contact and could partially be blocked by soluble recombinant m153.

Cells of the innate immune system coordinate the initial response to virus infections and help to shape the adaptive immune response. Dendritic and NK cells in particular are important in combating MCMV infection. Disruption of the activation of NK cells is a major target for several MCMV proteins, especially those from the m145 family. Dendritic cells can be infected by MCMV and the functional capacity of these cells is severely impaired at late times after infection. Due to the central role of DCs in the generation of an immune response the virus would benefit from also manipulating uninfected DCs. A recent study that investigated the effect of UL18-Fc fusion proteins on DCs showed that the UL18/LIR-1 interaction leads to the upregulation of CD83 and cytokine production in immature monocyte-derived DCs. UL18 also inhibited the chemotaxis of the DCs (Wagner et al., 2008). These results provide evidence that a viral MHC-I homolog can modulate DC function *in vitro*.

Our results indicate that MCMV m153 interacts specifically with both conventional and plasmacytoid DCs. We could not detect a specific effect of this interaction on the surface phenotype or migration ability of $CD11c^+$ DCs. The functional consequences of the interaction remain to be further explored. To best understand the function of m153 during MCMV infection, one needs to identify its ligand in the host. Based on our data, both conventional and plasmacytoid DCs present excellent target cell types for ligand identification. The m153-reporter cell line will be a useful tool to screen a DC-specific cDNA library to identify a ligand.

The m145 family of MCMV encodes a fascinating set of molecules with diverse functions that all presumably contribute to successful virus propagation. The original structural prediction has now been proven for two family members and it is clear that these MCMV proteins form part of the MHC superfamily. Many questions remain and it would be of great interest to determine which regions of the MHC-Iv molecules are involved in complex formation with their individual ligands. Further study of this MCMV family should yield great insight into the mechanisms MCMV and other herpesviruses employ to co-exist with their hosts.

REFERENCES

Adams, E.J., Juo, Z.S., Venook, R.T., Boulanger, M.J., Arase, H., Lanier, L.L., and Garcia, K.C. (2007). Structural elucidation of the m157 mouse cytomegalovirus ligand for Ly49 natural killer cell receptors. Proc Natl Acad Sci U S A *104*, 10128-10133.

Adams, P.C., and Barton, J.C. (2007). Haemochromatosis. Lancet *370*, 1855-1860.

Adams, P.D., Grosse-Kunstleve, R.W., Hung, L.W., Ioerger, T.R., McCoy, A.J., Moriarty, N.W., Read, R.J., Sacchettini, J.C., Sauter, N.K., and Terwilliger, T.C.

(2002). PHENIX: building new software for automated crystallographic structure determination. Acta Crystallogr D Biol Crystallogr *58*, 1948-1954.

Alcami, A., and Koszinowski, U.H. (2000). Viral mechanisms of immune evasion. Trends Microbiol *8*, 410-418.

Allen, H., Fraser, J., Flyer, D., Calvin, S., and Flavell, R. (1986). Beta 2-microglobulin is not required for cell surface expression of the murine class I histocompatibility antigen H-2D^{b} or of a truncated H-2D^{b}. Proc Natl Acad Sci U S A *83*, 7447-7451.

Andrews, D.M., Andoniou, C.E., Granucci, F., Ricciardi-Castagnoli, P., and Degli-Esposti, M.A. (2001). Infection of dendritic cells by murine cytomegalovirus induces functional paralysis. Nat Immunol *2*, 1077-1084.

Arase, H., Mocarski, E.S., Campbell, A.E., Hill, A.B., and Lanier, L.L. (2002). Direct recognition of cytomegalovirus by activating and inhibitory NK cell receptors. Science *296*, 1323-1326.

Attaya, M., Jameson, S., Martinez, C.K., Hermel, E., Aldrich, C., Forman, J., Lindahl, K.F., Bevan, M.J., and Monaco, J.J. (1992). Ham-2 corrects the class I antigen-processing defect in RMA-S cells. Nature *355*, 647-649.

Balthesen, M., Messerle, M., and Reddehase, M.J. (1993). Lungs are a major organ site of cytomegalovirus latency and recurrence. J Virol *67*, 5360-5366.

Banchereau, J., Briere, F., Caux, C., Davoust, J., Lebecque, S., Liu, Y.J., Pulendran, B., and Palucka, K. (2000). Immunobiology of dendritic cells. Annu Rev Immunol *18*, 767-811.

Beck, S., and Barrell, B.G. (1988). Human cytomegalovirus encodes a glycoprotein homologous to MHC class-I antigens. Nature *331*, 269-272.

Bendtsen, J.D., Nielsen, H., von Heijne, G., and Brunak, S. (2004). Improved prediction of signal peptides: SignalP 3.0. J Mol Biol *340*, 783-795.

Benedict, C.A., De Trez, C., Schneider, K., Ha, S., Patterson, G., and Ware, C.F. (2006). Specific remodeling of splenic architecture by cytomegalovirus. PLoS pathogens *2(3)*, e16.

Berman, H.M., Westbrook, J., Feng, Z., Gilliland, G., Bhat, T.N., Weissig, H., Shindyalov, I.N., and Bourne, P.E. (2000). The Protein Data Bank. Nucleic Acids Res *28*, 235-242.

Biron, C.A., Byron, K.S., and Sullivan, J.L. (1989). Severe herpesvirus infections in an adolescent without natural killer cells. The New England journal of medicine *320*, 1731-1735.

Bjorkman, P.J., and Parham, P. (1990). Structure, function, and diversity of class I major histocompatibility complex molecules. Annu Rev Biochem *59*, 253-288.

Bjorkman, P.J., Saper, M.A., Samraoui, B., Bennett, W.S., Strominger, J.L., and Wiley, D.C. (1987). Structure of the human class I histocompatibility antigen, HLA-A2. Nature *329*, 506-512.

Bowness, P. (2002). HLA B27 in health and disease: a double-edged sword? Rheumatology (Oxford) *41*, 857-868.

Brady, R.L., Dodson, E.J., Dodson, G.G., Lange, G., Davis, S.J., Williams, A.F., and Barclay, A.N. (1993). Crystal structure of domains 3 and 4 of rat CD4: relation to the NH2-terminal domains. Science *260*, 979-983.

Brewerton, D.A., Hart, F.D., Nicholls, A., Caffrey, M., James, D.C., and Sturrock, R.D. (1973). Ankylosing spondylitis and HL-A 27. Lancet *1*, 904-907.

Brigl, M., and Brenner, M.B. (2004). CD1: antigen presentation and T cell function. Annu Rev Immunol *22*, 817-890.

Brinkmann, U., Mattes, R.E., and Buckel, P. (1989). High-level expression of recombinant genes in Escherichia coli is dependent on the availability of the dnaY gene product. Gene *85*, 109-114.

Britt, W. (2006). Primate Models: Pros and Cons. In Cytomegaloviruses: Molecular Biology and Immunology, M.J. Reddehase, ed. (Norfolk, Caister Academic Press), pp. 591-605.

Brunger, A.T., Adams, P.D., Clore, G.M., DeLano, W.L., Gros, P., Grosse-Kunstleve, R.W., Jiang, J.S., Kuszewski, J., Nilges, M., Pannu, N.S.*, et al.* (1998). Crystallography & NMR system: A new software suite for macromolecular structure determination. Acta Crystallogr D Biol Crystallogr *54*, 905-921.

Bukowski, J.F., Warner, J.F., Dennert, G., and Welsh, R.M. (1985). Adoptive transfer studies demonstrating the antiviral effect of natural killer cells in vivo. J Exp Med *161*, 40-52.

Bukowski, J.F., Yang, H., and Welsh, R.M. (1988). Antiviral effect of lymphokine-activated killer cells: characterization of effector cells mediating prophylaxis. J Virol *62*, 3642-3648.

Burmeister, W.P., Gastinel, L.N., Simister, N.E., Blum, M.L., and Bjorkman, P.J. (1994a). Crystal structure at 2.2 Å resolution of the MHC-related neonatal Fc receptor. Nature *372*, 336-343.

Burmeister, W.P., Huber, A.H., and Bjorkman, P.J. (1994b). Crystal structure of the complex of rat neonatal Fc receptor with Fc. Nature *372*, 379-383.

Capps, G.G., Robinson, B.E., Lewis, K.D., and Zuniga, M.C. (1993). In vivo dimeric association of class I MHC heavy chains. Possible relationship to class I MHC heavy chain-beta 2-microglobulin dissociation. J Immunol *151*, 159-169.

Cerboni, C., Achour, A., Warnmark, A., Mousavi-Jazi, M., Sandalova, T., Hsu, M.L., Cosman, D., Karre, K., and Carbone, E. (2006). Spontaneous mutations in the human CMV HLA class I homologue UL18 affect its binding to the inhibitory receptor LIR-1/ILT2/CD85j. Eur J Immunol *36*, 732-741.

Cerwenka, A., and Lanier, L.L. (2003). NKG2D ligands: unconventional MHC class I-like molecules exploited by viruses and cancer. Tissue Antigens *61*, 335-343.

Chalupny, N.J., Rein-Weston, A., Dosch, S., and Cosman, D. (2006). Down-regulation of the NKG2D ligand MICA by the human cytomegalovirus glycoprotein UL142. Biochem Biophys Res Commun *346*, 175-181.

Chapman, T.L., and Bjorkman, P.J. (1998). Characterization of a murine cytomegalovirus class I major histocompatibility complex (MHC) homolog: comparison to MHC molecules and to the human cytomegalovirus MHC homolog. J Virol *72*, 460-466.

Chenna, R., Sugawara, H., Koike, T., Lopez, R., Gibson, T.J., Higgins, D.G., and Thompson, J.D. (2003). Multiple sequence alignment with the Clustal series of programs. Nucleic Acids Res *31*, 3497-3500.

Colbert, R.A. (2004). The immunobiology of HLA-B27: variations on a theme. Curr Mol Med *4*, 21-30.

Cosman, D., Fanger, N., Borges, L., Kubin, M., Chin, W., Peterson, L., and Hsu, M.L. (1997). A novel immunoglobulin superfamily receptor for cellular and viral MHC class I molecules. Immunity *7*, 273-282.

Cresswell, P., and Dawson, J.R. (1975). Dimeric and monomeric forms of HL-A antigens solubilized by detergent. J Immunol *114*, 523-525.

Cretney, E., Degli-Esposti, M.A., Densley, E.H., Farrell, H.E., Davis-Poynter, N.J., and Smyth, M.J. (1999). m144, a murine cytomegalovirus (MCMV)-encoded major histocompatibility complex class I homologue, confers tumor resistance to natural killer cell-mediated rejection. J Exp Med *190*, 435-444.

Dalod, M., Hamilton, T., Salomon, R., Salazar-Mather, T.P., Henry, S.C., Hamilton, J.D., and Biron, C.A. (2003). Dendritic cell responses to early murine

cytomegalovirus infection: subset functional specialization and differential regulation by interferon alpha/beta. J Exp Med *197*, 885-898.

Dalod, M., Salazar-Mather, T.P., Malmgaard, L., Lewis, C., Asselin-Paturel, C., Briere, F., Trinchieri, G., and Biron, C.A. (2002). Interferon alpha/beta and interleukin 12 responses to viral infections: pathways regulating dendritic cell cytokine expression in vivo. J Exp Med *195*, 517-528.

Davis, I.W., Leaver-Fay, A., Chen, V.B., Block, J.N., Kapral, G.J., Wang, X., Murray, L.W., Arendall, W.B., 3rd, Snoeyink, J., Richardson, J.S.*, et al.* (2007). MolProbity: all-atom contacts and structure validation for proteins and nucleic acids. Nucleic Acids Res *35*, W375-383.

Davis-Poynter, N.J., Lynch, D.M., Vally, H., Shellam, G.R., Rawlinson, W.D., Barrell, B.G., and Farrell, H.E. (1997). Identification and characterization of a G protein-coupled receptor homolog encoded by murine cytomegalovirus. J Virol *71*, 1521-1529.

Del Val, M., Hengel, H., Hacker, H., Hartlaub, U., Ruppert, T., Lucin, P., and Koszinowski, U.H. (1992). Cytomegalovirus prevents antigen presentation by blocking the transport of peptide-loaded major histocompatibility complex class I molecules into the medial-Golgi compartment. J Exp Med *176*, 729-738.

Del Val, M., Munch, K., Reddehase, M.J., and Koszinowski, U.H. (1989). Presentation of CMV immediate-early antigen to cytolytic T lymphocytes is selectively prevented by viral genes expressed in the early phase. Cell *58*, 305-315.

DeLano, W.L. (2002). The PyMOL User's Manual (Palo Alto, CA, USA, DeLano Scientific).

Emsley, P., and Cowtan, K. (2004). Coot: model-building tools for molecular graphics. Acta Crystallogr D Biol Crystallogr *60*, 2126-2132.

Farrell, H.E., Vally, H., Lynch, D.M., Fleming, P., Shellam, G.R., Scalzo, A.A., and Davis-Poynter, N.J. (1997). Inhibition of natural killer cells by a cytomegalovirus MHC class I homologue in vivo. Nature *386*, 510-514.

Finlay, B.B., and McFadden, G. (2006). Anti-immunology: evasion of the host immune system by bacterial and viral pathogens. Cell *124*, 767-782.

Fleming, P., Davis-Poynter, N., Degli-Esposti, M., Densley, E., Papadimitriou, J., Shellam, G., and Farrell, H. (1999). The murine cytomegalovirus chemokine homolog, m131/129, is a determinant of viral pathogenicity. J Virol *73*, 6800-6809.

Forbes, C.A., Brown, M.G., Cho, R., Shellam, G.R., Yokoyama, W.M., and Scalzo, A.A. (1997). The Cmv1 host resistance locus is closely linked to the Ly49 multigene family within the natural killer cell gene complex on mouse chromosome 6. Genomics *41*, 406-413.

Fremont, D.H., Matsumura, M., Stura, E.A., Peterson, P.A., and Wilson, I.A. (1992). Crystal structures of two viral peptides in complex with murine MHC class I H-2Kb. Science *257*, 919-927.

Garboczi, D.N., Hung, D.T., and Wiley, D.C. (1992). HLA-A2-peptide complexes: refolding and crystallization of molecules expressed in Escherichia coli and complexed with single antigenic peptides. Proc Natl Acad Sci U S A *89*, 3429-3433.

Gohda, T., Makita, Y., Shike, T., Tanimoto, M., Funabiki, K., Horikoshi, S., and Tomino, Y. (2003). Identification of epistatic interaction involved in obesity using the KK/Ta mouse as a Type 2 diabetes model: is Zn-alpha2 glycoprotein-1 a candidate gene for obesity? Diabetes *52*, 2175-2181.

Gold, M.C., Munks, M.W., Wagner, M., McMahon, C.W., Kelly, A., Kavanagh, D.G., Slifka, M.K., Koszinowski, U.H., Raulet, D.H., and Hill, A.B. (2004). Murine cytomegalovirus interference with antigen presentation has little effect on the size or the effector memory phenotype of the CD8 T cell response. J Immunol *172*, 6944-6953.

Gouet, P., Courcelle, E., Stuart, D.I., and Metoz, F. (1999). ESPript: analysis of multiple sequence alignments in PostScript. Bioinformatics *15*, 305-308.

Grundy, J.E., and Melief, C.J. (1982). Effect of Nu/Nu gene on genetically determined resistance to murine cytomegalovirus. J Gen Virol *61 (Pt l)*, 133-136.

Grundy, J.E., Trapman, J., Allan, J.E., Shellam, G.R., and Melief, C.J. (1982). Evidence for a protective role of interferon in resistance to murine cytomegalovirus and its control by non-H-2-linked genes. Infection and immunity *37*, 143-150.

Halaby, D.M., and Mornon, J.P. (1998). The immunoglobulin superfamily: an insight on its tissular, species, and functional diversity. J Mol Evol *46*, 389-400.

Hasan, M., Krmpotic, A., Ruzsics, Z., Bubic, I., Lenac, T., Halenius, A., Loewendorf, A., Messerle, M., Hengel, H., Jonjic, S.*, et al.* (2005). Selective down-regulation of the NKG2D ligand H60 by mouse cytomegalovirus m155 glycoprotein. J Virol *79*, 2920-2930.

Holm, L., and Sander, C. (1996). Mapping the protein universe. Science *273*, 595-603.

Holtappels, R., Gillert-Marien, D., Thomas, D., Podlech, J., Deegen, P., Herter, S., Oehrlein-Karpi, S.A., Strand, D., Wagner, M., and Reddehase, M.J. (2006). Cytomegalovirus encodes a positive regulator of antigen presentation. J Virol *80*, 7613-7624.

Hu, C.D., Chinenov, Y., and Kerppola, T.K. (2002). Visualization of interactions among bZIP and Rel family proteins in living cells using bimolecular fluorescence complementation. Mol Cell *9*, 789-798.

Iizuka, K., Naidenko, O.V., Plougastel, B.F., Fremont, D.H., and Yokoyama, W.M. (2003). Genetically linked C-type lectin-related ligands for the NKRP1 family of natural killer cell receptors. Nat Immunol *4*, 801-807.

Jahn, G., Stenglein, S., Riegler, S., Einsele, H., and Sinzger, C. (1999). Human cytomegalovirus infection of immature dendritic cells and macrophages. Intervirology *42*, 365-372.

Johansen, H., van der Straten, A., Sweet, R., Otto, E., Maroni, G., and Rosenberg, M. (1989). Regulated expression at high copy number allows production of a growth-inhibitory oncogene product in Drosophila Schneider cells. Genes & development *3*, 882-889.

Jones, E.Y., Davis, S.J., Williams, A.F., Harlos, K., and Stuart, D.I. (1992). Crystal structure at 2.8 Å resolution of a soluble form of the cell adhesion molecule CD2. Nature *360*, 232-239.

Jonjic, S., Mutter, W., Weiland, F., Reddehase, M.J., and Koszinowski, U.H. (1989). Site-restricted persistent cytomegalovirus infection after selective long-term depletion of CD4+ T lymphocytes. J Exp Med *169*, 1199-1212.

Jonjic, S., Pavic, I., Polic, B., Crnkovic, I., Lucin, P., and Koszinowski, U.H. (1994). Antibodies are not essential for the resolution of primary cytomegalovirus infection but limit dissemination of recurrent virus. J Exp Med *179*, 1713-1717.

Jordan, M.C., and Mar, V.L. (1982). Spontaneous activation of latent cytomegalovirus from murine spleen explants. Role of lymphocytes and macrophages in release and replication of virus. The Journal of clinical investigation *70*, 762-768.

Kane, J.F. (1995). Effects of rare codon clusters on high-level expression of heterologous proteins in Escherichia coli. Current opinion in biotechnology *6*, 494-500.

Kaptein, S.J.F., Vink, C., Bruggeman, C.A., and Stassen, F.R.M. (2006). The rat model for CMV infection and vascular disease. In Cytomegaloviruses: Molecular Biology

and Immunology, M.J. Reddehase, ed. (Norfolk, Caister Academic Press), pp. 502-523.

Kavanagh, D.G., Gold, M.C., Wagner, M., Koszinowski, U.H., and Hill, A.B. (2001). The multiple immune-evasion genes of murine cytomegalovirus are not redundant: m4 and m152 inhibit antigen presentation in a complementary and cooperative fashion. J Exp Med *194*, 967-978.

Kelley, L.A., MacCallum, R.M., and Sternberg, M.J. (2000). Enhanced genome annotation using structural profiles in the program 3D-PSSM. J Mol Biol *299*, 499-520.

Kerppola, T.K. (2008). Bimolecular fluorescence complementation: visualization of molecular interactions in living cells. Methods in cell biology *85*, 431-470.

Kirkpatrick, R.B., Ganguly, S., Angelichio, M., Griego, S., Shatzman, A., Silverman, C., and Rosenberg, M. (1995). Heavy chain dimers as well as complete antibodies are efficiently formed and secreted from Drosophila via a BiP-mediated pathway. J Biol Chem *270*, 19800-19805.

Kleijnen, M.F., Huppa, J.B., Lucin, P., Mukherjee, S., Farrell, H., Campbell, A.E., Koszinowski, U.H., Hill, A.B., and Ploegh, H.L. (1997). A mouse cytomegalovirus glycoprotein, gp34, forms a complex with folded class I MHC molecules in the ER which is not retained but is transported to the cell surface. The EMBO journal *16*, 685-694.

Koffron, A.J., Hummel, M., Patterson, B.K., Yan, S., Kaufman, D.B., Fryer, J.P., Stuart, F.P., and Abecassis, M.I. (1998). Cellular localization of latent murine cytomegalovirus. J Virol *72*, 95-103.

Krmpotic, A., Bubic, I., Polic, B., Lucin, P., and Jonjic, S. (2003). Pathogenesis of murine cytomegalovirus infection. Microbes Infect *5*, 1263-1277.

Krmpotic, A., Hasan, M., Loewendorf, A., Saulig, T., Halenius, A., Lenac, T., Polic, B., Bubic, I., Kriegeskorte, A., Pernjak-Pugel, E*., et al.* (2005). NK cell activation through the NKG2D ligand MULT-1 is selectively prevented by the glycoprotein encoded by mouse cytomegalovirus gene m145. J Exp Med *201*, 211-220.

Krmpotic, A., Messerle, M., Crnkovic-Mertens, I., Polic, B., Jonjic, S., and Koszinowski, U.H. (1999). The immunoevasive function encoded by the mouse cytomegalovirus gene m152 protects the virus against T cell control in vivo. J Exp Med *190*, 1285-1296.

Lawrence, M.C., and Colman, P.M. (1993). Shape complementarity at protein/protein interfaces. J Mol Biol *234*, 946-950.

Lebron, J.A., Bennett, M.J., Vaughn, D.E., Chirino, A.J., Snow, P.M., Mintier, G.A., Feder, J.N., and Bjorkman, P.J. (1998). Crystal structure of the hemochromatosis protein HFE and characterization of its interaction with transferrin receptor. Cell *93*, 111-123.

Lee, S.H., Zafer, A., de Repentigny, Y., Kothary, R., Tremblay, M.L., Gros, P., Duplay, P., Webb, J.R., and Vidal, S.M. (2003). Transgenic expression of the activating natural killer receptor Ly49H confers resistance to cytomegalovirus in genetically susceptible mice. J Exp Med *197*, 515-526.

Lenac, T., Budt, M., Arapovic, J., Hasan, M., Zimmermann, A., Simic, H., Krmpotic, A., Messerle, M., Ruzsics, Z., Koszinowski, U.H., *et al.* (2006). The herpesviral Fc receptor fcr-1 down-regulates the NKG2D ligands MULT-1 and H60. J Exp Med *203*, 1843-1850.

Li, P., McDermott, G., and Strong, R.K. (2002). Crystal structures of RAE-1beta and its complex with the activating immunoreceptor NKG2D. Immunity *16*, 77-86.

Li, P., Morris, D.L., Willcox, B.E., Steinle, A., Spies, T., and Strong, R.K. (2001). Complex structure of the activating immunoreceptor NKG2D and its MHC class I-like ligand MICA. Nat Immunol *2*, 443-451.

Lilley, B.N., and Ploegh, H.L. (2005). Viral modulation of antigen presentation: manipulation of cellular targets in the ER and beyond. Immunol Rev *207*, 126-144.

Lodoen, M., Ogasawara, K., Hamerman, J.A., Arase, H., Houchins, J.P., Mocarski, E.S., and Lanier, L.L. (2003). NKG2D-mediated natural killer cell protection against cytomegalovirus is impaired by viral gp40 modulation of retinoic acid early inducible 1 gene molecules. J Exp Med *197*, 1245-1253.

Lodoen, M.B., Abenes, G., Umamoto, S., Houchins, J.P., Liu, F., and Lanier, L.L. (2004). The cytomegalovirus m155 gene product subverts natural killer cell antiviral protection by disruption of H60-NKG2D interactions. J Exp Med *200*, 1075-1081.

Lodoen, M.B., and Lanier, L.L. (2005). Viral modulation of NK cell immunity. Nature reviews *3*, 59-69.

Loewendorf, A., Kruger, C., Borst, E.M., Wagner, M., Just, U., and Messerle, M. (2004). Identification of a mouse cytomegalovirus gene selectively targeting CD86 expression on antigen-presenting cells. J Virol *78*, 13062-13071.

Lu, X., Pinto, A.K., Kelly, A.M., Cho, K.S., and Hill, A.B. (2006). Murine cytomegalovirus interference with antigen presentation contributes to the inability of CD8 T cells to control virus in the salivary gland. J Virol *80*, 4200-4202.

Maley, F., Trimble, R.B., Tarentino, A.L., and Plummer, T.H., Jr. (1989). Characterization of glycoproteins and their associated oligosaccharides through the use of endoglycosidases. Anal Biochem *180*, 195-204.

Mans, J., Natarajan, K., Balbo, A., Schuck, P., Eikel, D., Hess, S., Robinson, H., Simic, H., Jonjic, S., Tiemessen, C.T.*, et al.* (2007). Cellular expression and crystal structure of the murine cytomegalovirus major histocompatibility complex class I-like glycoprotein, m153. J Biol Chem *282*, 35247-35258.

Margulies, D.H., Natarajan, K., Rossjohn, J., and McCluskey, J. (2007). Major Histocompatibility Complex (MHC) Molecules: Structure, Function, and Genetics. In Fundamental Immunology, W.E. Paul, ed. (Philadelphia, Lippincott, Williams, and Wilkins), p. in press.

Mathys, S., Schroeder, T., Ellwart, J., Koszinowski, U.H., Messerle, M., and Just, U. (2003). Dendritic cells under influence of mouse cytomegalovirus have a physiologic dual role: to initiate and to restrict T cell activation. The Journal of infectious diseases *187*, 988-999.

McDermott, L.C., Freel, J.A., West, A.P., Bjorkman, P.J., and Kennedy, M.W. (2006). Zn-alpha2-glycoprotein, an MHC class I-related glycoprotein regulator of adipose tissues: modification or abrogation of ligand binding by site-directed mutagenesis. Biochemistry *45*, 2035-2041.

McGeoch, D.J., Cook, S., Dolan, A., Jamieson, F.E., and Telford, E.A. (1995). Molecular phylogeny and evolutionary timescale for the family of mammalian herpesviruses. J Mol Biol *247*, 443-458.

McGeoch, D.J., Rixon, F.J., and Davison, A.J. (2006). Topics in herpesvirus genomics and evolution. Virus research *117*, 90-104.

Menard, C., Wagner, M., Ruzsics, Z., Holak, K., Brune, W., Campbell, A.E., and Koszinowski, U.H. (2003). Role of murine cytomegalovirus US22 gene family members in replication in macrophages. J Virol *77*, 5557-5570.

Mintern, J.D., Klemm, E.J., Wagner, M., Paquet, M.E., Napier, M.D., Kim, Y.M., Koszinowski, U.H., and Ploegh, H.L. (2006). Viral interference with B7-1 costimulation: a new role for murine cytomegalovirus fc receptor-1. J Immunol *177*, 8422-8431.

Moutaftsi, M., Mehl, A.M., Borysiewicz, L.K., and Tabi, Z. (2002). Human cytomegalovirus inhibits maturation and impairs function of monocyte-derived dendritic cells. Blood *99*, 2913-2921.

Murshudov, G.N., Vagin, A.A., and Dodson, E.J. (1997). Refinement of macromolecular structures by the maximum-likelihood method. Acta Crystallogr D Biol Crystallogr *53*, 240-255.

Mutter, W., Reddehase, M.J., Busch, F.W., Buhring, H.J., and Koszinowski, U.H. (1988). Failure in generating hemopoietic stem cells is the primary cause of death from cytomegalovirus disease in the immunocompromised host. J Exp Med *167*, 1645-1658.

Natarajan, K., Hicks, A., Mans, J., Robinson, H., Guan, R., Mariuzza, R.A., and Margulies, D.H. (2006). Crystal structure of the murine cytomegalovirus MHC-I homolog m144. J Mol Biol *358*, 157-171.

Natarajan, K., Li, H., Mariuzza, R.A., and Margulies, D.H. (1999). MHC class I molecules, structure and function. Rev Immunogenet *1*, 32-46.

Nielsen, H., Engelbrecht, J., Brunak, S., and von Heijne, G. (1997). Identification of prokaryotic and eukaryotic signal peptides and prediction of their cleavage sites. Protein engineering *10*, 1-6.

Nomura, M., Kurita-Taniguchi, M., Kondo, K., Inoue, N., Matsumoto, M., Yamanishi, K., Okabe, M., and Seya, T. (2002). Mechanism of host cell protection from complement in murine cytomegalovirus (CMV) infection: identification of a CMV-responsive element in the CD46 promoter region. Eur J Immunol *32*, 2954-2964.

Ohtsuka, M., Arase, H., Takeuchi, A., Yamasaki, S., Shiina, R., Suenaga, T., Sakurai, D., Yokosuka, T., Arase, N., Iwashima, M.*, et al.* (2004). NFAM1, an immunoreceptor tyrosine-based activation motif-bearing molecule that regulates B cell development and signaling. Proc Natl Acad Sci U S A *101*, 8126-8131.

Olson, R., Dulac, C., and Bjorkman, P.J. (2006). MHC homologs in the nervous system--they haven't lost their groove. Current opinion in neurobiology *16*, 351-357.

Olson, R., Huey-Tubman, K.E., Dulac, C., and Bjorkman, P.J. (2005). Structure of a pheromone receptor-associated MHC molecule with an open and empty groove. PLoS Biol *3*, e257.

Olson, S.A. (1994). MacVector: protein analysis. Methods in molecular biology (Clifton, NJ *25*, 237-246.

Onishi, M., Kinoshita, S., Morikawa, Y., Shibuya, A., Phillips, J., Lanier, L.L., Gorman, D.M., Nolan, G.P., Miyajima, A., and Kitamura, T. (1996). Applications of retrovirus-mediated expression cloning. Experimental hematology *24*, 324-329.

Otwinowski, Z., and Minor, W. (1997). Processing of X-ray Diffraction Data Collected in Oscillation Mode In Methods in Enzymology, pp. 307-326.

Painter, J., and Merritt, E.A. (2005). A molecular viewer for the analysis of TLS rigid-body motion in macromolecules. Acta Crystallogr D Biol Crystallogr *61*, 465-471.

Pereira, L., Maidji, E., McDonagh, S., and Tabata, T. (2006). Routes of human CMV transmission and infection at the uterine-placental interface. In Cytomegaloviruses: Molecular Biology and Immunology, M.J. Reddehase, ed. (Norfolk, Caister Academic Press), pp. 29-48.

Pinto, A.K., and Hill, A.B. (2005). Viral interference with antigen presentation to CD8+ T cells: lessons from cytomegalovirus. Viral immunology *18*, 434-444.

Pinto, A.K., Munks, M.W., Koszinowski, U.H., and Hill, A.B. (2006). Coordinated function of murine cytomegalovirus genes completely inhibits CTL lysis. J Immunol *177*, 3225-3234.

Polic, B., Hengel, H., Krmpotic, A., Trgovcich, J., Pavic, I., Luccaronin, P., Jonjic, S., and Koszinowski, U.H. (1998). Hierarchical and redundant lymphocyte subset control precludes cytomegalovirus replication during latent infection. J Exp Med *188*, 1047-1054.

Prod'homme, V., Griffin, C., Aicheler, R.J., Wang, E.C., McSharry, B.P., Rickards, C.R., Stanton, R.J., Borysiewicz, L.K., Lopez-Botet, M., Wilkinson, G.W.*, et al.* (2007). The human cytomegalovirus MHC class I homolog UL18 inhibits LIR-1+ but activates LIR-1- NK cells. J Immunol *178*, 4473-4481.

Raftery, M.J., Schwab, M., Eibert, S.M., Samstag, Y., Walczak, H., and Schonrich, G. (2001). Targeting the function of mature dendritic cells by human cytomegalovirus: a multilayered viral defense strategy. Immunity *15*, 997-1009.

Rawlinson, W.D., Farrell, H.E., and Barrell, B.G. (1996). Analysis of the complete DNA sequence of murine cytomegalovirus. J Virol *70*, 8833-8849.

Read, R.J. (2001). Pushing the boundaries of molecular replacement with maximum likelihood. Acta Crystallogr D Biol Crystallogr *57*, 1373-1382.

Reddehase, M.J., Balthesen, M., Rapp, M., Jonjic, S., Pavic, I., and Koszinowski, U.H. (1994). The conditions of primary infection define the load of latent viral genome

in organs and the risk of recurrent cytomegalovirus disease. J Exp Med *179*, 185-193.

Reddehase, M.J., Podlech, J., and Grzimek, N.K. (2002). Mouse models of cytomegalovirus latency: overview. J Clin Virol *25 Suppl 2*, S23-36.

Reddehase, M.J., Rothbard, J.B., and Koszinowski, U.H. (1989). A pentapeptide as minimal antigenic determinant for MHC class I-restricted T lymphocytes. Nature *337*, 651-653.

Reddehase, M.J., Weiland, F., Munch, K., Jonjic, S., Luske, A., and Koszinowski, U.H. (1985). Interstitial murine cytomegalovirus pneumonia after irradiation: characterization of cells that limit viral replication during established infection of the lungs. J Virol *55*, 264-273.

Redpath, S., Angulo, A., Gascoigne, N.R., and Ghazal, P. (1999). Murine cytomegalovirus infection down-regulates MHC class II expression on macrophages by induction of IL-10. J Immunol *162*, 6701-6707.

Reynolds, R.P., Rahija, R.J., Schenkman, D.I., and Richter, C.B. (1993). Experimental murine cytomegalovirus infection in severe combined immunodeficient mice. Laboratory animal science *43*, 291-295.

Riddell, S.R., Watanabe, K.S., Goodrich, J.M., Li, C.R., Agha, M.E., and Greenberg, P.D. (1992). Restoration of viral immunity in immunodeficient humans by the adoptive transfer of T cell clones. Science *257*, 238-241.

Risler, J.L., Delorme, M.O., Delacroix, H., and Henaut, A. (1988). Amino acid substitutions in structurally related proteins. A pattern recognition approach. Determination of a new and efficient scoring matrix. J Mol Biol *204*, 1019-1029.

Robbins, S.H., Bessou, G., Cornillon, A., Zucchini, N., Rupp, B., Ruzsics, Z., Sacher, T., Tomasello, E., Vivier, E., Koszinowski, U.H.*, et al.* (2007). Natural killer cells promote early CD8 T cell responses against cytomegalovirus. PLoS pathogens *3*, e123.

Roizman, B., and Sears, A.E. (1987). An inquiry into the mechanisms of herpes simplex virus latency. Annual review of microbiology *41*, 543-571.

Schleiss, M.R., and Lacayo, J.C. (2006). The guinea-pig model of congenital cytomegalovirus infection. In Cytomegaloviruses: Molecular Biology and Immunology, M.J. Reddehase, ed. (Norfolk, Caister Academic Press), pp. 525-550.

Schuck, P. (2000). Size-distribution analysis of macromolecules by sedimentation velocity ultracentrifugation and lamm equation modeling. Biophys J *78*, 1606-1619.

Schwartz, B.D., Kato, K., Cullen, S.E., and Nathenson, S.G. (1973). H-2 histocompatibility alloantigens. Some biochemical properties of the molecules solubilized by NP-40 detergent. Biochemistry *12*, 2157-2164.

Shanley, J.D., and Pesanti, E.L. (1986). Murine cytomegalovirus adrenalitis in athymic nude mice. Archives of virology *88*, 27-35.

Shiroishi, M., Kuroki, K., Ose, T., Rasubala, L., Shiratori, I., Arase, H., Tsumoto, K., Kumagai, I., Kohda, D., and Maenaka, K. (2006). Efficient leukocyte Ig-like receptor signaling and crystal structure of disulfide-linked HLA-G dimer. J Biol Chem *281*, 10439-10447.

Shortman, K., and Naik, S.H. (2007). Steady-state and inflammatory dendritic-cell development. Nat Rev Immunol *7*, 19-30.

Simon, C.O., Seckert, C.K., Grzimek, N.K.A., and Reddehase, M.J. (2006). Murine model of cytomegalovirus latency and reactivation: the silencing/desilencing and immune sensing hypothesis. In Cytomegaloviruses: Molecular Biology and Immunology, M.J. Reddehase, ed. (Norfolk, Caister Academic Press), pp. 483-500.

Sissons, J.G., Carmichael, A.J., McKinney, N., Sinclair, J.H., and Wills, M.R. (2002). Human cytomegalovirus and immunopathology. Springer seminars in immunopathology *24*, 169-185.

Smith, H.R., Chuang, H.H., Wang, L.L., Salcedo, M., Heusel, J.W., and Yokoyama, W.M. (2000). Nonstochastic coexpression of activation receptors on murine natural killer cells. J Exp Med *191*, 1341-1354.

Smith, H.R., Heusel, J.W., Mehta, I.K., Kim, S., Dorner, B.G., Naidenko, O.V., Iizuka, K., Furukawa, H., Beckman, D.L., Pingel, J.T.*, et al.* (2002). Recognition of a virus-encoded ligand by a natural killer cell activation receptor. Proc Natl Acad Sci U S A *99*, 8826-8831.

Smith, L.M., Shellam, G.R., and Redwood, A.J. (2006). Genes of murine cytomegalovirus exist as a number of distinct genotypes. Virology *352*, 450-465.

Steiner, I., Spivack, J.G., Deshmane, S.L., Ace, C.I., Preston, C.M., and Fraser, N.W. (1990). A herpes simplex virus type 1 mutant containing a nontransinducing Vmw65 protein establishes latent infection in vivo in the absence of viral

replication and reactivates efficiently from explanted trigeminal ganglia. J Virol *64*, 1630-1638.

Stoddart, C.A., Cardin, R.D., Boname, J.M., Manning, W.C., Abenes, G.B., and Mocarski, E.S. (1994). Peripheral blood mononuclear phagocytes mediate dissemination of murine cytomegalovirus. J Virol *68*, 6243-6253.

Sweet, C. (1999). The pathogenicity of cytomegalovirus. FEMS microbiology reviews *23*, 457-482.

Thale, R., Szepan, U., Hengel, H., Geginat, G., Lucin, P., and Koszinowski, U.H. (1995). Identification of the mouse cytomegalovirus genomic region affecting major histocompatibility complex class I molecule transport. J Virol *69*, 6098-6105.

Tortorella, D., Gewurz, B.E., Furman, M.H., Schust, D.J., and Ploegh, H.L. (2000). Viral subversion of the immune system. Annu Rev Immunol *18*, 861-926.

Townsend, A., Ohlen, C., Foster, L., Bastin, J., Ljunggren, H.G., and Karre, K. (1989). A mutant cell in which association of class I heavy and light chains is induced by viral peptides. Cold Spring Harb Symp Quant Biol *54 Pt 1*, 299-308.

Tripathy, S.K., Smith, H.R., Holroyd, E.A., Pingel, J.T., and Yokoyama, W.M. (2006). Expression of m157, a murine cytomegalovirus-encoded putative major histocompatibility class I (MHC-I)-like protein, is independent of viral regulation of host MHC-I. J Virol *80*, 545-550.

Vancikova, Z., and Dvorak, P. (2001). Cytomegalovirus infection in immunocompetent and immunocompromised individuals--a review. Current drug targets *1*, 179-187.

Villadangos, J.A., and Heath, W.R. (2005). Life cycle, migration and antigen presenting functions of spleen and lymph node dendritic cells: limitations of the Langerhans cells paradigm. Seminars in immunology *17*, 262-272.

Vink, C., Beuken, E., and Bruggeman, C.A. (2000). Complete DNA sequence of the rat cytomegalovirus genome. J Virol *74*, 7656-7665.

Voigt, V., Forbes, C.A., Tonkin, J.N., Degli-Esposti, M.A., Smith, H.R., Yokoyama, W.M., and Scalzo, A.A. (2003). Murine cytomegalovirus m157 mutation and variation leads to immune evasion of natural killer cells. Proc Natl Acad Sci U S A *100*, 13483-13488.

Wagner, C.S., Rolle, A., Cosman, D., Ljunggren, H.G., Berndt, K.D., and Achour, A. (2007). Structural elements underlying the high binding affinity of human cytomegalovirus UL18 to leukocyte immunoglobulin-like receptor-1. J Mol Biol *373*, 695-705.

Wagner, C.S., Walther-Jallow, L., Buentke, E., Ljunggren, H.G., Achour, A., and Chambers, B.J. (2008). Human cytomegalovirus-derived protein UL18 alters the phenotype and function of monocyte-derived dendritic cells. Journal of leukocyte biology *83*, 56-63.

Wills, M.R., Ashiru, O., Reeves, M.B., Okecha, G., Trowsdale, J., Tomasec, P., Wilkinson, G.W., Sinclair, J., and Sissons, J.G. (2005). Human cytomegalovirus encodes an MHC class I-like molecule (UL142) that functions to inhibit NK cell lysis. J Immunol *175*, 7457-7465.

Yokoyama, S. (2003). Protein expression systems for structural genomics and proteomics. Current opinion in chemical biology *7*, 39-43.

Zeng, Z., Castano, A.R., Segelke, B.W., Stura, E.A., Peterson, P.A., and Wilson, I.A. (1997). Crystal structure of mouse CD1: An MHC-like fold with a large hydrophobic binding groove. Science *277*, 339-345.

Zhang, M., and Atherton, S.S. (2002). Apoptosis in the retina during MCMV retinitis in immunosuppressed BALB/c mice. J Clin Virol *25 Suppl 2*, S137-147.

Ziegler, H., Muranyi, W., Burgert, H.G., Kremmer, E., and Koszinowski, U.H. (2000). The luminal part of the murine cytomegalovirus glycoprotein gp40 catalyzes the retention of MHC class I molecules. The EMBO journal *19*, 870-881.

Ziegler, H., Thale, R., Lucin, P., Muranyi, W., Flohr, T., Hengel, H., Farrell, H., Rawlinson, W., and Koszinowski, U.H. (1997). A mouse cytomegalovirus glycoprotein retains MHC class I complexes in the ERGIC/cis-Golgi compartments. Immunity *6*, 57-66.

LIST OF WEBSITES

AUC data analysis - SEDFIT: http://www.analyticalultracentrifugation.com

Hinge angle calculations - HINGE: http://sis.niaid.nih.gov/programs/hinge.html

N-linked glycosylation site prediction: http://www.cbs.dtu.dk/services/NetNGlyc

Signal peptide prediction: http://www.cbs.dtu.dk/services/SignalP

Structure validation - Molprobity: http://kinemage.biochem.duke.edu

APPENDIX A: Ethical clearance

UNIVERSITY OF THE WITWATERSRAND, JOHANNESBURG

STRICTLY CONFIDENTIAL

ANIMAL ETHICS SCREENING COMMITTEE (AESC)

CLEARANCE CERTIFICATE NO. 2007/74/4

APPLICANT: Ms J Mans

SCHOOL: Virology NIAID laboratory
DEPARTMENT:
LOCATION: Medical School

PROJECT TITLE: **Identifying and characterising the cellular ligand for the mouse cytomegalovirus glycoprotein m15?**

Number and Species

114 male and female mice

Approval was given for to the use of animals for the project described above at an AESC meeting held on 20071127. This approval remains valid until 20091127

The use of these animals is subject to AESC guidelines for the use and care of animals, is limited to the procedures described in the application form and to the following additional conditions:

Signed: _____ Date: 30/11/2007
(Chairperson, AESC)

I am satisfied that the persons listed in this application are competent to perform the procedures therein, in terms of Section 23 (1) (c) of the Veterinary and Para-Veterinary Professions Act (19 of 1982)

Signed: _____ Date: 30/11/2007
(Registered Veterinarian)

cc: Supervisor:
Director: CAS

Works 2000/lain0015/AESCCert.wps